1-1-1991

The orientation of low-molecular weight nematic liquid crystals in transverse electrical fields/

Kevin T. Schell
University of Massachusetts Amherst

THE ORIENTATION OF LOW-MOLECULAR WEIGHT NEMATIC LIQUID CRYSTALS IN TRANSVERSE ELECTRICAL FIELDS

A Dissertation Presented

by

KEVIN T. SCHELL

Submitted to the Graduate School of the
University of Massachusetts in partial fulfillment
of the requirements for the degree of

DOCTOR OF PHILOSOPHY

September 1991

Polymer Science and Engineering

THE ORIENTATION OF LOW-MOLECULAR WEIGHT NEMATIC LIQUID CRYSTALS IN TRANSVERSE ELECTRICAL FIELDS

A Dissertation Presented

by

KEVIN T. SCHELL

Approved as to style and content by:

Roger S. Porter
Roger S. Porter
Chairperson of Committee

Shaw L. Hsu
Shaw L. Hsu, Member

Hajime Sakai
Hajime Sakai, Member

William J. MacKnight
William J. MacKnight
Department Head
Polymer Science and
Engineering Department

ACKNOWLEDGEMENT

I would like to thank Professor Roger S. Porter for acting as my thesis advisor during the course of my studies at the University of Massachusetts. In the times of my own difficulty, Professor Porter demonstrated his continued support and patience without which this work would not have been possible. I remain in his debt as he went above and beyond the call of duty in his advisorial role.

I would also like to express my sincere thanks to Professors Shaw Ling Hsu and Hajime Sakai for serving on my committee. They guided me through many experimental and technical difficulties and offered helpful suggestions for my research.

I would also like to thank my former instuctors at North Carolina State University: Doctors Forest C. Hentz, Raymond E. Fornes and Richard D. Gilbert, for encouraging me to continue in my education.

Finally, I would like to thank my parents, Dr. and Mrs. Joseph F. Schell, and all my family for their moral support throughout my doctoral program. Also, thanks is extended to my personal friends Matthew Muir, James Bright, Kirk Johnson and Russel Clark for their humor, support and understanding during my more difficult times.

ABSTRACT

THE ORIENTATION OF LOW-MOLECULAR WEIGHT NEMATIC LIQUID CRYSTALS IN TRANSVERSE ELECTRICAL FIELDS

SEPTEMBER 1990

KEVIN T. SCHELL, B.S.

NORTH CAROLINA STATE UNIVERSITY

M.S., Ph.D., UNIVERSITY OF MASSACHUSETTS

Directed by: Professor Roger S. Porter

The orientation of nematic liquid crystals in electrical fields is commonplace in flat-panel watch and calculator displays. In 99% of these devices, the optical path and the electrical field are parallel to each other. When an alternating electrical field is applied perpendicular to the optical path unusual optical patterns result. The physics and properties of the wave-like optical pattern were previously unreported.

The geometry and wave-like optical pattern are described in chapter two for a room-temperature nematic liquid crystal: 4-4′-n-pentylcyanobiphenyl. Physical conditions of wave stability, i.e. temperature, field and frequency were investigated and discussed in terms of nematic liquid crystalline theory. It was determined that the wave pattern was stabilized at low temperatures and high

frequencies. It was also concluded that the mechanism of deformation was dielectric rather than ionic.

The macroscopic observations were quantified into two molecular orientation profiles in the succeeding chapter. The orientation profiles given are based on two possible cases of surface orientation for the nematic layer. The analysis of molecular orientation relies heavily on the theory of electrical deformation developed by Deuling.

To understand the importance of the material parameters of the nematic in relationship to the optical effect, binary blends of 4-4'-n-pentylcyanobiphenyl and 4-[4-alkylcyclo-hexyl]-cyanophenyl homologs were prepared. The complete phase behavior of these mixtures is the subject of chapter 4. A thorough physical characterization, regarding the dielectric and elastic properties, response times and threshold voltages, of four selected nematic fluids is given in chapter five. Finally, in chapter six, the effect of the blending on the electrical deformation of the nematic mesophase in a transverse-electrode cell is studied.

TABLE OF CONTENTS

Page

ACKNOWLEDGEMENTS.....iv

ABSTRACT.....v

LIST OF TABLES.....x

LIST OF FIGURES.....xi

CHAPTER

1. ELECTRO-OPTICS OF NEMATIC LIQUID CRYSTALS.....1

1.1 Liquid Crystal Cell Construction.....1
1.2 Physical Properties of Nematic Liquid Crystals.....4

1.2.1 Elastic Moduli.....4
1.2.2 Optical Properties.....7
1.2.3 Dielectric Properties.....7

1.3 Electro-optics.....9

1.3.1 Theory.....9
1.3.2 A Commercial Display.....15
1.3.3 A Research Example.....15
1.3.4 Transverse Electric Fields.....16

1.3.4.1 History.....16
1.3.4.2 Preliminary Work.....17
1.3.4.3 Research Objectives.....21
1.3.4.4 Current Speculation.....22

1.4 Scope.....24
1.5 Compositions and Equipment.....28
1.6 References.....31

2. WAVE STRUCTURES IN A NEMATIC LAYER: 4-4'-N-PENTYLCYANOBIPHENYL (K15).....33

2.1 Experimental.....34
2.2 Influence of DC Fields.....36
2.3 Influence of AC Fields.....37
2.4 Effect of Layer Thickness.....41
2.5 Effect of Temperature.....43
2.6 Analogy Between Interface Position and Work.....46
2.7 Explanation of the Wave Structure.....50
2.8 Conclusions.....53
2.9 References.....53

3. MOLECULAR ORIENTATION PROFILE IN A DEFORMED NEMATIC: 4-4′-N-PENTYLCYANOBIPHENYL.....55

3.1 Theory.....56
3.2 Experimental.....58
3.3 Molecular Orientation Profile.....59

3.3.1 Neglecting Boundary Effects.....59
3.3.2 Considering Boundary Effects.....62

3.4 Conclusions.....70
3.5 References.....71

4. BINARY PHASE STUDIES OF 4-4′-N-PENTYLCYANOBIPHENYL.....73

4.1 Theory of Eutectic Blending.....74
4.2 Experimental.....76
4.3 Binary Systems Studied.....79

4.3.1 N-Ethylcyclohexyl-p-cyanophenyl with K15....79
4.3.2 N-Butylcyclohexyl-p-cyanophenyl with K15....87
4.3.3 N-Heptylcyclohexyl-p-cyanophenyl with K15...87

4.4 Conclusions.....91
4.5 References.....93

5. ELECTRO-OPTICAL CHARACTERIZATION OF 60/40 BINARY MIXTURES.....94

5.1 Experimental.....94
5.2 Dielectric Properties.....96

5.2.1 Effect of Temperature.....98
5.2.2 Effect of Composition.....103

5.3 Response Time.....106

5.3.1 Effect of Voltage.....108
5.3.2 Effect of Temperature.....110
5.3.3 Effect of Layer Thickness.....110
5.3.4 Effect of Blending.....114

5.4 Elastic Constants.....117

5.4.1 Theory.....117
5.4.2 Effect of Temperature.....120
5.4.3 Effect of Blending.....120

5.5 Threshold Voltage.....120

5.5.1 Effect of Blending.....124

5.6 References.....128

6. ELECTRO-OPTICAL STUDIES OF BINARY NEMATIC MIXTURES....129

6.1 Experimental.....129
6.2 Transverse Electric-Field Deformation.....130

6.2.1 At Constant Temperature (14°C).....130
6.2.2 At Constant Sub-Clearing.....131

7. FUTURE WORK.....138

APPENDIX: MEASURING FILM THICKNESS INTERFEROMETRICALLY...141

BIBLEOGRAPHY.....143

LIST OF TABLES

1.1 Nomenclature, composition and chemical structure of nine LC mixtures.....26

1.2 Measurements of the elastic, dielectric and optical material properties made at constant temperature $(T_{NI}-10)^{o}C$.....29

1.3 Measurements of the elastic, dielectric and optical material properties made at constant temperature $(T_{NI}-10^{o}C)$..... 30

4.1. Thermal properties of 4 pure nematic liquid crystals compared with the literature.... 77

4.2. Heats of transition for K15/S1236 blends.....85

4.3. Heats of transition for K15/S1188 blends.....89

4.4. Heats of transition for K15/S1115 blends.....92

5.1 Composition and thermal properties of the eutectic for three binary systems as compared to pure K15.....97

5.2 Dielectric anisotropy for four pure nematic liquid crystals; [a]our measurements at $26^{o}C$, [b]EM catalog value (temperature not specified).105

5.3 A and x parameters for K15 in a 67 micron cell at $20^{o}C$.....111

6.1 Physical properties of four nematic systems at $14^{o}C$.....136

6.2 Electrical deformation data for four nematic fluids at $14^{o}C$.....136

6.3 Physical properties of four nematic systems at $(T_{NI}-7)^{o}C$.....137

6.4 Electrical deformation data for four nematic fluids at $(T_{NI}-7)^{o}C$.....137

LIST OF FIGURES

1.1 Three possible electrode structures for applying longitudinal or transverse electric fields to liquid crystal films.....3

1.2 Three cases of nematic liquid crystal alignment: a) homogeneous, b) tilted homeotropic and c) homeotropic alignment.....5

1.3 Four possible orderings of thin nematic films at E = 0.....6

1.4 The basic deformations of a nematic liquid crystal: a) splay, b) twist and c) bend.....8

1.5 Cell construction of a twisted nematic (TN) cell: a) polarizer, b) glass slide, c) transparent electrode, d) LC film and e) reflective tape.....11

1.6 The optical transmission of monochromatic light (λ = 633nm) as a function of voltage (a mixture of MBBA and EBBA, d = 12μm, T = 22^{o}C, field frequency = 60Hz).....14

1.7 Micrograph of an AC field alignment pattern for a positive nematic liquid crystal (n-pentyl-cyanobiphenyl, d = 12μm, T = 25^{o}C, field frequency = 60Hz).....19

1.8 Orientation pattern of nematic molecules in interdigital electrode device when the applied voltage is about 20% above threshold.....20

1.9 A molecular description of the wave-like deformation interface observed for several positive nematic LC's in AC fields: a) top view of cell, B, C, D and E denote planes of intersection, b) director profile in E plane, c) perspective view of cell and d) director profiles for planes B, C and D.....23

2.1 Geometry of a "thick"-electrode cell.....35

2.2 60 Hz AC deformation patterns for a "thick"-electrode cell with L = 2.2 mm and d = 12.4 microns.....38

2.3 Wavelength, wave-onset field, E_w, and threshold field, E_c, plotted versus reciprocal thickness.....42

2.4 Temperature dependence of wave structure for cells of two electrode geometries: □ - 14 micron, "thick"-electrode cell; △ - 12 micron, "thin"-electrode cell.....44

2.5 Square root of interface position versus electric field for a series of "thin"-electrode cells.....47

2.6 Interface position versus frequency for a cell with d = 14 microns, L = 1.98 mm and E = 700 V/cm.....48

3.1. Orientation of molecules and electric field of light ray for refractive indices, $n_{\parallel}$ and $n_{\perp}$.....57

3.2. Optical retardation as a function of normalized cell position.....60

3.3. Molecular orientation profile of a nematic layer neglecting boundary effects.....63

3.4. Molecular orientation profile of a nematic layer incorporating boundary effects.....66

3.5. Reduced voltage profile for a 12 micron layer at 900V/cm compared to theory.....68

4.1. Model phase diagram of a simple-eutectic mixture for two enantiotropic nematogens.....75

4.2. Phase diagram for K15 and S1236.....81

4.3. Schröder-van Laar theory versus experiment for K15/S1236 blend.....84

4.4. Phase diagram for K15 and S1188.....88

4.5. Phase diagram for K15 and S1115.....90

5.1. Dielectric constant of K15 as a function of temperature.....99

5.2. Dielectric constant of 60/40 mole percent mixture of K15/S1236 as a function of temperature.....100

5.3. Dielectric constant of 60/40 mole percent mixture of K15/S1188 as a function of temperature.....101

5.4. Dielectric constant of 60/40 mole percent mixture of K15/S1115 as a function of temperature.....102

5.5. Dielectric anisotropy of four nematic fluids plotted as a function of sub-clearing temperature.....104

5.6. Graphical description of response times: t_D, t_r and t_d.....107

5.7. Effect of voltage on the response times of a 67 micron layer of K15 at 20°C.....109

5.8. Effect of temperature on response times of K15. 112

5.9. Effect of layer thickness on the response times of K15 at 14°C.....113

5.10. Effect of average molecular length on the decay time of four nematic fluids.....115

5.11. Effect of dielectric anisotropy on the rise and delay times of four nematic fluids.....116

5.12. The three principle deformation modes of a nematic liquid crystal: a) splay. b) twist and c) bend.....118

5.13. Splay, K_{11}, and bend, K_{33}, elastic constants of K15 as compared with the literature.....121

5.14. Bend elastic constant versus sub-clearing temperature for four nematic fluids.....122

5.15. Splay elastic constant versus sub-clearing temperature for four nematic fluids.....123

5.16. Threshold voltage plotted against $(K_{11}/\Delta\varepsilon\varepsilon_o)^{-\frac{1}{2}}$ for four nematic fluids.....125

5.17. Threshold voltage versus sub-clearing temperature for four nematic fluids.....126

5.18. Dielectric anisotropy versus sub-clearing temperature for four nematic fluids.....127

6.1. Interface position vs electric field squared at 14°C.....133

6.2. Interface position vs electric field squared at (Tni-7)°C.....134

6.3. Slope of interface position vs. electric field squared curve plotted as a function of dielectric anisotropy.....135

6.4 Electrical deformation data for four nematic fluids at $(T_{NI}-7)^{o}C$.....137

A.1 Interference pattern for a 12 micron LC cell...142

CHAPTER 1

ELECTRO-OPTICS OF NEMATIC LIQUID CRYSTALS

Previous work has highlighted the importance of surfaces on the alignment of liquid crystalline materials[1-4]. Liquid crystals are also easily oriented by electrical fields. While investigating the strength of these effects on thin nematic layers, an interesting optical pattern was discovered. The pattern was observed in cross-polarized light and is characterized by a wave-like interface separating surface oriented and field oriented nematic. Searching the literature for similar work revealed only two related papers with little description of the wave pattern. Therefore, further work was undertaken to understand the physical and optical properties of this deformation.

1.1 Liquid Crystal Cell Construction

All LC optical display cells consist of a layered, sandwich-like construction. The most basic design has three layers: two glass plates separated by a liquid crystalline film. Depending on the desired display, more practical designs may include polarizing films and transparent electrode layers. A critical aspect of the display technology lies in the production of uniformly oriented LC

films. Since useful devices produce distinctive reflected or transmitted light patterns, a non-randomly oriented mesophase is required. Inherent to the science of LC electro-optics is a basic understanding and control of the surface alignment for the mesophase. Other engineering considerations include properly chosing the electrode geometry as well as an appropriate selection of the LC material.

Many different electro-optical effects have been reported in the literature[5] and each one has its own cell configuration. The optical effect demonstrated depends on the electrode geometry and the initial alignment of the NLC. To apply an electric field, three basic electrode geometries can be used. These are shown schematically in Figure 1.1. Conventionally, a longitudinal AC electric field is the most widely used. However, the electro-optical phenomenon of interest in this study is based upon a transverse electrode geometry and has an initial perpendicular molecular surface alignment of the NLC.

To discuss the surface alignment of a nematic LC, we must first introduce the concept of the director, **n**. The shape of a NLC molecule is typically elongated, ie. rod-like. The long axis of the rod is a useful reference axis and is called the nematic director (or director for short). On a molecular scale, the orientation of the director with respect to the plane of a substrate must fall into one of the three following cases: i) **n** is parallel to the plane,

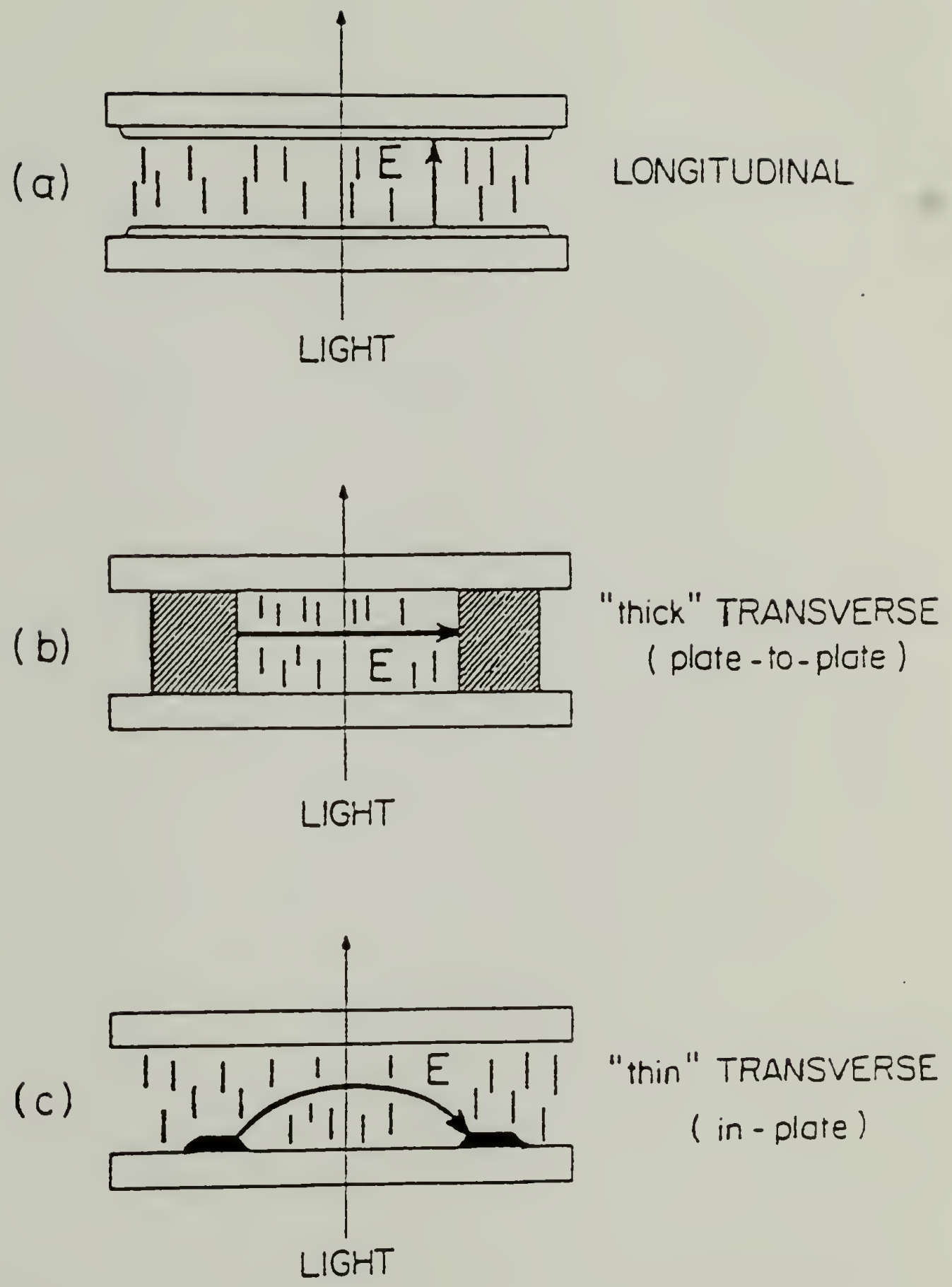

Figure 1.1 Three possible electrode structures for applying longitudinal or transverse electric fields to liquid crystal films.

ii) **n** is normal to the plane or iii) **n** forms an angle θ with the plane such that $0 < \theta < 90$. These three cases are shown schematically in Figure 1.2 and are given the names: a) homogeneous, b) homeotropic and c) tilted homeotropic surface alignment, respectively. Depending on the desired optical effect, several initial film orientations can be used. Some director configurations are shown in Figure 1.3.

1.2 Physical Properties of Nematic Liquid Crystals

1.2.1 Elastic Moduli

A proper treatment of the electro-optics of LC's requires an introductory word about the elastic properties of a mesomorphic medium. Liquid crystals exhibit elastic properties which can be described by the continuum theory proposed by Zocher[6] and Oseen[7]. Frank[8] presented this elastic theory in a more simple and comprehensive form.

The elastic continuum theory is based on the assumption that at each point within the liquid crystal a preferential direction for the molecular orientation is given which is described by a unit vector **n**, and which varies continuously from place to place - except for a few single points or lines. Any distortion of the undisturbed state requires a certain amount of energy, since elastic torques attempt to maintain the original configuration. The elastic energy density of a deformed nematic liquid crystal is given by

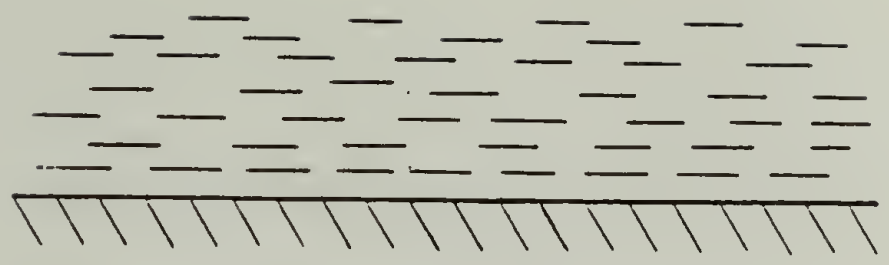

a) Homogeneous

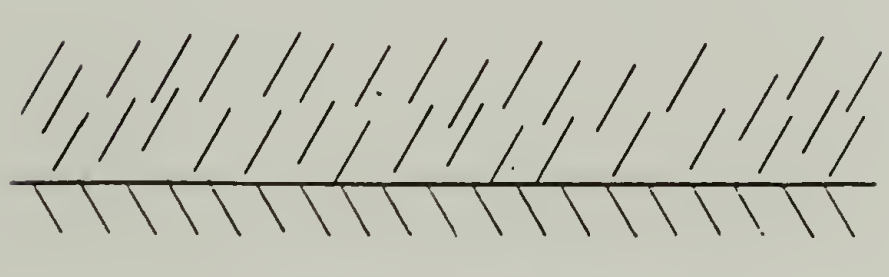

b) Tilted Homeotropic

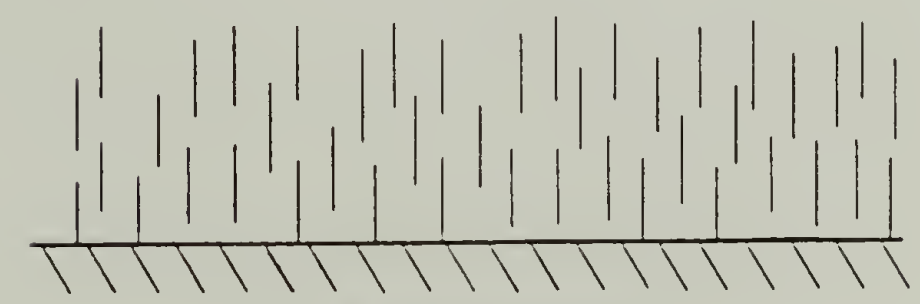

c) Homeptropic

Figure 1.2 Three cases of nematic liquid crystal alignment: a) homogeneous, b) tilted homeotropic and c) homeotropic alignment.

(a)

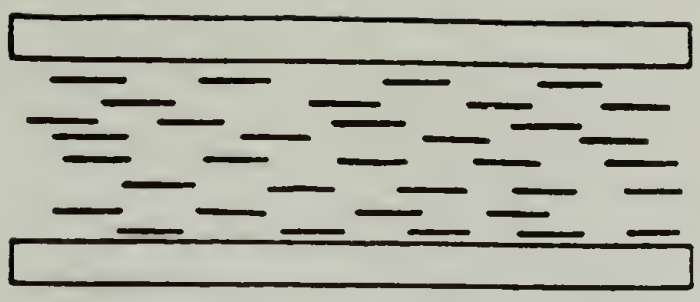

PARALLEL (homogenous)

(b)

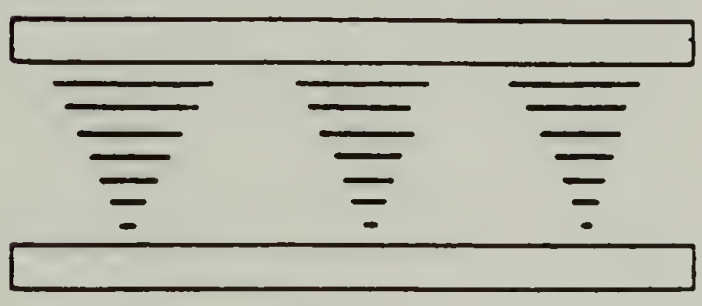

TWISTED PARALLEL

(c)

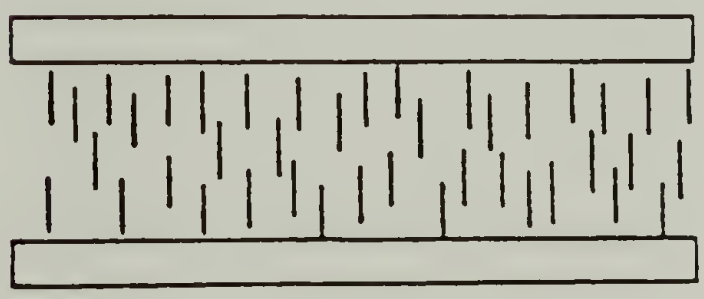

PERPENDICULAR
(homeotropic)

(d)

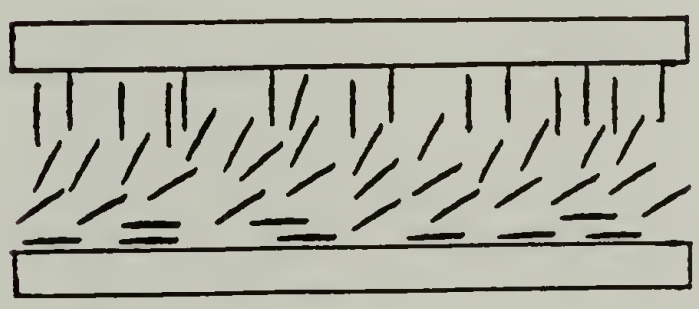

SPLAY NEMATIC

Figure 1.3 Four possible orderings of thin nematic films at E = 0. Side view of parallel-plate device is shown.

$$F = 1/2\ K_{11}(\text{div } \mathbf{n})^2 + K_{22}(\mathbf{n} \text{ curl } \mathbf{n})^2 + K_{33}(\mathbf{n} \times \text{curl } \mathbf{n})^2 \qquad (1.1)$$

where K_{11}, K_{22} and K_{33} are the elastic curvature constants of splay, twist and bend respectively. The elastic constants are of the order 10^{-5} to 10^{-6} dynes. The three fundamental deformations of a nematic liquid crystal are schematically represented in Figure 1.4.

1.2.2 Optical Properties

The domains of nematic liquid crystals (NLC's) are optically uniaxial. Visual effects of these materials can be most striking because of their relatively large optical anisotropy, $n = n_{11} - n_{\perp}$, i.e. the difference in the refractive index parallel and perpendicular to the optical axis of the molecule. The optical anisotropy for oriented polyolefins is typically in the range: $0.001 < \Delta n < .010$. For nematics, Δn occasionally exceeds 0.2! Liquid crystals have found a captive display market because of this feature in conjunction with other properties.

1.2.3 Dielectric Properties

The dielectric anisotropy ,$\Delta\epsilon$, is the difference between the parallel and perpendicular electric permitivity of the NLC as measured with respect to the director axis. The more positive the value of $\Delta\epsilon$, the easier the NLC can be reoriented with **n** parallel to the applied field, while the

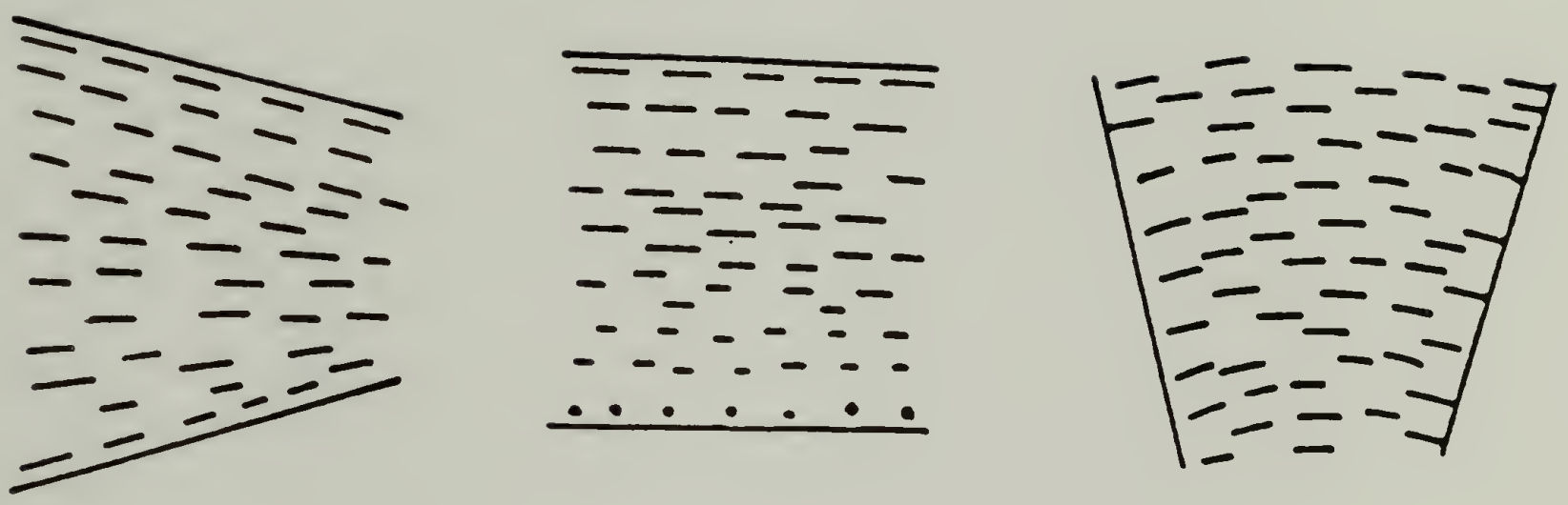

Figure 1.4 The basic deformations of a nematic liquid crystal: a) splay, b) twist and c) bend.

more negative the value of $\Delta\epsilon$ the easier the NLC can be reoriented with **n** perpendicular to the applied field. LC's for display applications can have positive and negative dielectric anisotropies with a magnitude ranging between 5 and 20. A material with $\Delta\epsilon = 0$ has no preferred alignment direction under the influence of an applied field and, thus, is not useful by itself for display devices. However, it is quite often the practice to blend several components together in order to obtain a broader mesomorphic range and enhance certain desirable properties. Although there are scientific bases for preparing these mixtures, the art of mixtures is more empirical than a fundamental science.

1.3 Electro-optics

1.3.1 Theory

The theory of electric alignment and the concurrent birefringence calculation[9,10] have been constructed by analogy with the treatment for the deformation of a NLC by a magnetic field[11]. In the case of electric "deformation" the anisotropy of the dielectric constant is no longer small in comparison with the average dielectric constant, as happens with the magnetic anisotropy in the case of magnetic deformation. The system of calculation follows.

First, one writes the expression for the free energy of the liquid crystal, F, as a function of the orientation of

the director axis, **n**, and the electric field, E, (in the CGSE system):

$$F = 1/2 \left[K_{11}(\text{div } \mathbf{n})^2 + K_{22}(\mathbf{n} \text{ curl } \mathbf{n})^2 + K_{33}(\mathbf{n} \times \text{curl } \mathbf{n})^2 - \frac{\Delta\varepsilon}{4\pi} E(\mathbf{n})^2 \right] dv \qquad (1.2)$$

Here, $\Delta\epsilon = \epsilon_{\parallel} - \epsilon_{\perp}$, while the meaning of the elastic constants, K_{ii}, have been discussed above.

Second, one solves Euler's equation corresponding to the functional, F, taking the boundary conditions into account. (The boundary conditions mathematically describe the initial orientation of the NLC at the enclosing surfaces (discussed above)). Thereby obtained is a steady-state solution that relates the director orientation angle, θ, to the coordinate along the z-axis (see Figure 1.5) and to the external field.

It can be shown that the process of reorientation of the liquid crystal shows threshold behavior. Reorientation does not begin until the critical voltage, V_c, is reached, which is given by

$$V_c = \sqrt{K_{ii}/\epsilon_o \Delta\epsilon} \qquad (1.3)$$

Here $K_{ii}=K_{11}$ for a splay deformation , $K_{ii}=K_{33}$ for a bend deformation and $K_{ii}=K_{11}+1/4(K_{33}-2K_{22})$ for a TN cell (see Figure 1.4). This equation shows that the Freederickz's transition (the onset of electrical reorientation) is not dependent on the thickness of the nematic layer. Physically,

a) Cell Geometry

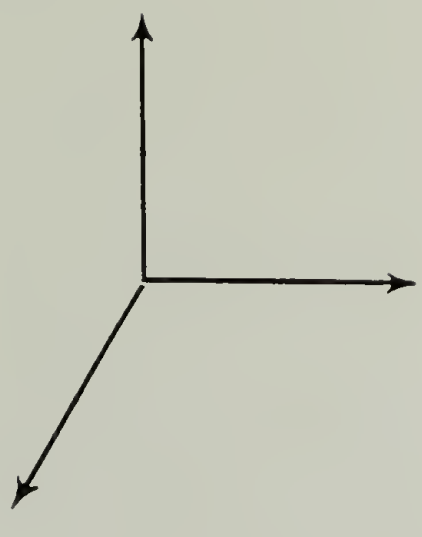

b) Side View

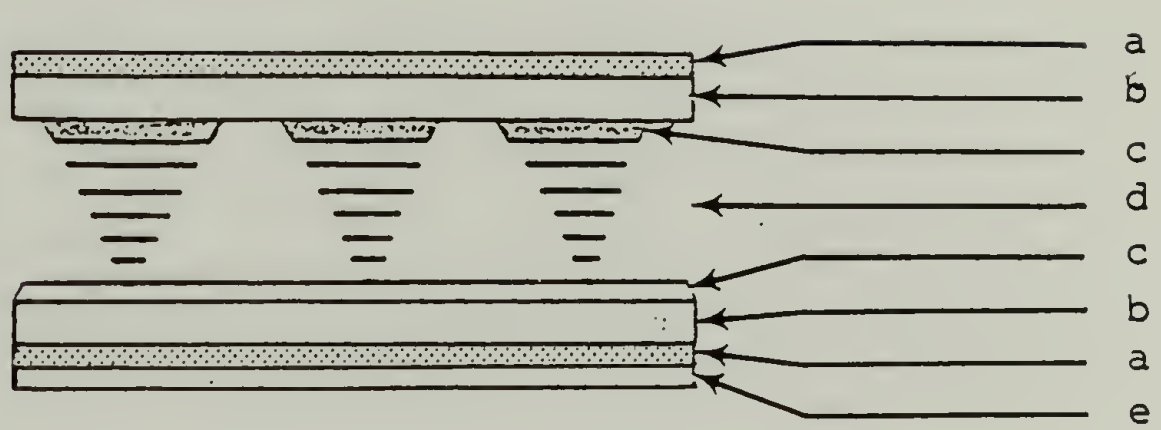

c) Perspective View

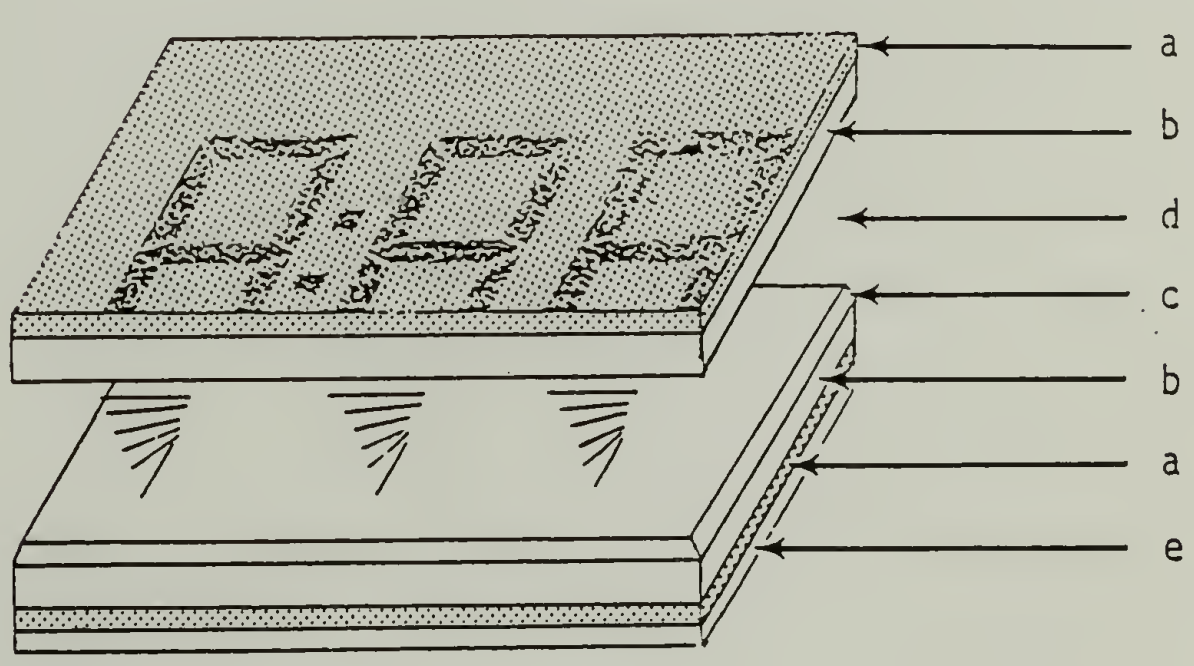

Figure 1.5 Cell construction of a twisted nematic (TN) cell: a) polarizer, b) glass slide, c) transparent electrode, d) LC film and e) reflective tape.

this is because in a thicker layer, for a given deviation θ_m of the director at the center, the deformation is of a longer wavelength and so requires a lower field strength to overcome the elastic forces. Thus, when the electrostatic energy density to be gained by reorientation matches the energy required for the "smoothest" of all possible deformation profiles given the initial boundary conditions, we have reached the threshold voltage.

The solution of Equation 1.2 yields an expression for the orientation angle of the optic axis $\theta(z)$ as a function of the position. Using this "deformation profile," one can find the distribution of the refractive indices across the cell from

$$n(z) = n_{\parallel} n_{\perp} / \left(n_{\perp}^2 \cos^2\theta(z) + n_{\parallel}^2 \sin^2\theta(z) \right)^{1/2}. \quad (1.4)$$

This expression allows calculations of the phase difference, $\Phi(E)$, between the "ordinary" ray and "extraordinary" rays at the exit face of the cell. The phase difference depends implicitly on the field intensity, E, through the expression for the refractive index, i.e.

$$\Phi(E) = \frac{2\pi}{\lambda} \int_0^d n(z)dz = 2\pi \frac{\overline{\Delta n(E)}}{\lambda} . \quad (1.5)$$

The intensity, I, of the light transmitted through the cell and analyzer is controlled by the degree of phase retardation according to

$$I = I_o \sin^2 2\beta \sin^2 (I/2) \quad . \qquad (1.6)$$

Here I_o is the intensity of the linearly polarized light incident on the cell, and β is the angle between the polarization vector of the incident ray and the optic axis of the NLC. The light intensity at the output of the analyzer oscillates depending on the voltage of the steady-state electric field (AC or DC) as might be expected (see Figure 1.6). This can be understood through Equation 1.6 and the coupling between the phase retardation and the applied field discussed above. The maximum amplitude of the oscillations is at $\beta = 45^o$. Several authors[9,10,12,13] have invoked the use of computers and numerical methods to calculate the parameters that enter into the culmination of the electro-optical theory given in Equation 1.6. Maze and Johnson[14] have found good fits of experiment to theory involving seven material parameters.

In summary, the construction and analysis of a LC cell in an electric field is an involved problem. To have a useful effect, one must consider and chose an appropriate LC system based on its dielectric and optical properties. Also, an initial molecular ordering and electrode geometry must be chosen. These decisions will determine when and if the original alignment can be overcome by the applied field. At voltages below threshold, the surface controlled-ordering will persist. Above the threshold, a new alignment will be stable with a characteristic, field and thickness dependent,

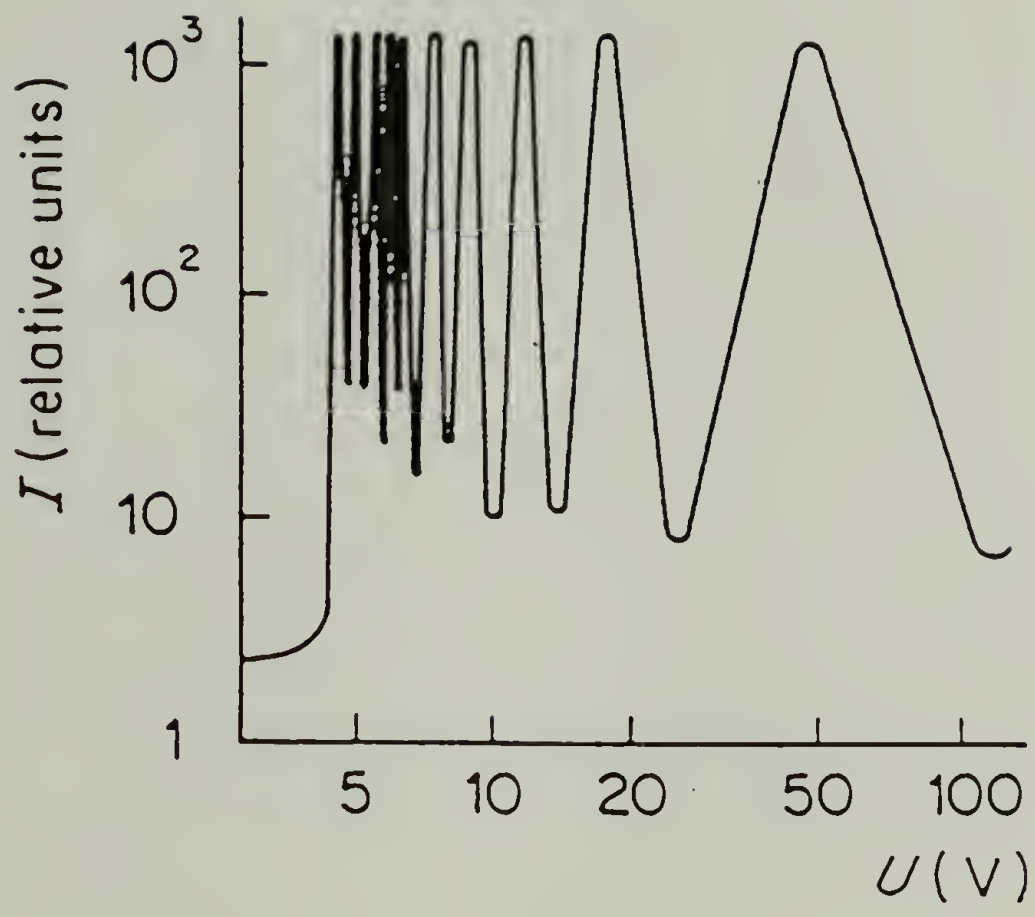

Figure 1.6 The optical transmission of monochromatic light (λ= 633 nm) as a function of voltage (a mixture of MBBA and EBBA, d = 12μm, T = 22°C, field frequency = 60 Hz).

deformation profile. Thus, the field modifies the optical birefringence, Δn, ie. the optical activity of the nematic film. This large scale change in optical properties is the basis for the utility of commercial display devices.

1.3.2 A Commercial Display

The most common, 99%, commercial display is of the twisted nematic (TN) variety[15]. The abbreviation TN denotes a particular cell design and hence a specific electro-optical phenomenon. LC cells consist of two transparent plates which induce a uniform parallel (homogeneous) alignment of the NLC and are separated by a thin film of the NLC. The plates, however, are oriented with respect to one another in such a manner that the director of the LC rotates through some angle θ in travelling from the top to the bottom substrate (see Figure 1.5). The preferred value of θ for the commercial devices is 90^{o}. Thus, the LC director rotates 1/4 of a turn across the thickness of the film. Typical film thicknesses are between 10 and 30 microns (1 μm = 10^{-6} meters). Transparent electrodes of tin oxide, SnO_2, or indium oxide, In_2O_3, are in direct contact with the liquid crystal. It is through these electrodes that the realigning electric field is applied.

1.3.3 A Research Example

Electrical fields applied perpendicular to the direction of light propagation are defined as transverse

electrical fields (Figure 1.1b and c), while electrical fields applied parallel to the direction of light propagation are known as longitudinal electrical fields (see Figure 1.1a). The use of transparent electrodes to establish a longitudinal field is the most common commercial arrangement. There is considerable literature on longitudinal field effects.

In contrast, literature discussing the use of transverse fields is limited both in number and scope. A computer search of Science Citations over the last seventeen years (1969-1986) uncovered only 13 papers related to this subject. The search listed all publications appearing from the intersection of "liquid crystals" and "transverse electric fields" used as key words or phrases. In contrast there are over 18,000 publications cited over the same time period found for the keyword "liquid crystal" alone.

1.3.4 Tranverse Electric Fields

1.3.4.1 History

The first observation of strong scattering by an LC in an electric field was made by Freederickzs and Tsvetkov[16]. They found that if the critical voltage V_c, is exceeded by 10-20 volts, the flow becomes turbulent and the LC becomes optically non-uniform, scattering light in all directions. Kapustin and Larinova[17] were next, 28 years later. In their brief communication, surface alignment was not mentioned.

Excitement in 1968 at RCA laboratories over alternative display technologies was stimulated by a rediscovery of dynamic scattering[18] and the economic potential of LC substances in low power-consumption displays. This led to further LC research including some using transverse electrode geometries[19-20]. Apparently, the lack of optical uniformity and the emergence of the more promising TN technology led to the rapid decline of research devoted to transverse-electrode LC cells. The one further work found was the research of Soref[21-24] carried out at Sperry Rand. He was the first to investigate the electro-optic effects of positive nematic materials ($\Delta\epsilon > 0$) in transverse fields. His study was to design a useful display device using the thin-electrode design of Figure 1.1c. He chose small plate spacings ($d < 10\mu m$) and narrow electrode separations ($9 < L < 30\mu m$). The results of this work were compiled in a twenty-six page company report[25].

1.3.4.2 Preliminary Work

Transverse electric-field cells of the thin-electrode geometry (Figure 1.1c) were constructed at Umass by sputtering gold films on previously treated and masked glass slides. LC films of the nematic compounds n-pentylcyano-biphenyl and n-pentoxycyanobiphenyl were used. LC film thickness was varied from 4 to 80 μm using polyimide spacers. The initial homeotropic alignment of these LC's was

generated by treating the glass microscope slide and coverslip with dichlorodimethylsilane.

Reorientation by DC fields from 0-1500 volts demonstrated threshold behavior and a time dependent interface position. The surface aligned LC appears dark in cross polarized light. The electrically realigned regions of the cell show birefringent interference colors. The degree of reorientation, indicated by the Newton interference colors, is highest at the electrode boundaries and decreases toward the deformation interface. Deformation always occurs at the cathode in DC fields.

Reorientation by AC fields from 0-300 volts at 60 Hz demonstrated threshold behavior and stable interface positions. The deformation interface between the initial homeotropic alignment and the electrically realigned LC occurs simultaneously at both electrodes and exhibits a distinct sawtooth (or sinusoidal) appearance (see Figure 1.7). Soref has noted similar patterns in his work. As mentioned previously, Soref studied only nematic LC mixtures having a positive dielectric anisotropy. The explanation he offers to account for such a curious pattern is shown schematically in Figure 1.8. In words:

> "Groups of molecules tilting to the left and to the right in Figure 1.8 join each other in a homeotropic boundary region midway in the gap. As the voltage goes up, the tilt angles increase towards 90^{o} at mid-gap and the width of the homeotropic interface shrinks. The interface layer vanishes at high voltages[25]".

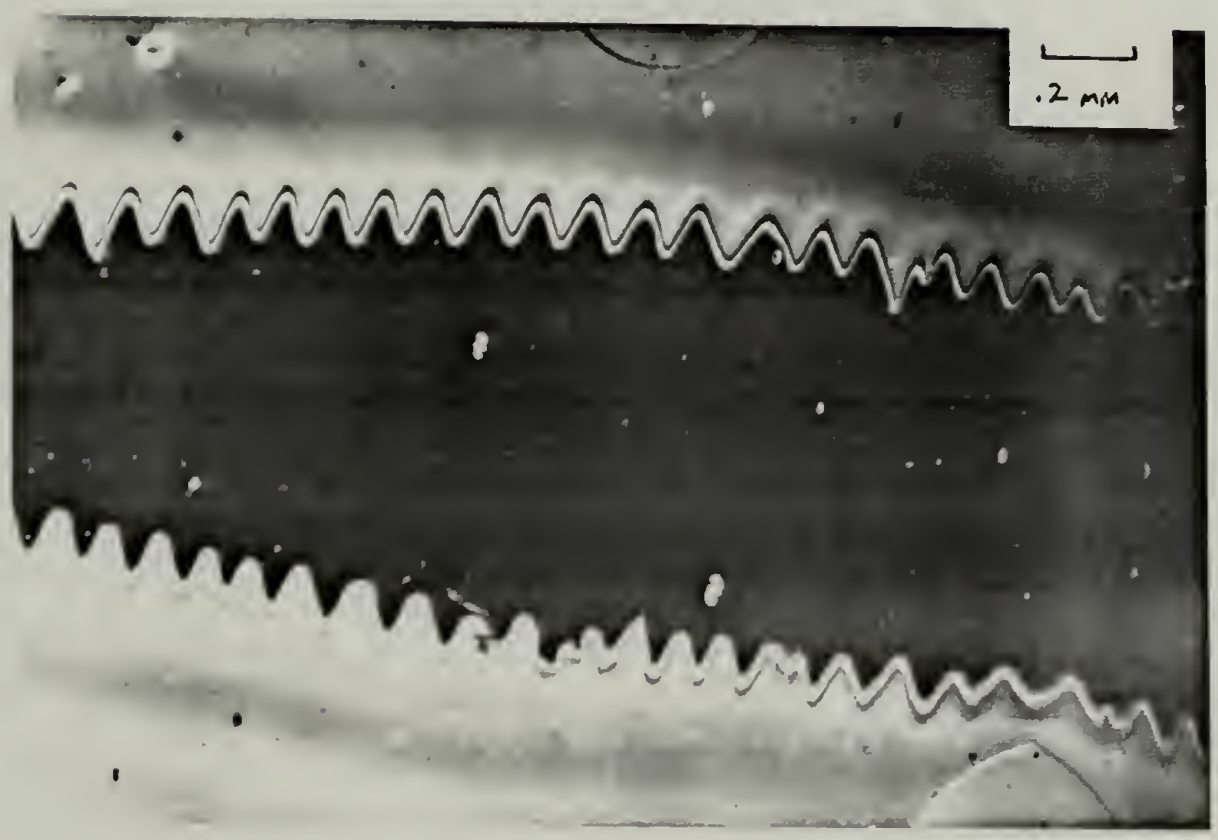

Figure 1.7 Micrograph of an AC field alignment pattern for a positive nematic liquid crystal (n-pentylcyanobiphenyl, d = 12μm, T = 25^{o}C, field frequency = 60Hz).

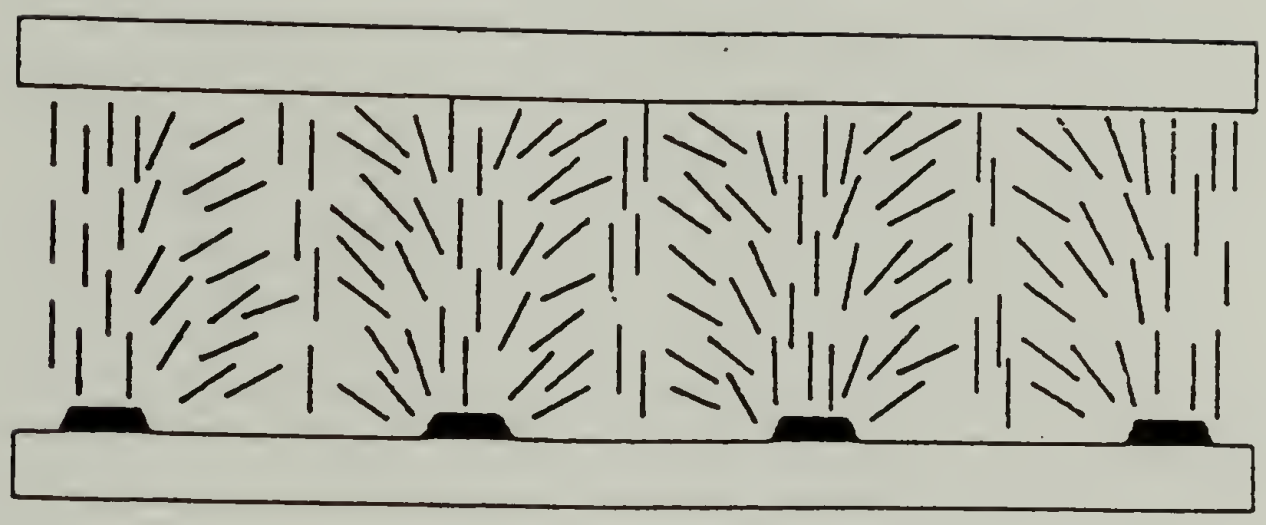

Figure 1.8 Orientation pattern of nematic molecules in interdigital electrode device when the applied voltage is about 20% above threshold. Side view of device is shown.

This explanation is unsatisfying. If the nematic director profile in Figure 1.8 is accurate, one would expect to see a somewhat different optical pattern. From Figure 1.8, the director is shown with the greatest distortion away from perpendicularity near the center of an electrode gap. As one approaches either electrode from the central region, the director gradually becomes less and less distorted, i.e. more nearly homeotropic. This would result in high optical phase differences at the center of the electrode gap and gradually decreasing phase differences moving towards the electrodes. Consequently, this would produce a series of Newton interference colors in a sequence exactly opposite to the one observed experimentally.

1.3.4.3 Research Objectives

We would like to investigate and understand the physical basis which accounts for the optical pattern observed in Figure 1.7. What is the director profile and what causes the wave-like interface? We would also like to observe what effect adding blending a second liquid crystalline material has on the electro-optical pattern, if any. It is possible that a thorough analysis of the deformation interface may yield a technique for measuring all three elastic constants simultaneously.

1.3.4.4 Current Speculation

A material property believed to be of fundamental importance is the ratio of the splay and twist elastic constants, K_{11}/K_{22}. If this ratio is unity, one might predict the deformation interface to be linear; whereas, when this ratio is large, one might expect the deformation interface to support larger amplitude teeth. This speculation can be rationalized with the aid of Figure 1.9.

We postulate a director profile resembling the contour commonly shown for a Freederickz's transition for three different planes which cut the cell normal to the y-axis. These three planes intersect the wave interface at three distinct points: the "trough", the point of maximum slope and the "crest" of the sinusoidal curve. We assume that the director profiles for all three cuts are the same with the exception of the distance, x, which indicates the horizontal position away from the electrode, where the first "column" of nematic molecules is perfectly homeotropic. The value of x will increase from its minimum value for the plane cutting a "trough", to a maximum for the plane cutting a "crest". A plane slicing a point of maximum slope will have an intermediate value of x.

Neglecting edge effects, planes B and D (see Figure 1.9c) are planes of symmetry. Any distortion in a plane parallel to plane B or D, but offset some arbitrary value +y in the y-direction is mirrored in a plane offset -y in the

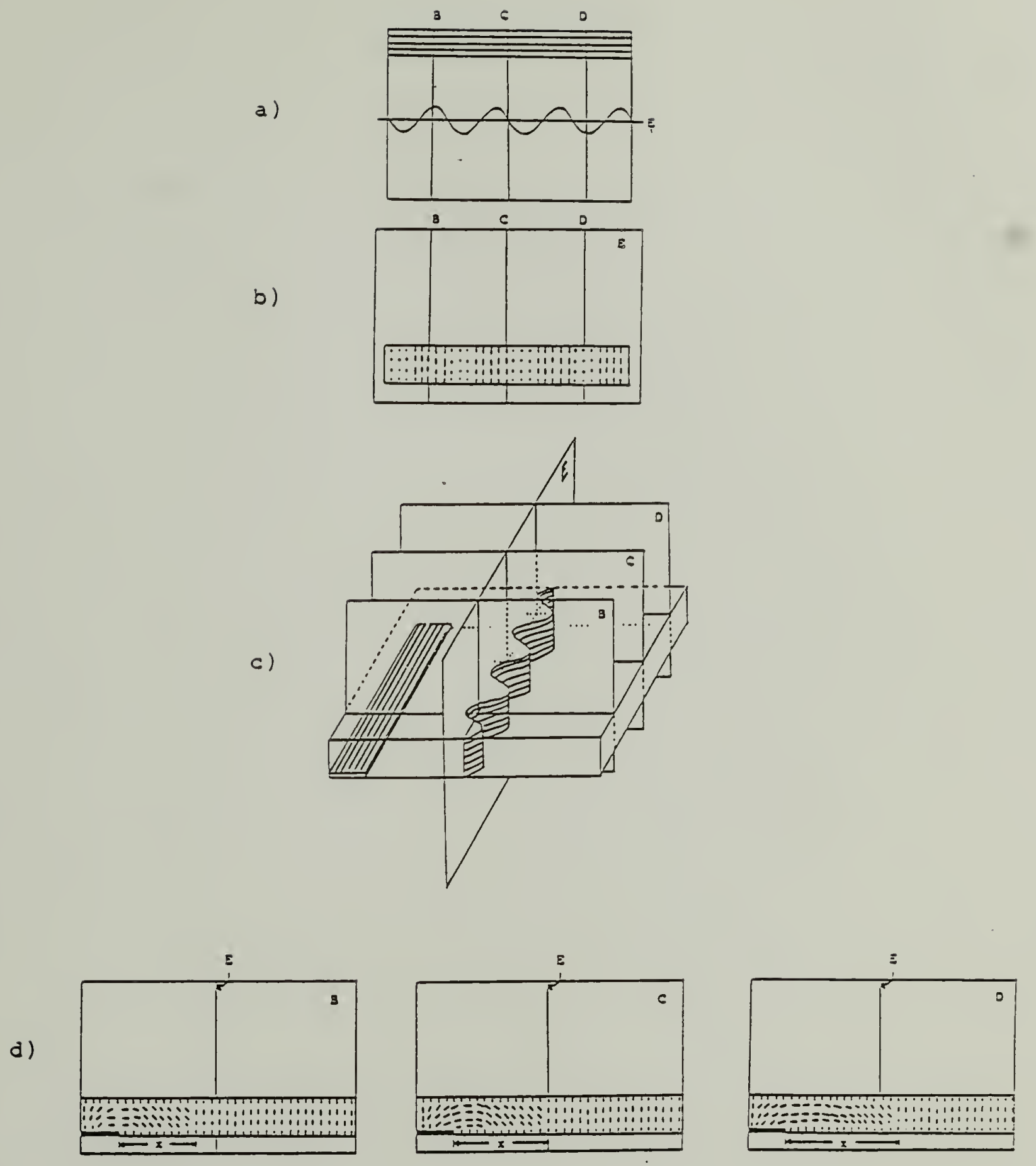

Figure 1.9 A molecular description of the wave-like deformation interface observed for several positive nematic LC's in AC fields: a) top view of cell, B, C, D and E denote planes of intersection, b) director profile in E plane, c) prespective view of cell and d) director profiles for planes B, C, and D.

y-direction. Thus, no net torque can be imposed on the molecules lying in the "trough" and "crest" planes.

A torque can be imposed on molecules lying within any other plane normal to the y-axis but different from planes B and D. By plane C, we denote the plane which lies midway between planes B and D and cuts the deformation interface at a point of maximum slope. Molecules lying within this plane are subject to the greatest torsional deformation arising from the ordering of molecules in adjacent planes.

Plane C is a plane of assymetry. The molecular ordering pattern in a neighboring plane an arbitrary distance +y from plane C is not identical to the molecular ordering pattern in a plane -y units away from plane C. Thus, large torsional forces can be exerted on the molecules in this plane from reoriented molecules in neighboring planes.

A hypothetical director configuration showing the twist deformation which can arise by the above mentioned speculation is shown in Figure 1.9b. In this schematic, we have sliced the cell normal to the x-axis and half-way between the "troughs" and "crests" of the wave contour.

1.4 Scope

The goal of this work is to determine the effect of the elastic constants (K_{ii}), film thickness, electrode separation, temperature, and the AC voltage and frequency on the wavelength and amplitude of the deformation interface. Preliminary work varying these parameters indicates their

significance to a complete understanding of the electro-optical phenomenon.

This study will be limited to positive nematic LC's ($\Delta\epsilon > 0$) because of the wide availability of compositions with this specification. Also, chosing this condition, defines an initial director configuration which can be easily obtained and identified for reference purposes (see Figure 1.3c). (The homeotropic alignment of a thin NLC film appears dark between crossed-polars and shows a readily identifiable cross-shaped interference pattern).

Various techniques for controlling surface alignment may be used. The desired "spontaneous" initial alignment is homeotropic. Preliminary work with dichlorodimethylsilane as a surface coupling agent has been successful in generating reproducible perpendicular orientation. Other possible techniques for generating homeotropic alignment include other silane coupling reagents, chromic acid cleaning[2], and surfactant additives[26].

Nine liquid crystal mixtures have been selected for study from a field of eighteen binary mixtures belonging to twelve chemical structures and markedly different LC classes. The composition and chemical structure of these nine LC's are shown in Table 1.1. Six compositions are mixtures within a single chemical class while three others are blends of two different chemical classes. The blending of LC's within the homologous series of a single chemical composition provides a broader mesomorphic temperature

Table 1.1 Nomenclature, composition and chemical structure of nine LC mixtures.

Material	Composition	Molar Ratio	Chemical Structure
E	(E5,E7)	(40,60)	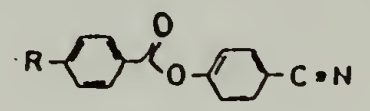
K	(K15,K21)	(40,60)	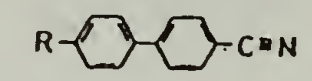
P	($P_3$5,$P_3$7)	(40,60)	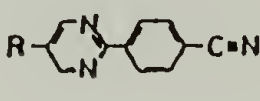
P_{pdo}	(5PDO3,$P_3$7)	(40,60)	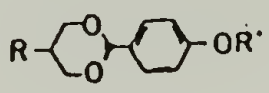
P_{82}	($P_3$7,5EH_2O3)	(80,20)	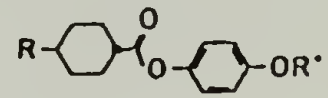
P_{64}	($P_3$7,5EH_2O3)	(60,40)	
PD	(PD5,7)	(40,60)	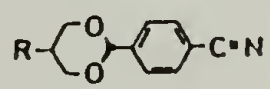
S	(S5,S7)	(40,60)	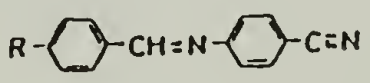
PE	(PCHE5,7)	(40,60)	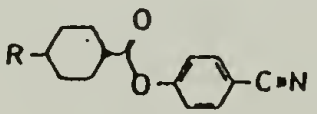

range. With the exception of material "K", the unsubscripted numbers in the composition column of Table 1.1 designate the number of carbon atoms in the alkyl group of the chemical structure.

The nine LC's of Table 1.1 are regrouped in Tables 1.2 and 1.3 according to their physical properties reported by Schadt and Gerber[27]. The four LC's listed in Table 1.2 span the entire range of K_{11}/K_{33} values ($0.7 < K_{11}/K_{33} < 1.70$) given by their comprehensive study. Table 1.3 shows mixtures spanning as large a range of K_{11}/K_{22} as possible, while holding other important material properties nearly constant. The elastic constants for these compounds have been previously reported[27].

The plate spacing, d, and electrode separation, L, will be extended beyond the values used by Soref[21]. Values of d up to 100 μm will be used. (Increasing the plate spacing, and hence the film thickness, much beyond this results in a decay of the homeotropic alignment).

1.5 Compositions and Equipment

Liquid crystal compositions might be chosen from the nine binary mixtures shown in Table 1.1. These mixtures can be divided into two groups. The first four form a series of compositions ranging in the material constant K_{33}/K_{11} from 0.76 to 1.67 (see Table 1.2). The remaining five have been chosen to determine the effect of the material constant ratio K_{22}/K_{11} (see Table 1.3).

Table 1.2 Measurements of the elastic, dielectric and optical material properties made at constant temperature (T_{NI}-10°C).

Material	K_{33}/K_{11}	K_{22}/K_{11}	$\Delta\epsilon/\epsilon_{\perp}$	Δn
E	1.67	0.60	2.263	0.149
K	1.34	0.54	1.939	0.177
P	1.16	0.55	2.263	0.183
P_{pdo}	0.76	0.52	2.032	0.130

Table 1.3 Measurements of the elastic, dielectric and optical material properties made at constant temperature (T_{NI}-10°C).

Material	K_{22}/K_{11}	K_{33}/K_{11}	$\Delta\epsilon/\epsilon_{\perp}$	Δn
P_{82}	0.55	0.92	1.907	0.133
P_{64}	0.47	0.90	1.591	0.119
PD	0.64	1.43	1.495	0.089
PE	0.57	1.55	1.032	0.086
S	0.51	1.39	1.750	0.204

Most optical measurements will be made on a Vickers optical microscope at low power (30-100X) in cross polarized light. Precise temperature control is imperative since refractive indices and elastic constants are temperature sensitive. Temperature can be adequately regulated by an Omega Model 921 PID temperature controller. Film thicknesses will be controlled by polyimide spacers and measured interferometrically using a Perkin-Elmer UV-Vis spectrophotometer (see Appendix 1).

1.6 References

1. F. Kahn, G.N. Taylor and H. Schonhorn, Proc. IEEE **61**, 823 (1973).

2. L.T. Creagh and A.R. Kmetz, Mol. Cryst. Liq. Cryst. **24**, 59 (1974).

3. J.C. Dubois, M. Gazard and A. Zann, J. Appl. Phys. **47**, 1270 (1976).

4. T. Uchida, M. Ohgawara and Y. Shibata, Mol. Cryst. Liq. Cryst. **98**, 149 (1983).

5. M.F. Schiekel and K. Fahrenschon, Appl. Phys. Lett. **19**, 391 (1971).

6. H. Zocher, Z. Phisik **28**, 790 (1927).

7. C.W. Oseen, Arkiv Matematik Astron. Fysik **A19**, 1 (1925), Fortschr. Chem. Physik u. Physik Chem. **20**, 1 (1929), Trans. Faraday Soc. **29**, 883 (1933).

8. F.C. Frank, Disc. Faraday Soc. **25**, 19 (1958).

9. H. Gruler, T.J. Scheffer and G. Meier, Z. Naturforsch. **27A**, 966 (1972).

10. H.J. Dueling, Mol. Cryst. Liq. Cryst. **19**, 123 (1972).

11. A. Saupe, Z. Naturforsch. **15a**, 815 (1960); P. Pincus, J. Appl. Phys. **41**, 974 (1970).

12. P.D Berezin, I.N. Kompanets, V.V. Nikitin, and S.A. Pikin, Zh. Esp. Teor. Fiz. **64**, 599 (1972) [Sov. Phys. JETP **37**, 305 (1973)].

13. E. Jakeman and E.P. Raynes, Phys. Lett. **A39**, 69 (1972). Orsay Liquid Crystal Group, J. Chem. Phys. **54**, 816 (1969).

14. C. Maze and D. Johnson, Mol. Cryst. Liq. Cryst. **33**, 213 (1976).

15. B. Bihrandar, Mol. Cryst. Liq. Cryst. **99**, 345 (1983).

16. V. Freederickz and I.V. Tsvetkov, Dokl. Akad. Nauk. SSSR **4**, 123 (1935).

17. A. P. Kapustin and L.S. Larinova, Kristallogr. **9**, 297 (1974).

18. G.H. Heilmeier and L.A. Zanoni, Appl. Phys. Lett. **13**, 91 (1968).

19. R. Williams, J.Chem. Phys. **56**, 147 (1971).

20. L.K. Vistin and V.M. Ivanov, 1st Scientific Conference on Liquid Crystals, Ivanovo Pedagogical Institute, Ivanovo (1970).

21. R.A. Soref, Appl. Phys. Lett. **22**, 165 (1972).

22. R.A. Soref, S.I.D. Symposium, New York, 1973.

23. R.A. Soref, J. Appl. Phys. **45**, 5466 (1974).

24. R.A. Soref, Proc. IEEE **62**, 1710 (1974).

25. R.A Soref, Sperry Rand Research Report SRRC-RR-73-1, (1973).

26. I. Haller, Appl. Phys. Lett. **24**, 349 (1974).

27. M. Schadt and P.R. Gerber, Z. Naturforsch. **37a**, 165 (1982).

CHAPTER 2

WAVE STRUCTURES IN A NEMATIC LAYER: 4-4′-N-PENTYLCYANOBIPHENYL (K15)

Mono-domains of nematic liquid crystals are readily deformed by electrical fields. The study of these deformations and resultant structures by optical methods fall within the field of electro-optics. In the past 20 years, many interesting effects, including dynamic scattering[1-2] and dielectric reorientation[3-5] phenomena, have been reported.

In this chapter we report an interesting and reproducible wave structure found in electro-optical cells using a transverse-field geometry. Although this geometry (in which the electric field is produced by an in-plane electrode structure) has been used by previous researchers[6-8], a detailed study of this is structure is missing from the literature. The remarkable wave pattern studied here occurs at the interface between electrically and surface aligned molecules of a thin nematic layer. Establishing the stable wavelike interface depends on the conditions of field strength, frequency, temperature and layer thickness. Thus, we have undertaken a fundamental study of these conditions and explain the wave structure as a dielectric orientation pattern.

2.1 Experimental

The compound, 4-4'-n-pentylcyanobiphenyl (K15), was chosen for study because of its large dielectric anisotropy ($\Delta\epsilon \approx 9$) and nematic state at ambient temperature. These features facilitate dielectric reorientation of the molecules parallel to an applied field due to the highly polar cyano end group. This compound, as supplied by Merck, has a bulk ionic conductivity ($\sigma = 0.6 \times 10^{-10}$ nS/cm) and was used without further purification.

The nematic range for the commercial material as measured by DSC is given below:

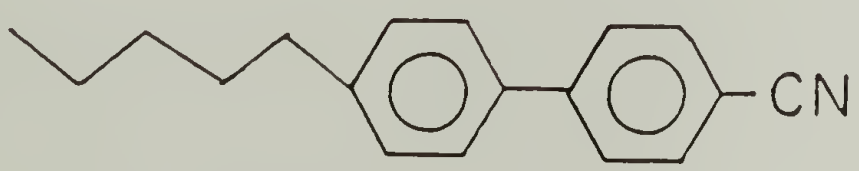

22.3°C 35.1°C

solid <----> nematic <----> isotropic

T_{KN} T_{NI}

The cell geometry for our transverse-field observation is shown in Figure 2.1. The cell consists of a nematic liquid crystalline layer sandwiched between two glass plates. The glass plates were chemically cleaned and treated with dichlorodimethyl silane to produce spontaneous, homeotropic alignment of the nematic molecules perpendicular to the glass. The plate separation, d, was varied from 2.5 to 42 microns and measured interferometrically. An electric field is applied across the nematic layer by means of two

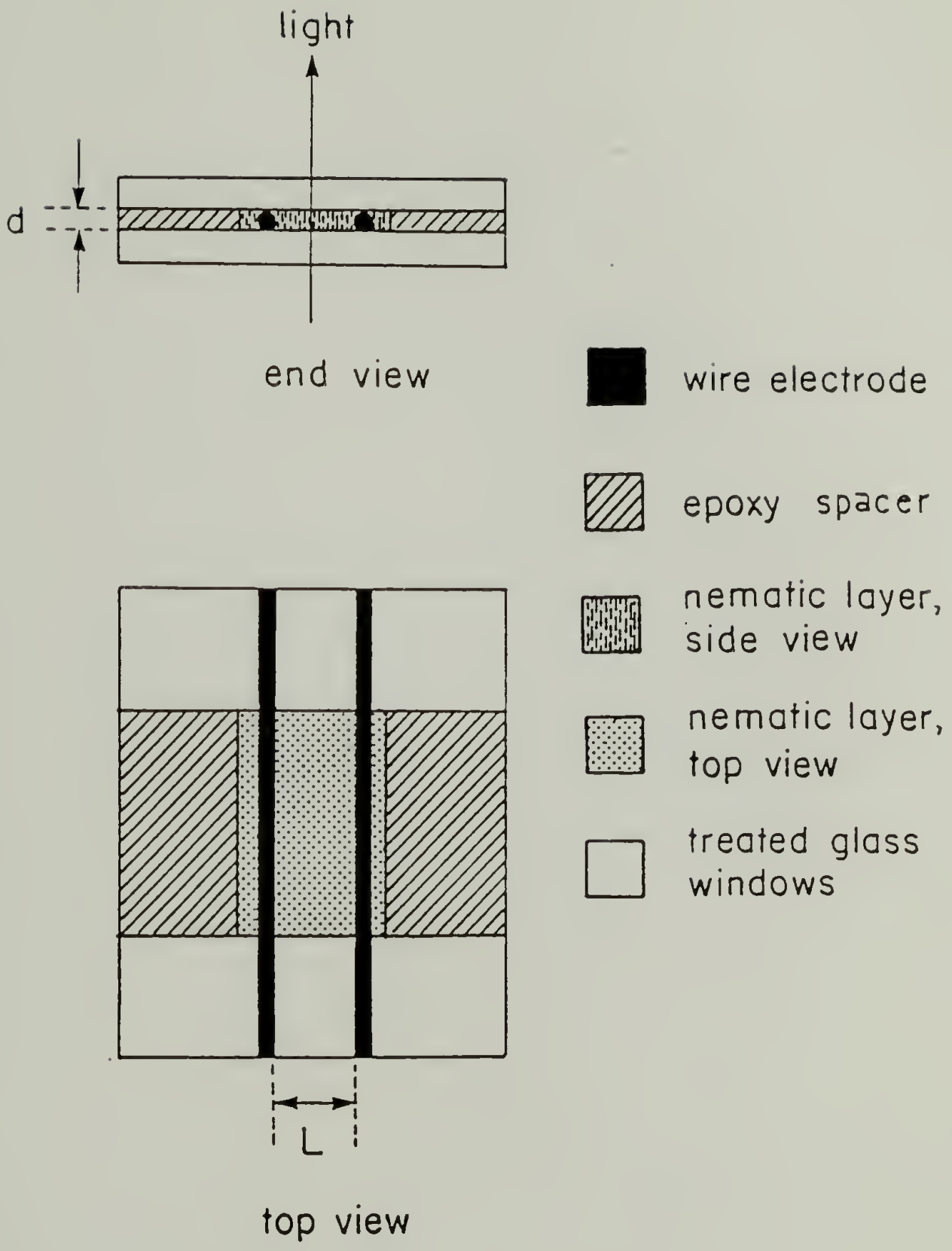

Figure 2.1 Geometry of a "thick"-electrode cell.

electrodes. The electrodes may be as thick as d ("thick"-electrodes) or much thinner ("thin"-electrodes). The "thick"-electrode construction uses fine diameter wire as the electrodes; whereas, the "thin"-electrode construction uses thin films (about 1 micron) of conducting indium oxide. The electrode separation, L, was varied between 1 and 4 mm. Because the field is perpendicular to the direction of light through the cell (see Figure 2.1), the assembly is called a transverse-field cell[8].

Optical observations of the field-induced deformation structures were made using a Zeiss polarizing microscope at low magnification (typically 30X).

2.2 Influence of DC Fields

Without field, the nematic between the two electrodes appears black in cross-polarized light. This condition remains when the sample stage is rotated through 360^{o}. When conoscopic light is used, the interference pattern shows an optically-centered cross. This indicates the molecules are perpendicular to the glass surface.

As the electric field is increased above a critical value, E_c, deformation occurs at the cathode. This deformation is recognized by an increase in the birefringence at this electrode. Because there is a small amount of birefringence at the metal electrode even at zero voltage, determining E_c precisely is sometimes difficult.

As the field is increased further, additional nematic in the vicinity of the cathode becomes birefringent. A sharp interface separates the surface oriented nematic from the electrically oriented nematic. The interface is nearly parallel to the electrode. The distance between the cathode and the interface is time dependent. At long times the interface eventually reaches the anode. Bands of Newton's interference color can be seen between the interface and the cathode.

2.3 Influence of AC Fields

When an AC voltage is applied, colorful birefringent patterns are produced. Figure 2.2 shows a typical series of patterns produced by applying a 60 Hz AC signal across a cell with an L = 2.2mm and d = 12.4 microns. The observations made in cross-polarized light are summarized below.

The inter-electrode area is entirely dark until a threshold field, E_C, is reached. At this field, birefringence is first perceptible at both electrodes. As the field strength is increased further, the birefringent regions near both electrodes increase, forming a symmetrical pattern (Figure 2.2a). A series of colored bands, indicating the degree of molecular reorientation, exists between the linear interface and the electrode. At a field for wave-onset, E_W, perturbations in the linear interfaces are just perceptible (see Figure 2.2b). Above E_W, the amplitude of the

Figure 2.2 60Hz AC deformation patterns for a "thick"-electrode cell with L = 2.2mm and d = 12.4 microns. Field strengths are: a) 900 V/cm, b) 1100 V/cm (E_w), c) 1250 V/cm and d) 1450 V/cm.

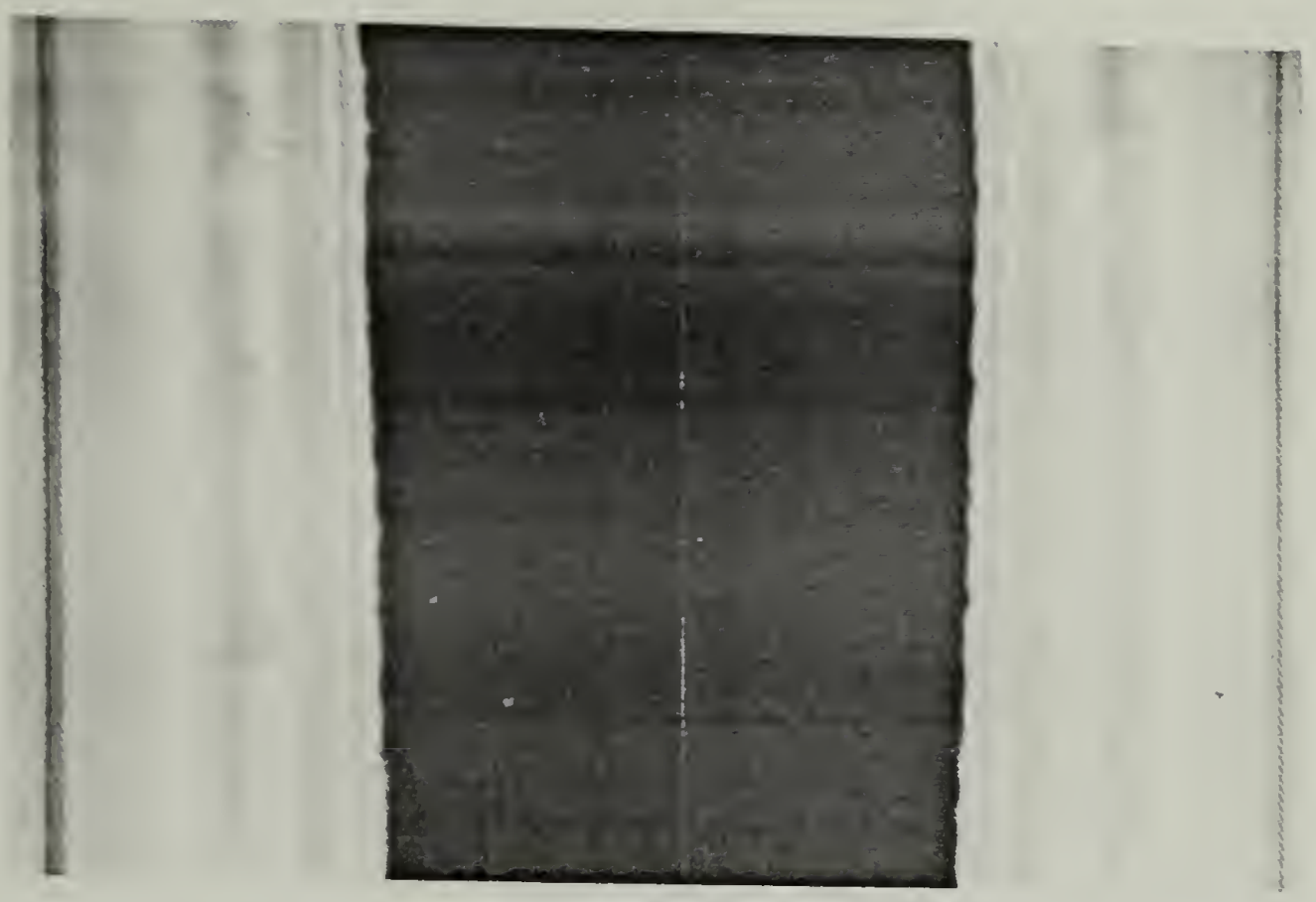

(a)

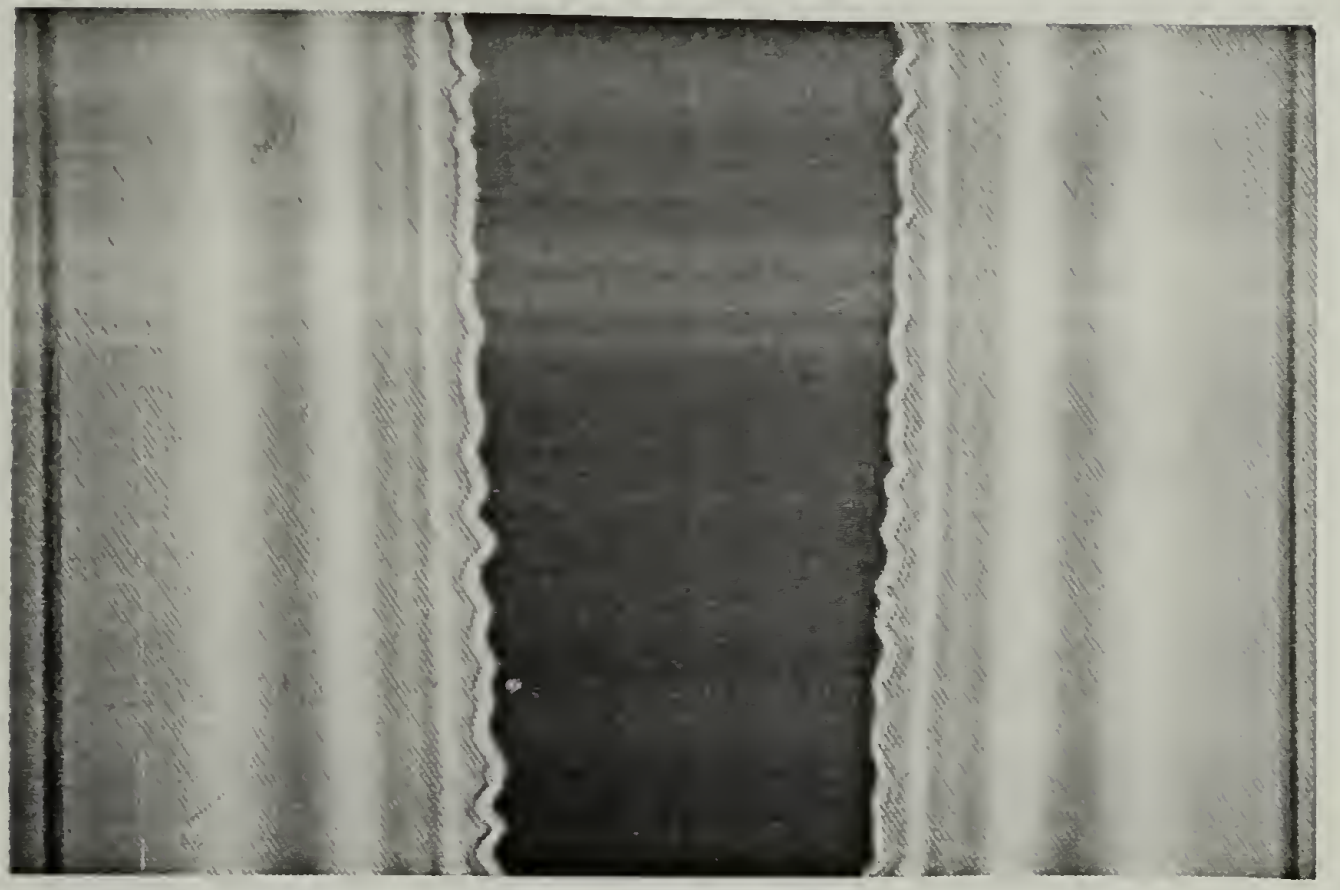

(b)

continued next page

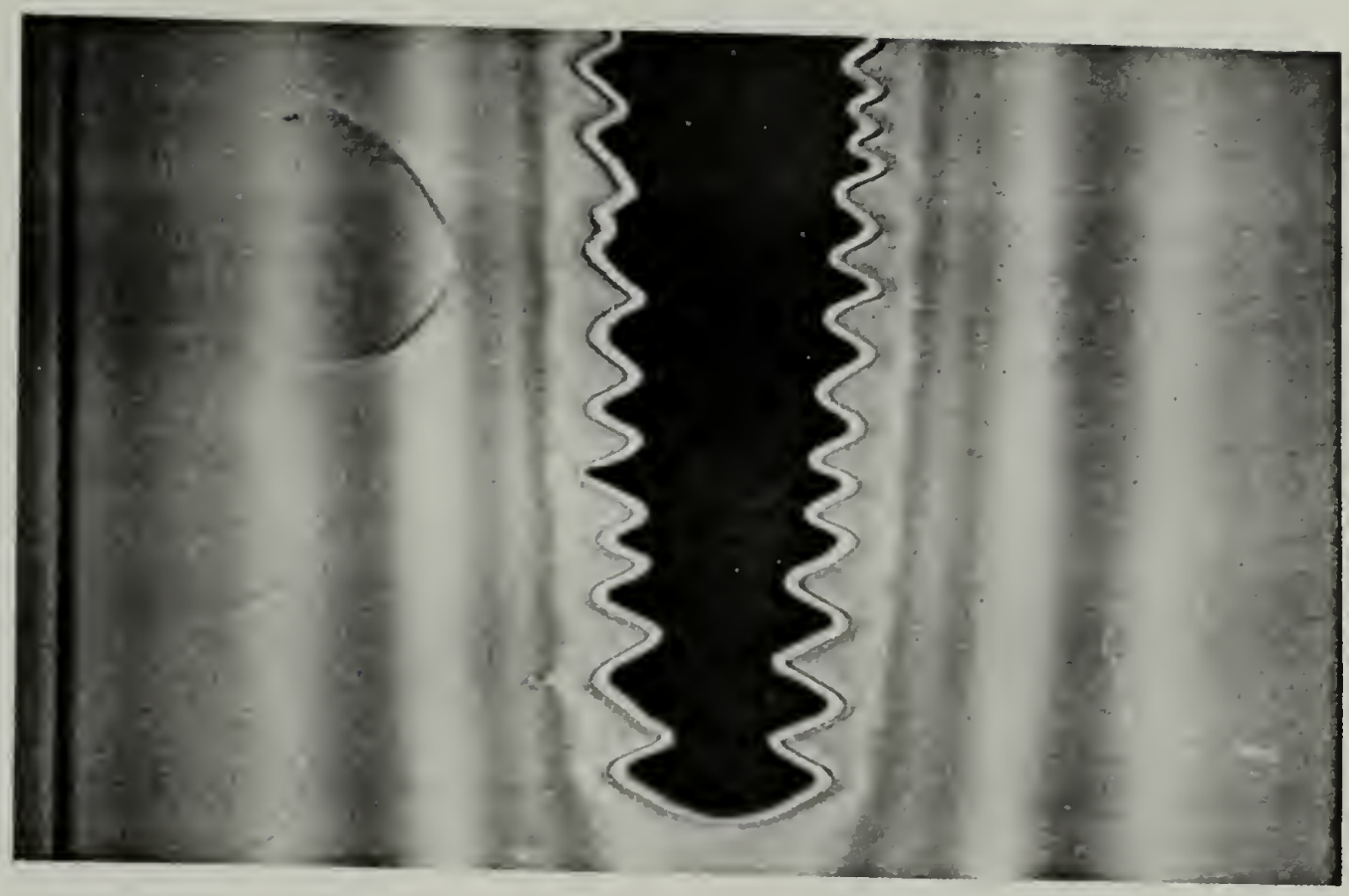

(c)

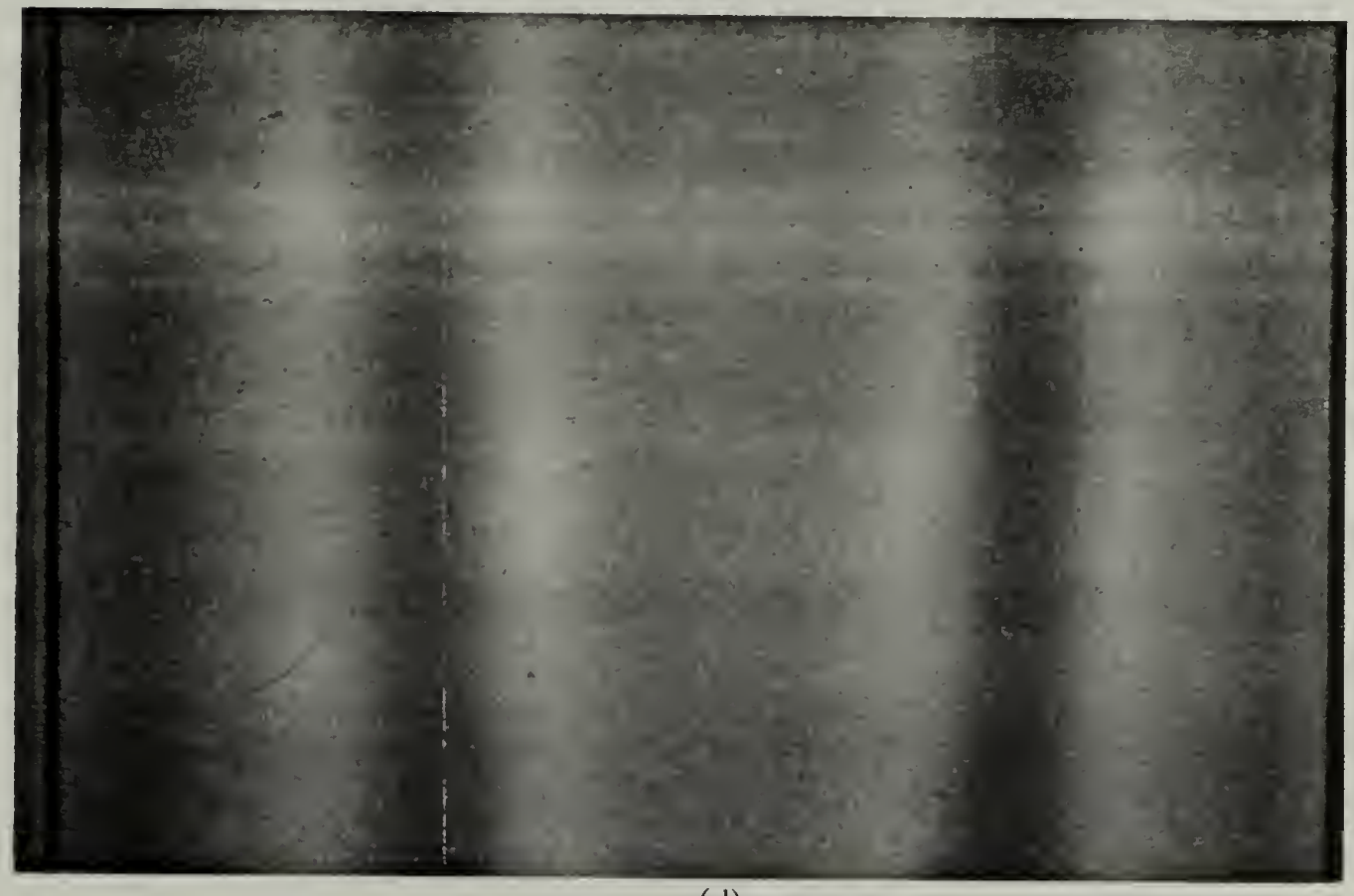

(d)

Figure 2.2 (continued)

perturbations increases and a regular wave pattern is developed (Figure 2.2c). The wavelength, λ, depends on the cell thickness and temperature. Eventually, the birefringent regions emanating from either electrode merge in the center of the inter-electrode region (Figure 2.2d). When this occurs, the wave structure collapses. This can be accompanied by a complete coalescence of the advancing birefringent regions; or a black disclination line may remain, dividing the two regions. These observations are reversed upon reducing the field strength.

2.4 Effect of Layer Thickness

The effect of layer thickness on the wavelength of the wave structure is shown in Figure 2.3. The values reported were measured at 22°C using a 140 volt, 60 Hz AC signal. The data are plotted versus reciprocal thickness to emphasize the limiting effects of the glass surfaces on thick and thin layers. From this figure, two thickness regimes can be identified. Layers thinner than about 10 microns ($1/d < 0.1$) have a constant wavelength of about 20 microns. For thicker layers, the wavelength of the structure scales linearly with reciprocal thickness. The y-intercept of this line predicts the wavelength of an infinitely thick layer to be 330 microns. Experimentally, however, waves could not be established in layers thicker than 42 microns because the two interfaces merged in the center of the cell before wave forming conditions were met. These results suggest that: 1)

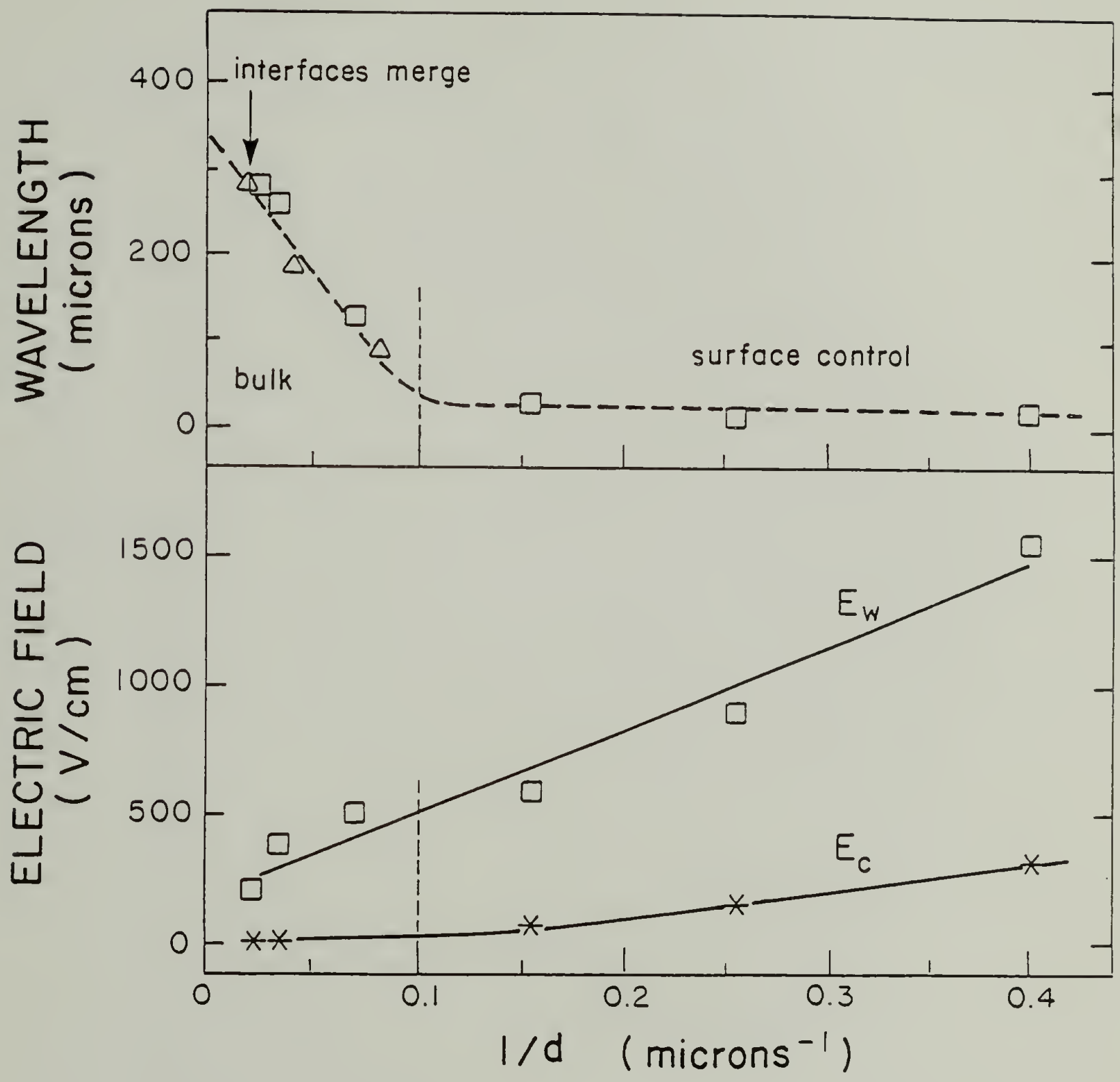

Figure 2.3 Wavelength, wave-onset field, E_w, and threshold field, E_c, plotted versus reciprocal thickness.

the glass surface plays a stabilizing role in the production of the wave structure and 2) the bulk properties of the nematic become more important for layers thicker than 10 microns.

The threshold field dependence, E_c, also demonstrates two regime behavior (Figure 2.3). For layers thinner than 10 microns, E_c scales linearly with reciprocal thickness. This trend is expected. Soref[8] predicts E_c to obey the equation:

$$E_c = (\pi/d)(K_{33}/\Delta\epsilon\epsilon_o)^{\frac{1}{2}} \qquad (2.1)$$

where K_{33} is the elastic constant for bend deformation and ϵ_o is the permittivity constant for a vacuum. Thus, from the slope of our curve, we calculate K_{33} to be 9.1×10^{-6} dynes. This is within a decade of the value of 1.69×10^{-6} dynes reported for the same compound by Karat and Madhusudana[9]. For thicker layers, E_c is small (of the order of 10 V/cm).

The wave onset field, E_w, was found to scale linearly with reciprocal thickness as shown in Figure 2.3.

2.5 Effect of Temperature

The temperature dependence of the wave structure at a constant applied voltage is shown in Figure 2.4. "Thick"- and "thin"-electrode configurations gave equivalent results. The wavelength of the waves increased linearly with temperature from 22 to 32°C. Concomitantly, the definition

Figure 2.4 Temperature dependence of wave structure for cells of two electrode geometries: □ - 14 micron, "thick"-electrode cell; △ - 12 micron, "thin"-electrode cell.

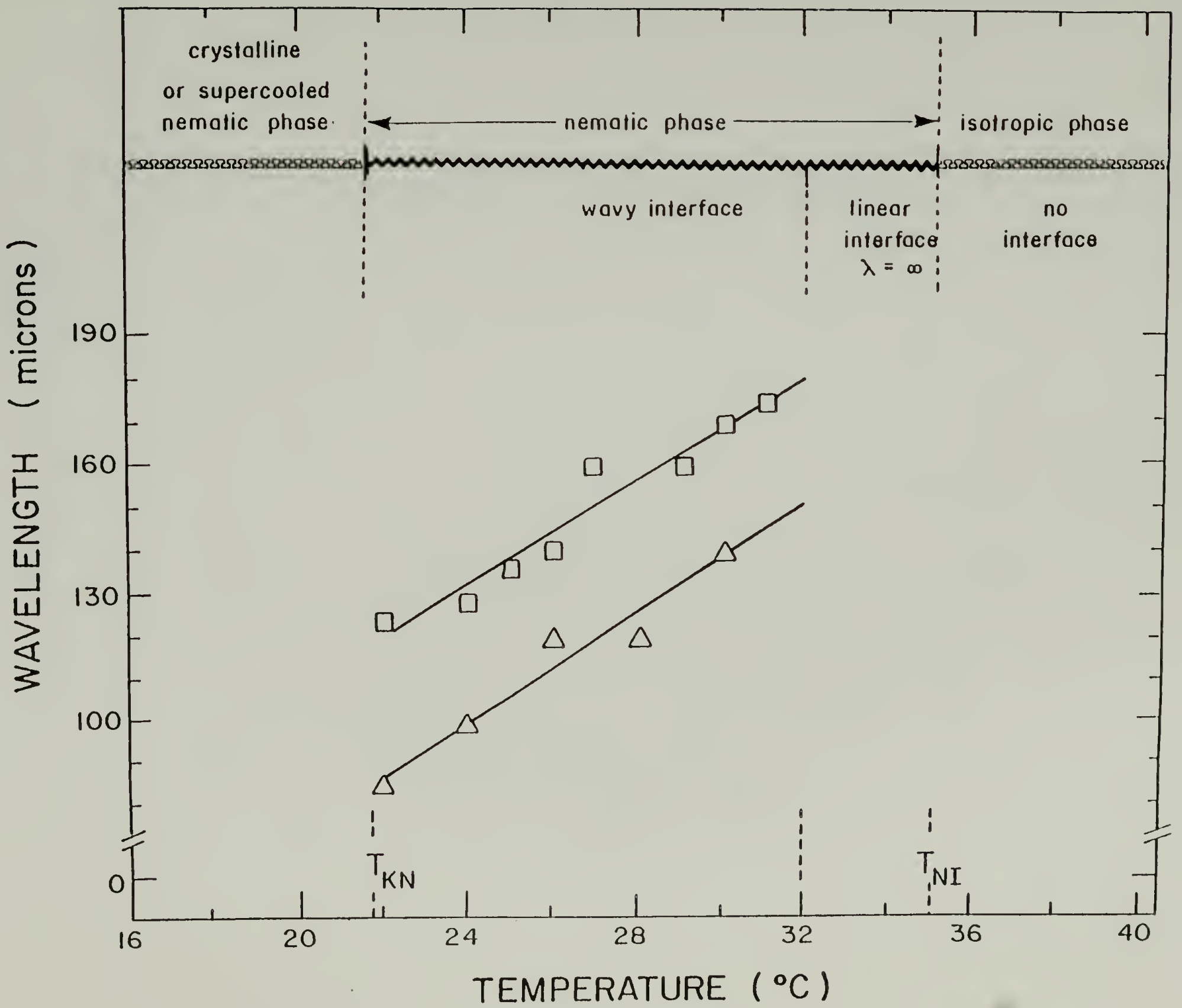
crystalline
or supercooled
nematic phase
nematic phase
isotropic phase
wavy interface
linear
interface
λ = ∞
no
interface
WAVELENGTH (microns)
190
160
130
100
0
T_{KN}
T_{NI}
16
20
24
28
32
36
40
TEMPERATURE (°C)

of the wave structure became more diffuse with increasing temperature. From 32 to 35°C, the wave structure destabilized entirely and the interface became linear. These results will be discussed in the following section. Above the clearing point (35°C), no birefringence and no wave structures were observed as expected.

The conditions of temperature and frequency which stabilize the wave structure are shown in Figure 2.5. The data span a frequency range from 200 to 2000 Hz at constant voltage and cover the entire nematic temperature range. This Figure shows that high frequencies and low temperatures promote the formation of the wave structure. These are conditions where the nematic mesophase responds to a deformation more like an elastic solid than a viscous liquid. The definition of the wave pattern also sharpens under these conditions.

2.6 Analogy Between Interface Position and Work

The interface position may be quantified by a dimensionless number, x/L, where x is the distance from the electrode to the interface. Values range from 0 (for $E < E_c$) to 0.5, where the two interfaces merge in the center of the cell. For reasons which will become apparent later, the square-root of this quantity is plotted versus electric field for a series of "thin"-electrode cells in Figure 2.6. The interface is linear at low fields, and wavy at high fields. The wave onset field, E_w, is encircled. As the field

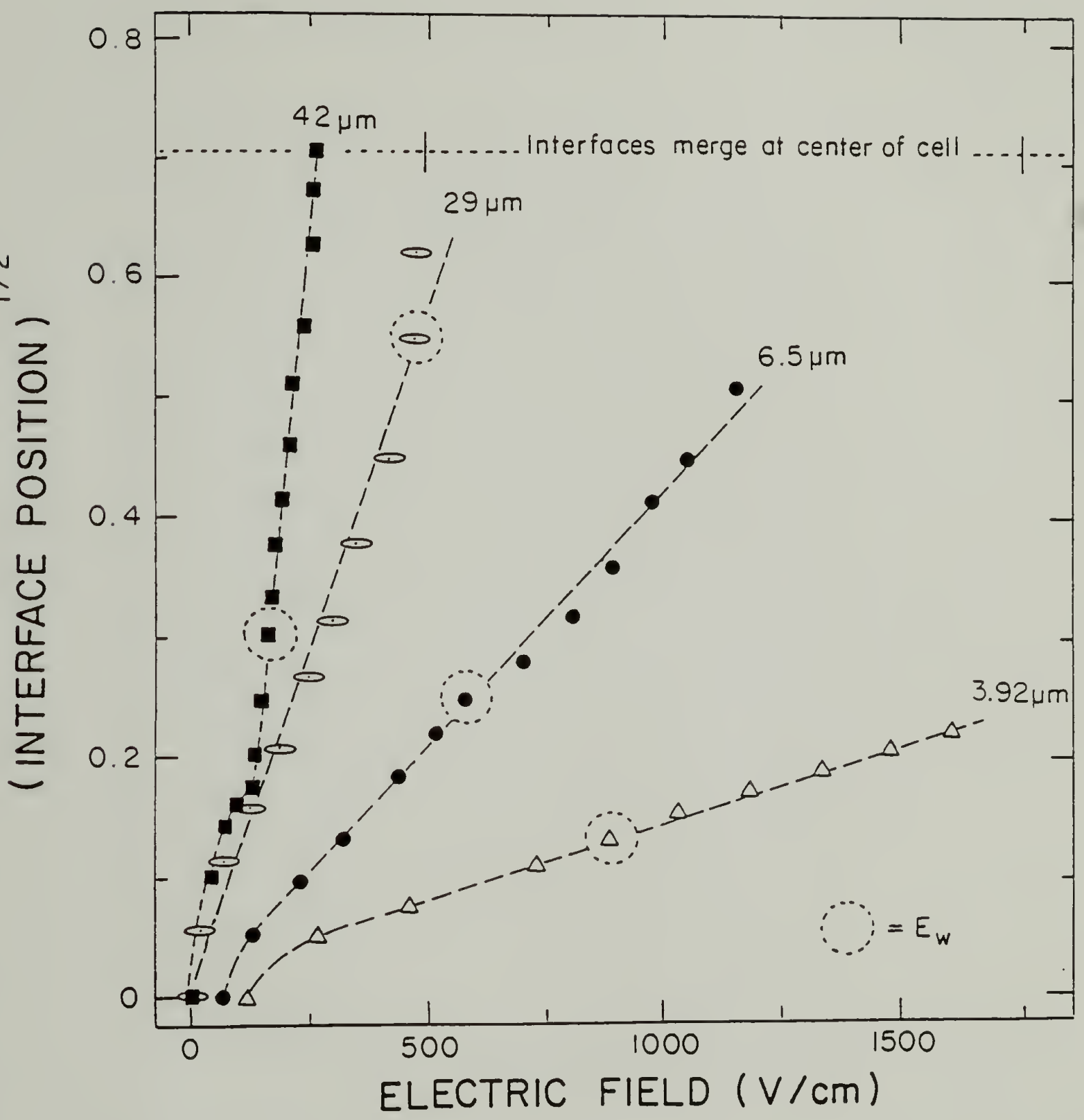

Figure 2.5 Square root of interface position versus electric field for a series of "thin"-electrode cells.

Figure 2.6 Interface position versus frequency for a cell with d = 14 microns, L = 1.98 mm and E = 700 V/cm.

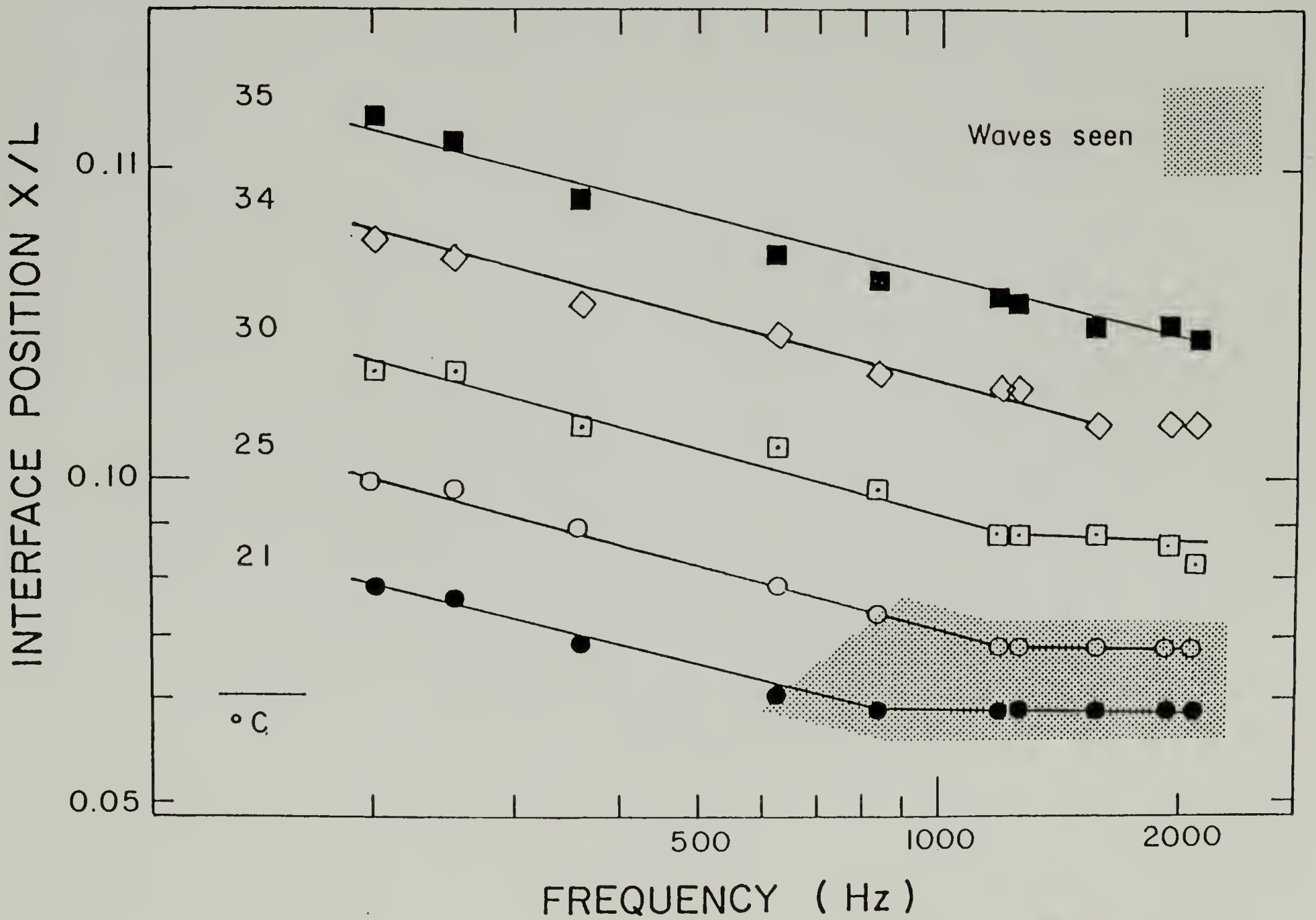
INTERFACE POSITION X/L
0.11
0.10
0.05
35
34
30
25
21
°C
Waves seen
500
1000
2000
FREQUENCY (Hz)

is increased above this level, the amplitude and definition of the waves increase. Typically, waves occur closer to the center of the cell for thicker layers.

Figure 2.6 also shows a linear relationship between $\sqrt{x/L}$ and E. Since L is identical for these cells and V = EL, it follows that x/L scales linearly with V^2. The equation for energy storage as a function of time, W(t), in a parallel plate capacitor is given by:

$$W(t) = CV^2(t)/2 \qquad (2.2)$$

where C is the capacitance of the cell driven by the time dependent voltage V(t). Thus, an analogy is made between the interface position and the electrical work done on the nematic. Deviations from linearity in the initial regions of the $\sqrt{x/L}$ vs E^2 curves can be either positive or negative. For thin samples, where the initial deformation is dominated by the surface and E_C was found to be large, the deviations are negative. For thick samples, where bulk properties become more important and E_C was found to be small, the deviations are positive.

2.7 Explanation of the Wave Structure

The birefringent patterns shown in Figure 2.2 are the result of electrically induced torques acting on the nematic. The origin of these torques can be either ionic or dielectric in nature. Defining the space-charge relaxation frequency[8], f_C, as

$$f_c = \sigma_\perp / 2\pi\epsilon_\perp\epsilon_o \qquad (2.3)$$

where $\sigma_\perp$ and $\epsilon_\perp$ are the perpendicular components of the anisotropic conductivity and permittivity, respectively, two regimes can be identified. For $f < f_c$, the cell operates in the conductive regime: for $f > f_c$, the cell operates in the dielectric regime. In the conductive regime, ionic impurities, injected charges or ions formed by dissociative processes have ample time to migrate during one-half cycle of the voltage. Thus, orientation caused by shear-induced torques are possible. In this regime a frequency dependent interface position is expected. In the dielectric regime, ionic motion is limited and orientation caused by dielectric torques predominate. Here, a frequency independent interface position is expected (in contrast to the threshold field dependency). This suggests that the frequency independent region of the curves in Figure 2.5 correspond to the dielectric regime and the negatively sloped linear portions correspond to the conduction regime.

For 4-4'-n-pentylcyanobiphenyl at 21^oC[10], we calculate f_c to be about 240 Hz. From the equivalent temperature curve of Figure 2.5, the wave structure is observed above 625 Hz. Thus, the wave structure occurs in the dielectric regime. The absence of dust particle motion at the wave-like interface supports this conclusion since it rules out ionic flow.

Because the regular wave pattern produced here is similar to the schematic pattern shown in the paper by

Helfrich[11], we believe the wave structure is the result of space-charge build-up[11,12]. As the nematic reorients, the dielectric constant of the liquid increases ($\epsilon_{\parallel} \approx 15$, $\epsilon_{\perp} \approx 6$). This increases the charge storing capacity of the liquid and allows the field to penetrate further.

At $f > f_c$, charges can accumulate locally[11], disrupting the homogeneity of the dielectric field. According to the theory[11], as simplified by deGennes[13], an instability in the orientation pattern can occur when the dimensionless parameter δ^2 is greater than unity. This parameter is given by

$$\delta^2 = \left(1 - \frac{\sigma_{\perp}}{\sigma_{\parallel}} \frac{\epsilon_{\parallel}}{\epsilon_{\perp}}\right)\left(1 + \frac{\alpha_2}{\eta_c} \frac{\epsilon_{\parallel}}{\Delta\epsilon}\right) \qquad (2.4)$$

where α_2 and η_c are viscosity coefficients and the other parameters have been defined previously. Substituting the viscosity values of MBBA[14] for our sample, we calculate[10] δ^2 to be 33.5 at 21°C and 1000Hz. Thus, the wave instability is predicted from theory and confirmed experimentally (see Figure 2.5). The temperature dependence of δ^2 is non-trivial because all six of the material parameters in equation 4 are temperature dependent. However, these parameters vary slowly for temperatures well below the nematic-isotropic transition. Thus, we expect the wave instability criterion, δ^2, to continue to be met in this temperature region. This is confirmed from Figure 2.4 where a wavelength can be measured between 22 and 32°C. As the nematic-isotropic transition is approached to within 3 or 4 degrees, the

material parameters vary more rapidly and change in such as manner as to lower δ^2 below unity. Here, no wave pattern is established and the interface becomes linear (see Figure 2.4). As for the temperature dependence of the wavelength, we speculate this depends critically on the elastic constants of the sample. The loss of sharpness in the wave-like interface with temperature is attributed to increased thermal fluctuations.

At $f < f_c$, destabilization of the wave structure occurs. In this regime, conduction currents are allowed to flow. These currents neutralize the space-charges thus destroying the wave structure.

2.8 Conclusions

Orientation patterns caused by the action of an electrical field on a mono-domain nematic liquid crystal are varied and interesting. This chapter describes an interesting wave structure observed in thin nematic layer of 4-4'-n-pentylcyanobiphenyl for a particular electrode geometry. The regular wave structure occurs in the dielectric regime of an electrical deformation and is believed to be the result of space-charge build-up.

2.9 References

1. G.H. Heilmeier, L.A. Zanoni and L.A. Barton, Proc. IEEE, **56**, 1162 (1968).

2. W.W. Hollaway, Jr. and M.J. Rafuse, J. Appl. Phys., **42**, 5395 (1971).

3. M.J. Schiekel and K. Fahrenschon, Appl. Phys. Lett., **19**, 391 (1971).

4. W. Haas, J. Adams and J.B. Flannery, Phys. Rev. Lett., **25**, 1326 (1970).

5. F.J. Kahn, Appl. Phys. Lett., **20**, 199 (1972).

6. I.G. Chistyakov and L.K. Vistin, Kristallografiya, **19**, 195 (1974).

7. A.P. Kapustin and L.S. Larinova, Kristallografiya, **9**, 297 (1963).

8. R.A. Soref, Appl. Phys. Lett., **22**, 165 (1973).

9. P.P. Karat and N.V. Madhusudana, Mol. Cryst. Liq. Cryst., **40**, 239 (1977).

10. $\sigma_\perp = 0.83 \times 10^{-10}$ nS/cm, $\sigma_\parallel = 0.13 \times 10^{-10}$ nS/cm, $\epsilon_\perp = 6.0$, $\epsilon_\parallel = 15.3$. All measurements taken at 21^{o}C and 1000Hz.

11. W. Helfrich, J. Chem Phys., **51**, 4092 (1969).

12. E. Dubois-Violette, P.G. deGennes and O. Parodi, J. Physique, **32**, 305 (1971).

13. P.G. DeGennes, The Physics of Liquid Crystals, Oxford Press University, Oxford, 1974.

14. $\alpha_2 = -77.5$ poise, $\eta_c = 41.6$ poise; from reference 13.

CHAPTER 3

MOLECULAR ORIENTATION PROFILE IN A DEFORMED NEMATIC: 4-4'-N-PENTYLCYANOBIPHENYL

Most optical displays begin with a thin, uniformly oriented nematic layer. The molecular orientation in the off-state is controlled by the bounding surfaces[1-6]. By applying an electric field across the layer, the alignment of the molecules is altered. This change in alignment affects the optical properties of the nematic layer. Such a device is called an electro-optic cell.

The dielectric orientation of aligned nematic layers is a well known electro-optical phenomenon[7-8]. This phenomenon is the basis for the popular twisted-nematic (TN) effect[9] used in watch and calculator displays[10-12]. It was Kahn who first demonstrated spatially-uniform tunable birefringence for a nematic layer between two transparent electrodes[1] in 1971. Shortly after him, Soref[13] first reported on spatially varying birefringent patterns in nematic layers using a transverse electrode geometry. In this geometry, the electric field and the light propagation directions are perpendicular (see Figure 2.1). The orientation pattern observed consists of a series of birefingent bands parallel to the electrodes. An ordered and symmetrical sequence of colors is generated between the electrodes. A sharp interface between electrically oriented and surface oriented nematic is readily defined at low voltages. To explain his

results, Soref later published his view of the molecular orientation profile inside the deformed layer[14].

We have repeated Soref's experiment using a different nematic liquid crystal and found similar optical patterns[15]. However, the molecular orientation profile given by Soref[14] is incorrect. Using the theory of electrical deformation for a nematic developed by Deuling[16], we calculate the correct orientation profile. Thus, in this chapter the birefringence patterns of chapter 2, observed for 4-4'-n-pentylcyano-biphenyl, are converted into absolute molecular orientation values. The orientation profile so calculated should describe any positive nematic ($\Delta\epsilon > 0$) in a similar electro-optic cell.

3.1 Theory

A uniformly oriented nematic layer is optically uniaxial. There are two principal refractive indices given for such a system: $n_{\parallel}$ and $n_{\perp}$. These are the values of the refractive index when the electric field vector of the probing light ray and the molecular axis of the nematic are parallel and perpendicular to each other, respectively (see Figure 3.1). It can be shown geometrically that the refractive index for any intermediate angle of orientation, Θ, is given by:

$$n(\Theta) = n_{\parallel} n_{\perp} / \sqrt{n_{\parallel}^2 \sin^2\Theta + n_{\perp}^2 \cos^2\Theta} \qquad (3.1)$$

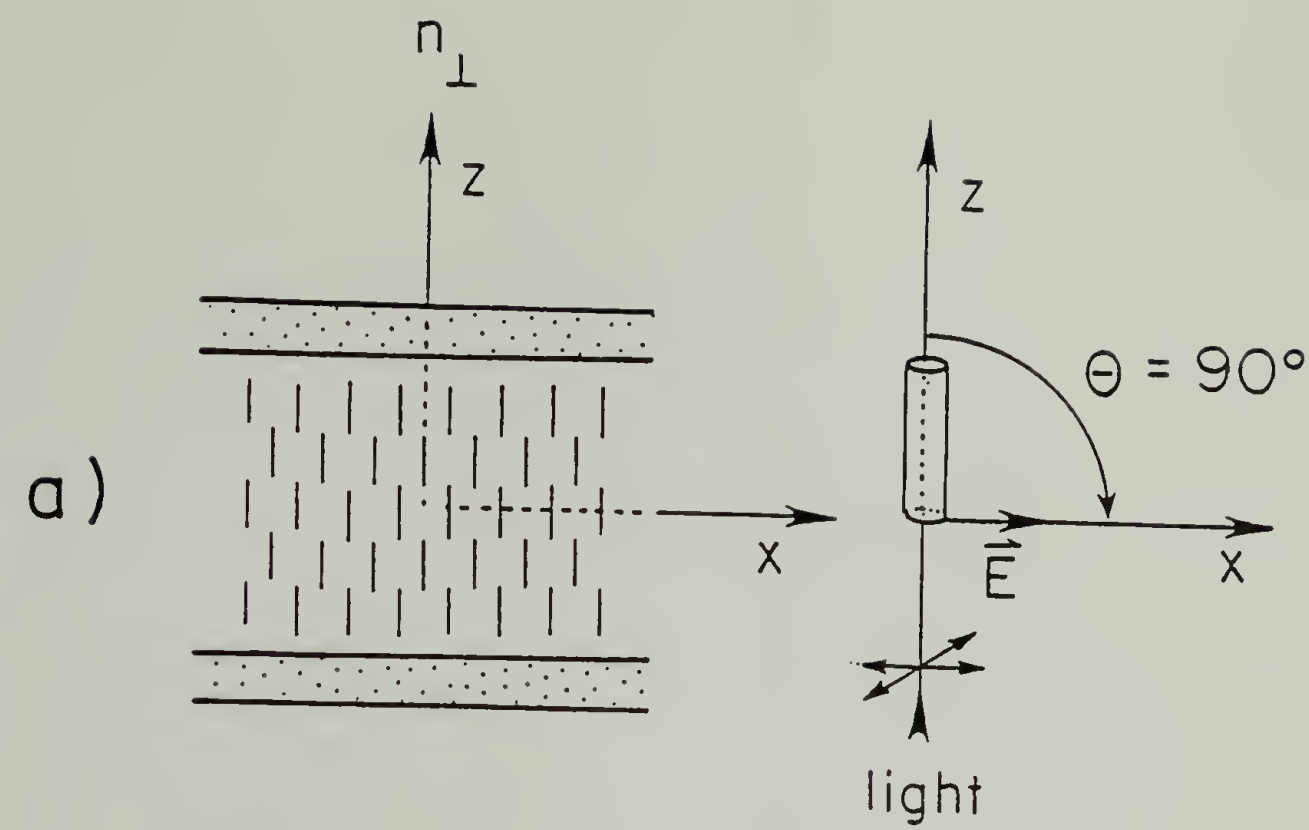

Figure 3.1 Orientation of molecules and electric field of light ray for refractive indices, $n_{||}$ and $n_\perp$.

The birefringence, Δn, of such a system is defined by

$$\Delta n = n(\Theta) - n_{\perp} \qquad (3.2)$$

From equations (3.1) and (3.2), it can be shown that the birefringence has a maximum value, $(n_{\parallel} - n_{\perp})$, when $\Theta = 0^{o}$ and is 0 when $\Theta = 90^{o}$. The birefringence decreases monotonically between these two extremes. The optical retardation, R, is related to the birefringence through the expression:

$$R = \{n(\Theta) - n_{\perp}\}d \qquad (3.3)$$

where d is the layer thickness. Thus, the molecular orientation profile can be determined from the spatial dependence of retardation for the nematic layer.

In this chapter, two molecular orientation profiles are discussed. In the simplest case, the orientation profile is independent of the z- (or thickness) direction. This has the effect of ignoring any boundary effects due to the surfaces of the glass. In a more sophisticated approach, we develop the concept of an equivalent cell. In this case, boundary effects are considered implicitly by using Deuling's theory of deformation for a nematic layer[16].

3.2 Experimental

The geometry of the electro-optical cell is given in Figure 2.1. The cell consists of a 12 micron layer of 4-4'-n-pentylcyanobiphenyl (K15) sandwiched between two glass

plates. K15 is a room temperature nematic liquid crystal having a $T_{KN} = 22.3^{o}$ and $T_{NI} = 35.1^{o}C$. The spontaneous homeotropic alignment of the nematic is produced by chemically treating the glass substrates with dichlorodimethylsilane. The spacing of the plates, d, was controlled by the diameter of the wire electrodes and confirmed by interferometry. The separation of the wires, L, was 2.2 mm. Two strips of an epoxy-coated polyester film were cured two hold the plates together once the cell was constructed.

The cell was placed between crossed-polars so that the length of the wires made an angle of 45^{o} with respect to the analyzer and polarizer directions. (The orientation of maximum intensity). A 60 Hz AC field was applied across the electrodes, transverse to the viewing direction. Color micrographs of the inter-electrode area were taken at several voltages and are reproduced as Figures 2.2a-d. The colored birefringent bands are then converted into optical retardation values by a standard Michel-Levy chart and finally into a molecular orientation. The assignments are unique.

3.3 Molecular Orientation Profile

3.3.1 Neglecting Boundary Effects

The optical retardation for each colored is plotted as a function of normalized cell position, x/L, in Figure 3.2.

Figure 3.2 Optical retardation as a function of normalized cell position. Legend: ⧈ - 900 V/cm, ◆ - 1100 V/cm (crest), ◘ - 1100 V/cm (trough), ◇ - 1250 V/cm (crest), ■ -1250 V/cm (trough), □ - 1450 V/cm.

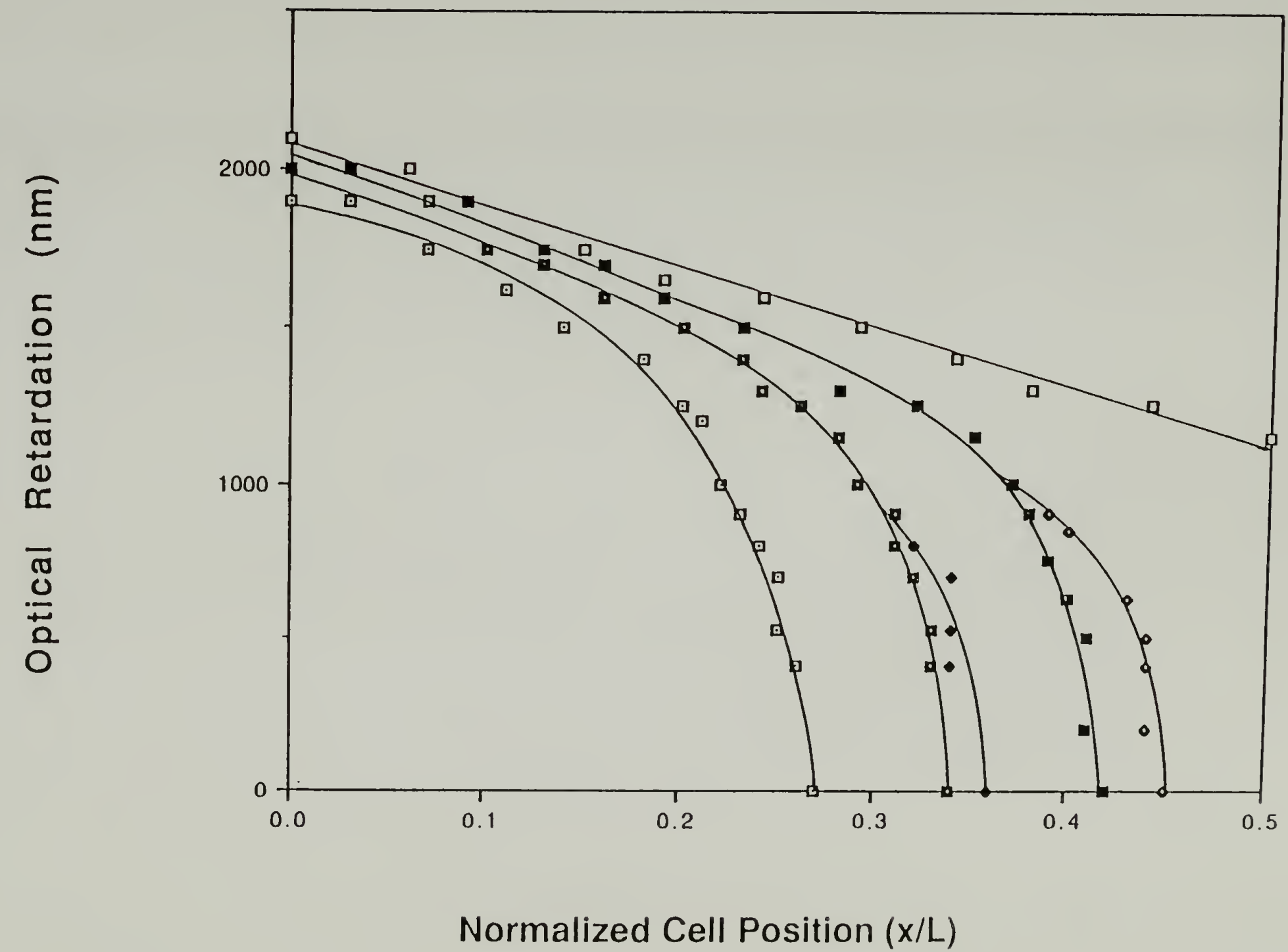
Optical Retardation (nm)
2000
1000
0
0.0
0.1
0.2
0.3
0.4
0.5
Normalized Cell Position (x/L)

The Figure shows the retardation has a maximum value at the electrode (x/L = 0) and decays monotonically to zero at the interface (where the birefringence stops, see Figure 2.2). Two "branches" are shown below R = 800 nm for the two intermediate field strengths. These correspond to "slices" taken through the layer intersecting crest and trough positions of the wavy interface.

From the data of Figure 3.2 and equations (3.1) through (3.3), angular orientation at each cell position can be calculated. Defining the orientation angle ϕ as 90 - Θ, we plot the angle of orientation as a function of position in Figure 3.3. The Figure shows the nematic is most highly oriented near the electrode. The maximum value of 70^{o} suggests orientation is not complete. Moving away from the electrode, the orientation declines gradually. A precipitous drop in ϕ occurs just before the interface position is reached. This drop is believed to be due to the inability of this model to account for boundary effects in the z-direction.

3.3.2 Considering Boundary Effects

To incorporate z-dependent orientation in the deformation profile, the concept of an equivalent cell is developed. The equivalent cell contains a homeotropically aligned nematic between two parallel-plate electrodes spaced by the distance, d. The nematic has the physical properties of K15 (i.e. Δn, $\Delta \epsilon$, K_{ii}) except that values of the parallel

Figure 3.3 Molecular orientation profile of a nematic layer neglecting boundary effects. Legend: ⧈ - 900 V/cm, ◆ - 1100 V/cm (crest), ◘ - 1100 V/cm (trough), ◈ - 1250 V/cm (crest), ■ -1250 V/cm (trough), ▫ -1450 V/cm.

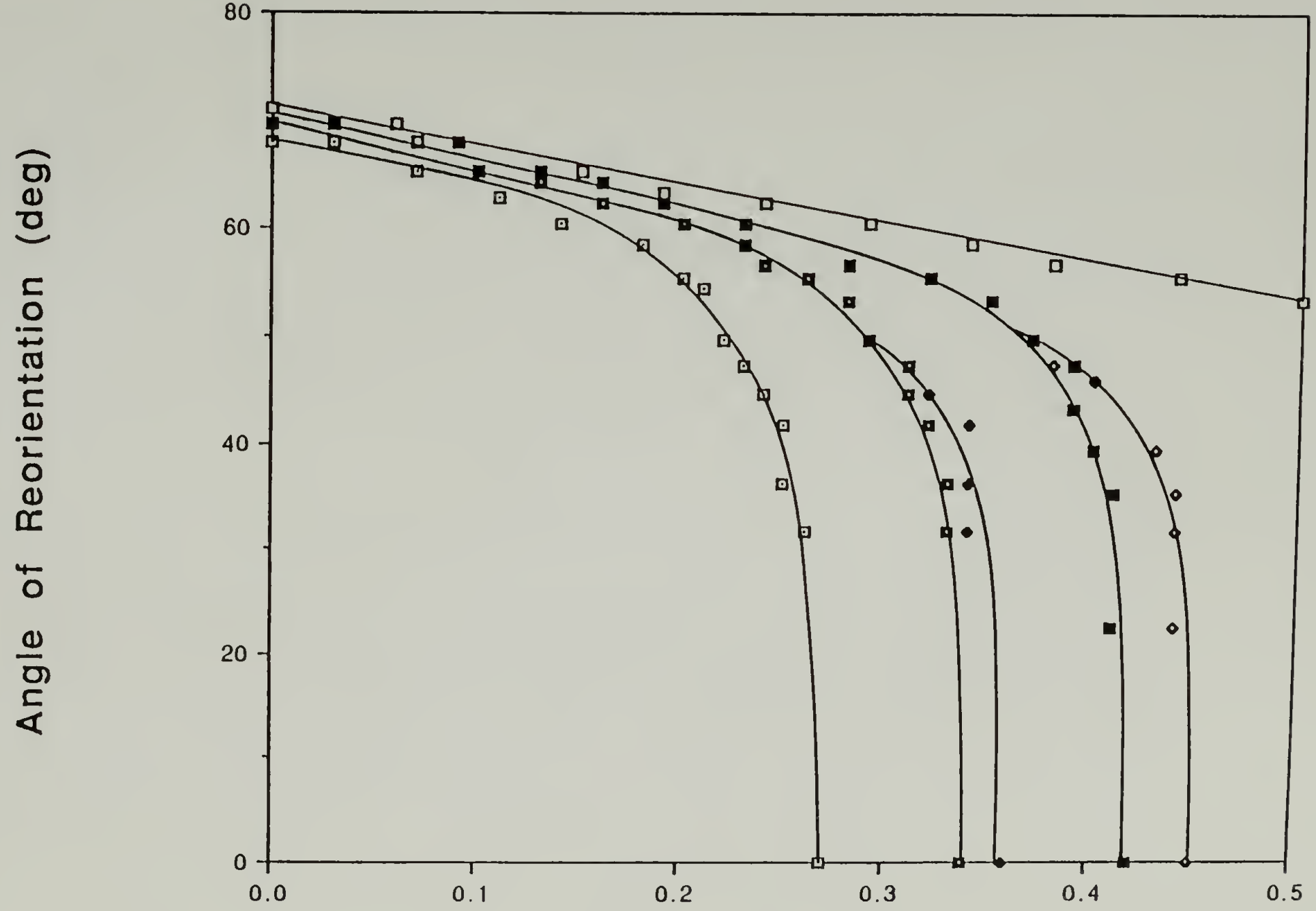
Angle of Reorientation (deg)
80
60
40
20
0
0.0
0.1
0.2
0.3
0.4
0.5
Normalized Cell Position (x/L)

and perpendicular dielectric constant are interchanged. In this fashion, molecules at the center of the equivalent cell will rotate in a similar manner (perpendicular to the direction of light propagation) as those of the cell being modeled. The material parameters for K15 at 24°C were taken from the literature[17-19] and used to calculate ϕ_m for each measured retardation. Here, ϕ_m is the maximum orientation angle at the center of the equivalent cell in accordance with Deuling's theory[16]. This is plotted as a function of cell position in Figure 3.4. The equivalent cell model yields a more gradual orientation profile for the electrically aligned nematic as compared to the previous model.

Using the equivalent cell model it is also possible to assign a reduced voltage to several relative cell positions. Thus, a reduced-voltage profile is obtained. This has been done for the 900V/cm deformation structure and is compared to a theoretical curve in Figure 3.5. The theoretical curve is based on the voltage profile expected for a uniform dielectric between parallel conducting cylinders[20]. The theoretical curve was normalized by setting the reduced voltage at the interface position equal to unity. Thus, the analogy is drawn that the voltage at the interface of the transverse-electrode cell is the threshold voltage of the equivalent cell. Both curves show a similar trend. However, the reduced voltage decays toward unity more rapidly for the equivalent cell model than the theoretical curve. This is

Figure 3.4 Molecular orientation profile of a nematic layer incorporating boundary effects. Legend: ⊡ - 900 V/cm, ◆ - 1100 V/cm (crest), ◘ - 1100 V/cm (trough), ◇ - 1250 V/cm (crest), ■ -1250 V/cm (trough), □ -1450 V/cm.

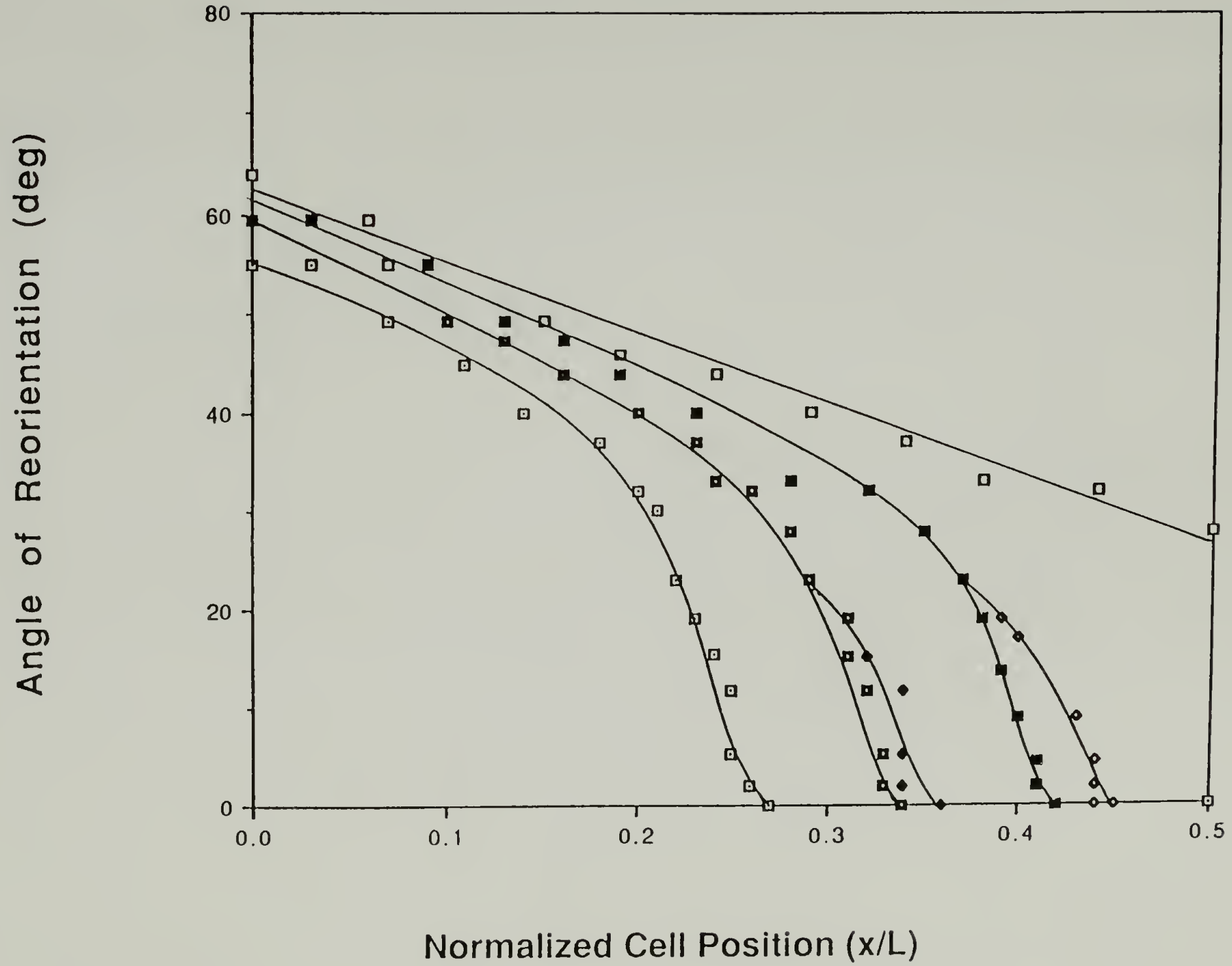
Angle of Reorientation (deg)
80
60
40
20
0
0.0
0.1
0.2
0.3
0.4
0.5
Normalized Cell Position (x/L)

Figure 3.5 Reduced voltage profile for a 12 micron layer at 900 V/cm compared to theory.

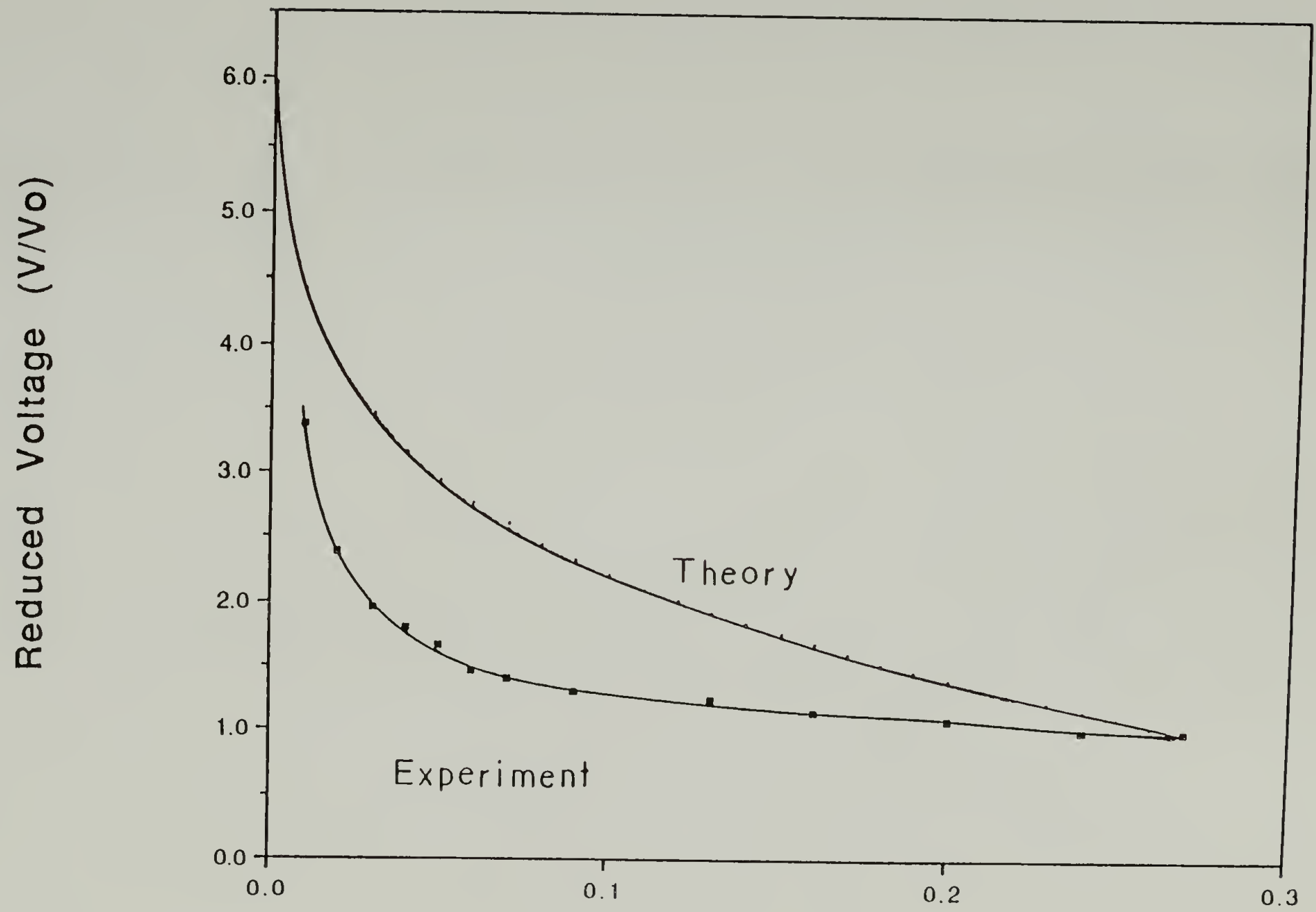
Reduced Voltage (V/Vo)
6.0
5.0
4.0
3.0
2.0
1.0
0.0
0.0
0.1
0.2
0.3
Theory
Experiment
Normalized Cell Position (x/L)

most likely due to the non-uniform dielectric constant of the system being modelled. The difference is in the direction that would be expected for a dielectric medium with a higher value near the electrode (i.e. $\approx\epsilon_{11}$) and a lower value at the interface ($\epsilon_{\perp}$). Thus, the equivalent cell model appears to be of some use in analyzing the deformation structures generated in transverse-electrode cells.

3.4 Conclusions

We have analyzed the birefringent patterns of the nematic liquid crystal, 4-4'-n-pentylcyanobiphenyl, in a thin layer. Our observations are similar to those of Soref who studied a nematic mixture of a different chemical class. Thus, we believe the orientation profiles calculated here can be generalized to other positive ($\Delta\epsilon > 0$) nematic systems.

We have calculated the molecular orientation profile from the birefringent patterns using two different methods. In the first method, boundary effects of the glass substrates are neglected. The molecular orientation profile for this case changes dramatically near the deformation interface. In the second method, we take boundary effect into account. The molecular orientation profile for this case is more gradual. This latter method also allows a reduced-voltage profile to be calculated within the nematic layer. Comparison of our experimental results with theoretical predictions confirm the usefulness of this

method. Thus, the equivalent cell method is preferred because of its greater accuracy and versatility in determining the molecular orientation profile between the electrodes.

3.5 References

1. F.J. Kahn, G.N. Taylor and H. Schonhorn, Proc. IEEE, **61**, 823 (1973).

2. W. Urbach M. Boix and E. Guyon, Appl. Phys. Lett., **25**, 479 (1974).

3. L.T. Creagh and A.R. Kmetz, Mol. Cryst. Liq. Cryst., **24**, 59 (1974).

4. J.C. Dubois, M. Gazard and A. Zann, J. Appl. Phys., **47**, 1270 (1975).

5. T. Uchida, M. Ohgawara and Y. Shibata, Mol. Cryst. Liq. Cryst., **98**, 149 (1983).

6. H.L. Ong, A.J. Hurd and R.B. Meyer, J Appl. Phys., **57**, 186 (1984).

7. F.J. Kahn, Appl. Phys. Lett., **20**, 199 (1971).

8. R.A. Soref and M.J. Rafuse, J. Appl. Phys., **43**, 2029 (1971).

9. M. Schadt and W. Helfrich, Appl. Phys Lett., **18**, 127 (1971).

10. D.W. Berreman, in Nonemissive Electro-optic Displays, edited by A.R. Kmetz and F.K. Willisen (Plenum Press, New York and London, 1975), p9.

11. P.A. Penz, Proc. S.I.D., **19**, 43 (1978).

12. E.P. Raynes, IEEE Trans. Electr. Dev., **26**, 1116 (1979).

13. R.A. Soref, Appl. Phys. Lett., **22**, 165 (1973).

14. R.A. Soref, in S.I.D. Symposium Digest of Technical Papers (Lewis Winner, New York, 1972), p34.

15. K.T. Schell and R.S.Porter, Mol. Cryst. Liq. Cryst., **174**, 141 (1989).

16. H.J. Deuling, Mol. Cryst. Liq Cryst., **19**, 123 (1972).

17. R.G. Horn, J. Physique, **39**, 105 (1978).

18. J.D. Bunning, T.E. Faber and P. L. Sherrell, J. Physique, **42**, 1175 (1981).

19. B.R. Ratna and R. Shashidar, Mol. Cryst. Liq. Cryst., **42**, 113 (1977).

20. S. Ramo, J.R. Whinnery, T.V. Duzer, Fields and Waves in Communication Electronics, John Wiley & Sons, Inc., New York, 1965, p186.

CHAPTER 4

BINARY PHASE STUDIES OF 4-4′-N-PENTYLCYANOBIPHENYL

Mixtures of liquid crystalline materials and their phase diagrams have been studied for various reasons: both theoretical[1-2] and applied[3]. Recently, we have demonstrated[4] an interesting electro-optical effect for the room-temperature liquid crystal 4-4′-n-pentylcyanobiphenyl (K15). This effect involves the reorientation of thin layers of K15 in transverse electric fields. Under the appropriate conditions, wave structures are established[4]. Preliminary studies indicate the wave structure depends on the dielectric anisotropy of the nematic. In an effort to control and modify this parameter, blends of K15 with a second liquid crystalline compound were prepared. In this paper, we present the phase behavior of three binary systems having K15 as one of the two components. Based on this work, appropriate compositions for further electro-optical studies will be chosen.

The homologous series 4-[4-n-alkylcyclohexyl]-cyanophenyl was selected for blending purposes with K15 because it spans a wide range of dielectric anisotropy ($8 < \Delta\epsilon < 14$) and is chemically similar to K15. Members of the homologous series and K15 all have a terminal cyano group which lies in the principle molecular axis. This strong dipolar group facilitates electrical orientation of the mesophase. The n-ethyl, n-butyl and n-heptyl compounds

were chosen from among this series. Both n-ethyl and n-butyl are monotropic liquid crystals and have limited nematic temperature ranges for electro-optical studies. However, through blending with K15, a eutectic composition with a suitable nematic temperature range is predicted from the Schröder-van Laar (S-vL) equation. To test this prediction, and to explore the compositional range for electro-optical studies, the phase diagram of these systems were constructed.

4.1 Theory of Eutectic Blending

The phase diagram for a simple eutectic mixture of two nematic liquid crystals is shown in Figure 4.1. The nematic-isotropic transition temperature is the linear weighted average of the two T_{NI} for the pure components[5]. The crystal-nematic transition temperature for any mixture and the eutectic (lowest transition) composition can be predicted from the Schröder-van Laar (S-vL) equation[1-2,6]. The system of equations for a binary mixture is given below:

$$-\ln x_1 = \frac{\Delta H_{f_1}}{R}\left(\frac{1}{T} - \frac{1}{T_1}\right) \qquad (4.1)$$

$$-\ln (1-x_1) = \frac{\Delta H_{f_2}}{R}\left(\frac{1}{T} - \frac{1}{T_2}\right) \qquad (4.2)$$

where T, T_1 and T_2 are the crystal-nematic transitions for component 1 and component 2, respectively, and H_{f1} and H_{f2} are the heats of the crystal-nematic transition for the two

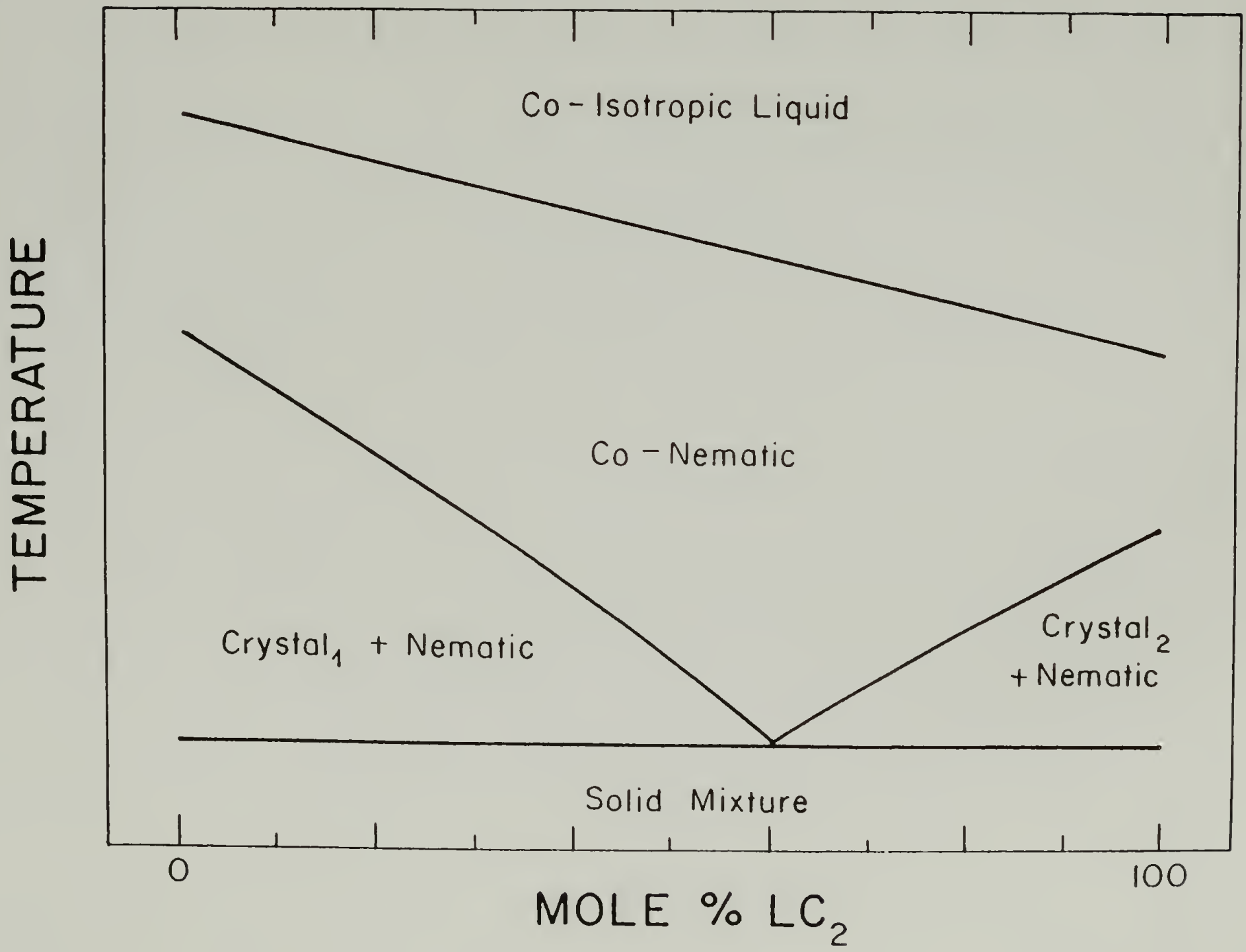

Figure 4.1 Model phase diagram of a simple-eutectic mixture for two enantiotropic nematogens.

pure components, x_1 is the mole fraction of component 1 and R is the gas constant. The assumptions involved in this equation are: a) the two components form pure crystals and do not co-crystallize in the solid phase, b) the two components form an ideal mesophase (i.e. co-mesophase across the entire range of compositions) and c) the heat of mixing is negligible. To some extent, assumptions a) and b) are incompatible. The more similar the molecules, the more likely they are to co-crystallize, as well as form an ideal mesophase.

4.2 Experimental

The chemical structure of 4-4'-n-pentylcyanobiphenyl (K15) and the homologous series 4-[4-n-alkylcyclohexyl]-cyanophenyl are given below.

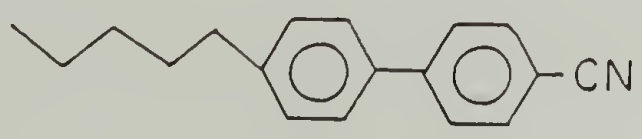

4-4'-n-pentylcyanobiphenyl

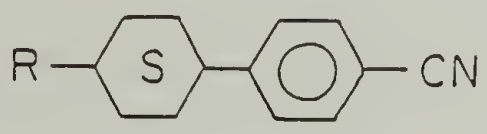

4-[4-alkylcyclohexyl] cyanophenyl

Abbreviations for the chemical structures are shown in Table 4.1. These compounds, obtained from Merck, were estimated to have a purity >99% by elemental analysis and were used without further purification.

Table 4.1 Thermal properties of 4 pure nematic liquid crystals compared with the literature.

	T_{KN} (°C)		ΔH_{KN} cal/g		T_{NI} (°C)		T_{KN} (°C)	ΔH_{kn} cal/g
Compound	EXP	LIT	EXP	LIT	EXP	LIT	van't	Hoff
K15	22.3	24	15.7	16.1	35.1	35.3	22.7	18.3
S1236	40.5	40	24.5	24.4	(-1.5)	(4)	37.1	24.0
S1188	40.7	41	21.8	22.0	39.0	41	40.1 41.5	15.8 23.5
S1115	29.8	30	22.0	22.6	55.8	57	----	----

Thermal transitions and transition heats between -30 and 60°C were measured by a Perkin-Elmer DSC-2 apparatus under an atmosphere of dry nitrogen. Transition temperatures and transition heats were calibrated using benzophenone, cyclohexane and water standards. Thermal programming and data aquisition was performed by a supporting Perkin-Elmer TADS data station. A Vickers polarizing optical microscope was used to determine the mesophase structure and assess the DSC results. To achieve the sub-ambient temperatures required, an aluminum block was designed to mount on top of the microscope stage through which a cooling fluid could circulate. The entire microscope assembly was housed inside a glove bag which was purged continuously with dry nitrogen to prevent condensation.

Crystallization of all binary mixtures was slow. This was evidenced by the fact that all compositions supercooled by 10°C or more, even at a slow cooling rate of 1.25°C/min; and that the heats of transition were reduced by rapid cooling. To promote maximum crystallization, all mixtures were cooled from the isotropic state at the rate of -1.25°C/min down to -30°C. Even then not all the samples crystallized, particularly those near the eutectic point. For these samples, crystallization was initiated, where possible, by immersing the sample in liquid nitrogen just prior to placing it in a cold (<0°C) DSC sample chamber. Further crystallization was monitored by scanning between -30 and 0°C until no further endo- or exotherms were observed

in this temperature range and the baseline was flat. The phase diagrams were constructed from heating curves obtained at a slow scan rate of either 1.25° or 5.0°C/min.

4.3 Binary Systems Studied

The thermal transitions of the four pure components are compared with those reported by Merck[7] in Table 4.1. The experimental values agree with those reported to within ±2°C with the exception of T_{NI} for S1236. This value is determined by an extrapolation procedure[8,9] discussed in the following section. Merck reports T_{NI} = 4°C for S1236. Our value of -1.5°C yields a difference of 5.5°C. The phase behavior for all three binary systems will be discussed separately. The chemical abbreviations used in the headings are identified in Table 4.1. The mixture of the first homolog, 4-[4-ethylcyclohexyl]cyanophenyl, with 4-4'-n-pentylcyano-biphenyl gives the most interesting and complicated phase diagram. We begin our discussion with this system below.

4.3.1 N-Ethylcyclohexyl-p-cyanophenyl with K15

The S1236/K15 phase diagram is shown in Figure 4.2. The T_{NI} of pure S1236 was determined by extrapolation to be -1.5°C. This procedure was used since the isotropic phase of S1236 cannot be cooled rapidly enough to measure T_{NI} directly. When blended with an enantiotropic liquid crystal such as K15, the T_{NI} of pure S1236 is found by extrapolating

the nematic-isotropic transition line, defined by the high mole % K15 samples, back to 0 mole % K15. This procedure has been used previously[8,9]. It is not always reliable since curvature may occur below the crystal-isotropic portion of the phase diagram. Nonetheless, the value we report is within 4°C of the 1.9°C, reported by Osman[10]. Thus, we feel confident in applying this method here.

The phase diagram is interesting. Figure 4.2 shows a nematic co-mesophase forms over the entire binary compositional range. This co-mesophase, however, is divided into 2 separate regions. Optical microscopy reveals the co-nematic is homogeneous for compositions > 62 mole % K15. Below 46 mole % K15, the co-nematic mesophase is in equilibrium with S1236 crystals. Therefore, a phase line is constructed between the eutectic point and the T_{NI} for the 46 mole % K15 blend.

The T_{NI} for the co-nematic increases linearly for compositions between 46 and 100 mole % K15 (see Figure 4.2). For compositions between 22 and 46 mole % K15, T_{NI} remains constant at 14°C. This suggests the composition of the co-nematic is constant (at ≈46 mole % K15). Below 22 mole % K15, T_{NI} is 1 to 2°C lower than 14°C; suggesting the co-nematic contains < 46 mole % K15.

Figure 4.2 also shows that three independent phenomena occur at ≈10 mole % K15: 1) the T_{NI} increases, 2) a new phase develops and 3) the lowest temperature transition increases. All 3 transitions stabilize to constant values

Figure 4.2 Phase diagram for K15 and S1236. ♦ - T_{KN} of minor component; ◊ -T_{KS} crystal to smectic (?); ▲ - T_{SN} smectic to nematic; ◪ - T_{KN} of eutectic mixture; □ - T_{NI} of 45 mole % K15 blend; ○ -T_{NI} of mixture; ● - T_{KI} crystal to isotropic.

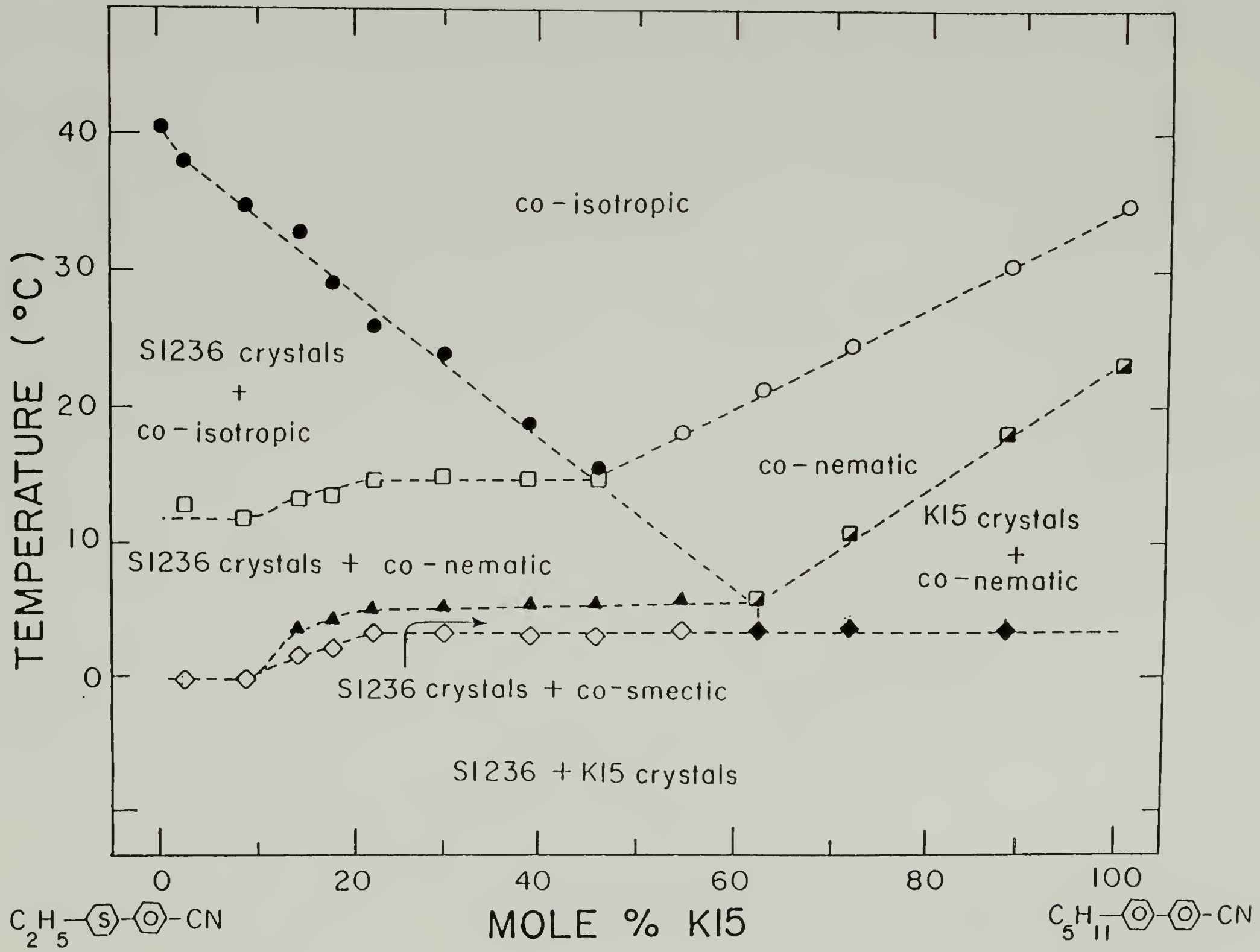
TEMPERATURE (°C)
40
30
20
10
0
co - isotropic
S1236 crystals
+
co - isotropic
co - nematic
K15 crystals
+
co - nematic
S1236 crystals + co - nematic
S1236 crystals + co - smectic
S1236 + K15 crystals
0
20
40
60
80
100
MOLE % K15
C2H5-(S)-(O)-CN
C5H11-(O)-(O)-CN

when the gross composition exceeds 22 mole % K15. We note that, at this composition, crystal and mesophase formation occur at the same temperature (i.e. ≈8°C) on cooling from the co-isotropic liquid. Thus, below 22 mole % K15, S1236 crystallizes from the co-isotropic phase; whereas, above 22 mole % K15, S1236 crystallizes from the co-nematic. We suggest the new phase, between 10 and 62 mole % K15, might be a co-smectic and do not preclude the possibility of co-crystallization for this system. However, experimental confirmation is lacking because of the small percentage of sample in this new phase (as determined by low enthalpy of melting values, < 1.5 cal/g), the narrow temperature range of it's existence and the encumbrances of sub-ambient x-ray analysis. Although co-crystallization is rare, it has been observed in systems where the two components are very similar chemically[11].

The eutectic composition contains 62 mole % K15, which compares favorably with the S-vL prediction[1-2,6] of 66 mole % K15. However, the predicted crystal transitions (T_{KI} and T_{KN}) do not agree well with experiment (see Figure 4.3). This difference is believed to be due to a non-negligible heat of mixing which is consistent with the observation of a new phase. The eutectic mixturer has a T_{NI} of 20.3°C and a co-nematic range of ≈16°C.

The transition heats for all phase changes are given in Table 4.2. These curves were constructed primarily as a means of assessing whether each mixture was fully

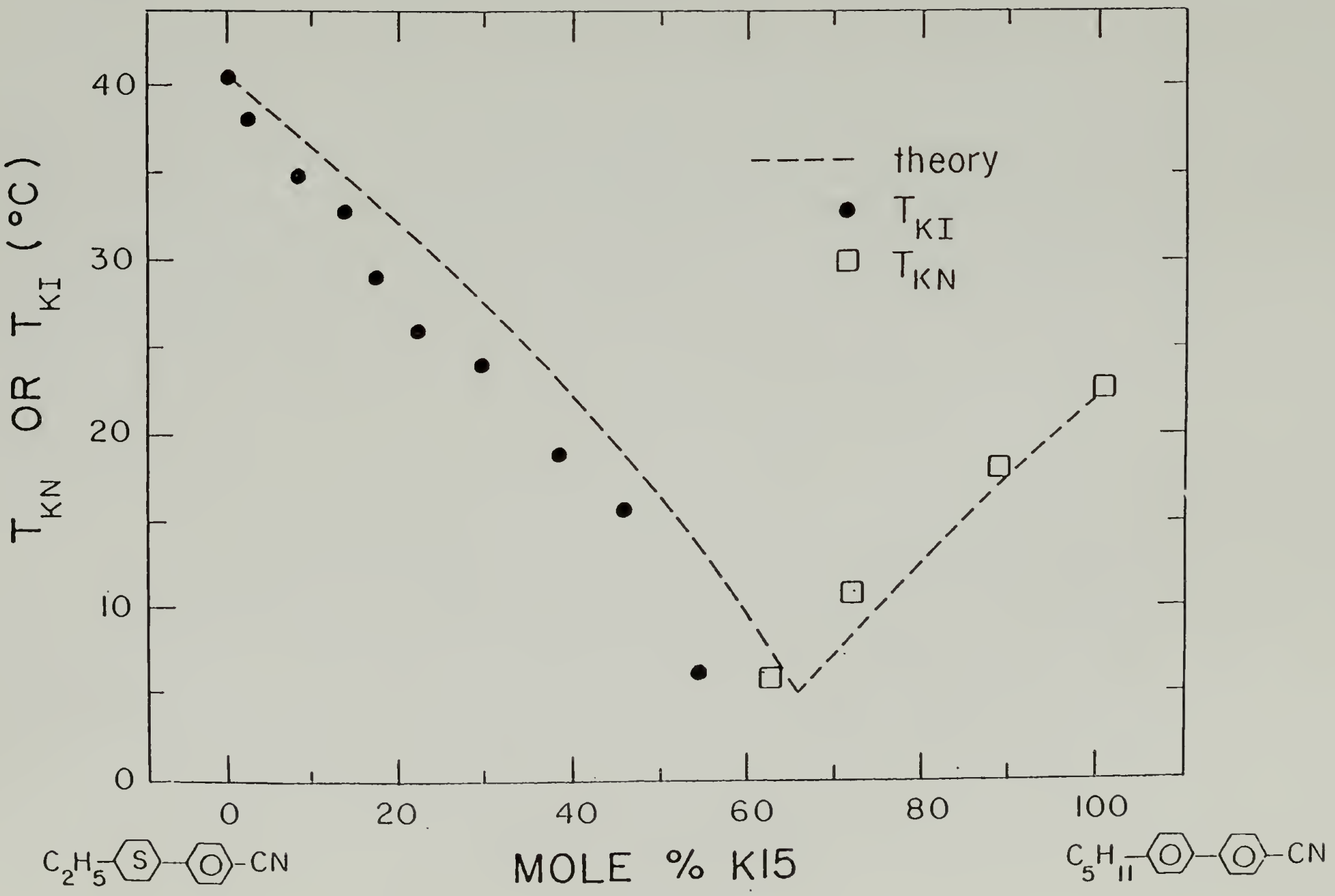

Figure 4.3 Schroder-van Laar theory versus experiment for K15/S1236 blend.

Table 4.2 Heats of transition for K15/S1236 blends.

Mole % KI5	ΔH_{KN} a) (cal/g)	ΔH_{KS} b) (cal/g)	ΔH_{SN} b) (cal/g)	ΔH_{NI} (cal/g)	ΔH_{KI} (cal/g)	ΔH_{KN} c) (cal/g)	$\Sigma \Delta H$ (cal/g)
0	—	—	—	—	24.5	—	24.5
2.3	0.4	—	—	0.04	21.3	—	21.7
8.5	2.1	—	—	0.17	19.8	—	22.0
14.0	—	3.6	0.06	0.22	18.9	—	22.8
17.5	—	4.4	0.23	0.28	14.6	—	19.0
22.1	—	6.4	0.15	0.34	13.1	—	20.0
29.4	—	7.4	0.27	0.45	11.7	—	19.8
38.5	—	9.6	0.22	0.50	8.2	—	18.5
45.6	—	9.8	0.37	0.11	4.7	—	15.0
54.3	—	14.1	1.34	0.33	—	—	15.8
62.2	0.7	14.6	?	0.46	—	0	15.8
71.4	8.4	—	—	0.54	—	6.2	15.1
88.2	3.9	—	—	0.66	—	13.8	18.4
100.0	—	—		0.70	—	15.5	16.2

a) of minor component; b) of major component; c) smectic phase is conjectural

crystallized or not and are included here for the sake of completeness. There is a discontinuity in the total heat of transition curve which occurs at a composition of 46 mole % K15. This is the composition where T_{KI} and T_{NI} lines intersect (see Figure 2).

4.3.2 N-Butylcyclohexyl-p-cyanophenyl with K15

The S1188/K15 phase diagram is shown in Figure 4.4. S1188 is a monotropic liquid crystal. Because the suppression of T_{NI} below T_{KN} is only 1-2^{o}C, the phase diagram appears similar to an ideal eutectic mixture (see Figure 4.1). However, a slight non-ideal depression occurs in the T_{NI} curve for this system.

The eutectic composition is ≈60 mole % K15, which agrees favorably with the S-vL prediction of 66 mole %. The eutectic has a T_{NI} of 32.5^{o}C and a co-nematic range of ≈27^{o}C. The transition heats are shown in Table 4.3.

4.3.3 N-Heptylcyclohexyl-p-cyanophenyl with K15

The S1115/K15 phase diagram is shown in Figure 4.5. A single co-nematic mesophase is exhibited for all compositions. Of the three systems studied, this is the only one where both components are enantiotropic. The compositional dependence of T_{NI} is almost linear, demonstrating nearly ideal eutectic behavior (Figure 4.5).

The eutectic composition of this binary system, as predicted by the S-vL equation, is 63 mole % K15. However,

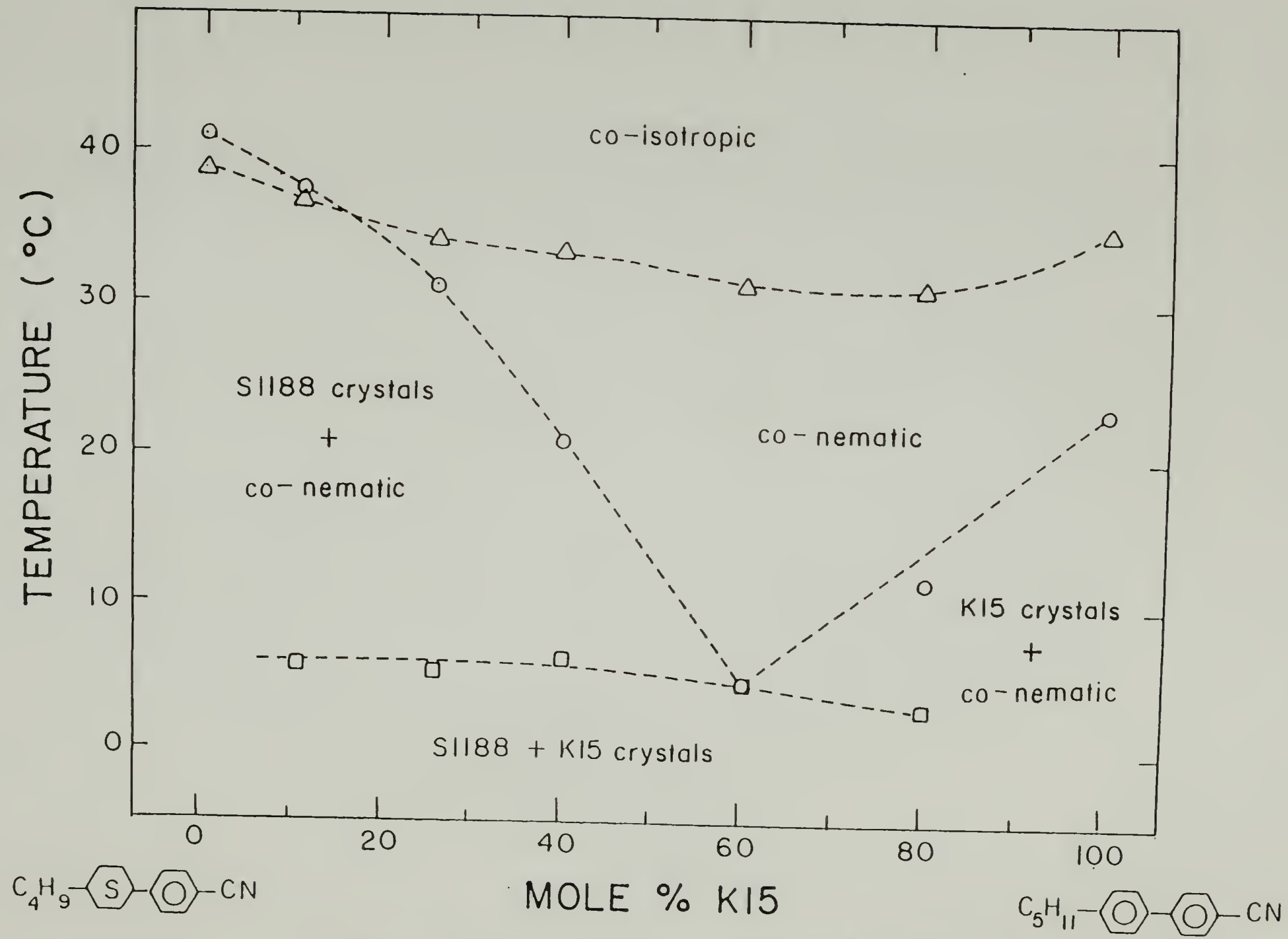

Figure 4.4 Phase diagram for K15 and S1188.

Table 4.3 Heats of transition for K15/S1188 blends.

Mole % K15	ΔK_{KN} [a] (cal/g)	ΔH_{KN} [b] (cal/g)	ΔH_{NI} (cal/g)	$\Sigma \Delta H$ (cal/g)
0	—	21.9	0.86	22.8
10.9	1.9	18.1	0.74	20.8
26.2	4.9	13.4	0.48	18.8
40.2	9.3	8.3	0.50	18.1
59.8	?	15.6	0.43	16.0
80.0	6.2	8.0	0.86	15.1
100.0	—	15.5	0.70	16.2

a) of minor component; b) of major component.

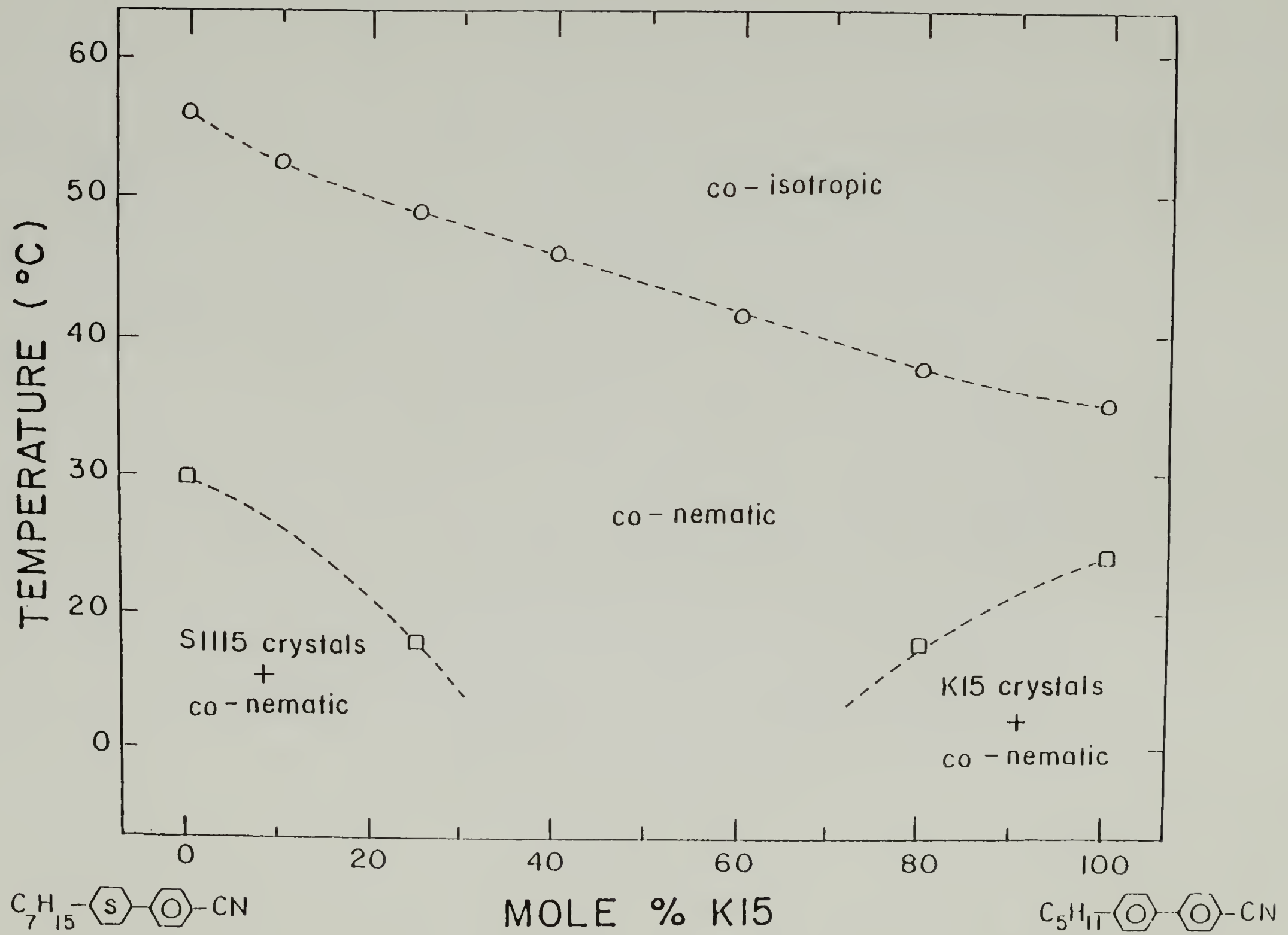

Figure 4.5 Phase diagram for K15 and S1115.

compositions between 25 and 80 mole % K15 did not crystallize after slow cooling or repeated immersion in liquid nitrogen. Thus, the eutectic composition is bracketed between 25 and 80 mole % K15. Optical microscopy revealed the 60 mole % K15 composition was still liquid crystalline at $-7^{o}C$ (the lowest temperature experimentally achievable). The nematic range of the 60 mole % K15 composition is $>40^{o}C$. T_{NI} for this composition is $41.5^{o}C$.

Only two transition heats are given for this system: ΔH_{KN} and ΔH_{NI} (see Table 4.4). This Table shows that ΔH_{NI} decreases linearly with composition of K15, while ΔH_{KN} is strongly depressed from the pure component values for intermediate compositions.

4.4 Conclusions

The phase behavior of 4-4'-n-pentylcyanobiphenyl (K15) when mixed with a second component from the homologous series, 4-[4-alkylcyclohexyl]cyanophenyl, has been explored. A broadening of the co-nematic mesophase at the eutectic composition was found for all three binary systems studied. The eutectic composition for each systems contains ≈60 mole % K15, which agrees favorably with the predictions from the S-vL theory.

The phase behavior of K15 and 4-[4-ethylcyclohexyl]-cyanophenyl is interesting. A new phase transition, not present in either of the two starting materials, was

Table 4.4 Heats of transition for K15/S1115 blends.

Mole % K15	ΔH_{KN} (cal/g)	ΔH_{NI} (cal/g)	$\Sigma \Delta H$ (cal/g)
0	22.0	1.2	23.2
10	11.5	1.1	12.6
25	8.3	0.9	9.2
40	—	0.9	0.9
60	—	0.7	0.7
80	9.7	0.6	10.3
100	15.5	0.7	16.2

demonstrated for compositions between 10 and 62 mole % K15. This new phase is believed to be a co-smectic.

4.5 References

1. D. Demus, C. Fietkau, R. Schubert and H. Kehlen, Mol. Cryst. Liq. Cryst., **25**, 215 (1972).

2. A.V. Ivashcenko, V.V. Titov and E.I. Kovshev, Mol. Cryst. Liq. Cryst., **33**, 195 (1976).

3. M. Schadt and P.R. Gerber, Z. Naturforsch., **37A**, 165 (1982).

4. K.T. Schell and R.S. Porter, Mol. Cryst. Liq. Cryst., **174**, 141 (1989).

5. J.S. Dave and K.L. Vasanth, Ind. J. Chem., **7**, 498 (1968).

6. E.C.H. Hsu and J.F. Johnson, Mol. Cryst. Liq. Cryst., **27**, 95 (1973).

7. EM Chemicals, Licristal Liquid Crystals Catalogue, p6 (1984).

8. A. Bogojawlensky and N. Winogradow, Z. Physik. Chem. (Leipzig), **60**, 433 (1907).

9. R. Walter, Ber. Deut. Chem. Ges., **58**, 2303 (1925).

10. M.A. Osman, Z. Naturforsch., **38A**, 779 (1983).

11. B. Engelen and F. Schneider, Z. Naturforsch., **33A**, 1077 (1978).

CHAPTER 5

ELECTRO-OPTICAL CHARACTERIZATION OF 60/40 BINARY MIXTURES

In the previous chapter we studied the phase behavior of n-pentylcyanobiphenyl as it was blended with 4-[4-alkyl-cyclohexyl]-cyanophenyl homologs. In this chapter, we will see how this blending modifies the electro-optical properties of n-pentylcyanobiphenyl. The electro-optical properties of interest include the response times, the dielectric and elastic constants, and the threshold voltage. These properties can all be obtained from capacitance versus time and capactitance versus voltage experiments.

5.1 Experimental

For both experiments, the nematic liquid crystal is sandwiched between two indium oxide coated glass plates. The active electrode area measured 380 mm^2 and was surrounded by a guard ring to eliminate stray capacitances. The thickness of the nematic layer was controlled between 12 and 70 microns by a spacer window.

Uniaxial rubbing of the indium oxide surfaces generated uniform, planar alignment[1] of the nematic. This orientation was confirmed by the four-fold extinction pattern of the sample when it was rotated through 360° in cross-polarized light.

All measurements were made in an inert nitrogen atmosphere with the temperature regulated to ±1°C by a

Neslab circulating water bath. The electrical resistivities of all LC samples were between 10^9 and 10^{10} ohm-cm, indicating high ionic purity.

Both C_{11} and $C_{\perp}$ were measured at 1 KHz using a Gen-Rad 1689 DigiBridge reading to an accuracy of 0.1%. This frequency was chosen because it eliminates low-frequency conduction and is the conventional frequency used when reporting the dielectric properties of nematics. The perpendicular capacitance, $C_{\perp}$, was measured using a 500 mV driving voltage. This was below the threshold voltage, V_c, of all the mixtures. Thus, molecular orientation was controlled solely by the substrate surfaces. Voltage controlled orientation was produced by increasing the test voltage above V_c. The maximum 1.275 driving voltage of the bridge was extended to 12.75V by a 10:1 operational amplifier inserted on the high side of the signal. Consequently, a voltage divider was inserted between the test cell and the bridge on the low side of the loop. The parallel capacitance, C_{11}, was taken as the capacitance of the nematic sample at 12.75V, well above the threshold voltage where the molecules are oriented nearly parallel to the field.

The capacitance values were checked by using freshly distilled toluene and known LC mixtures as reference materials. The values obtained agreed to within 4% of the standard values. The relative variation of C_{11} and $C_{\perp}$ were

measured to within ±0.5%. The absolute accuracy in capacitance measurements is believed to be ±4%.

For convenience, only the 60/40 mole percent K15/homolog mixture was chosen from each of the three binary systems studied in chapter 4. This composition is very near the eutectic composition, thus affording the largest available temperature range for the mixed nematic (see Table 5.1).

5.2 Dielectric Properties

Perhaps the single most important parameter governing the electro-optics of a nematic fluid is its dielectric anisotropy. The magnitude of this value influences the speed of the optical transition, whereas, the sign governs the cell geometry needed to achieve the desired effect. For these reasons, previous researchers have measured the dielectric properties of various nematic compounds[2-4].

The parallel and perpendicular dielectric constants, ϵ_{11} and $\epsilon_{\perp}$, can be calculated from the capacitance measurements of oriented samples using the definitions:

$$\epsilon_{11} = C_{11}/C_o \qquad (5.1)$$

$$\epsilon_{\perp} = C_{\perp}/C_o \qquad (5.2)$$

where C_o is the capacitance of the empty cell and C_{11} and $C_{\perp}$ have been defined above.

Table 5.1 Composition and thermal properties of the eutectic for three binary systems as compared to pure K15.

	Eutectic Composition		Property of Eutectic Mixture		
Binary System	(Mole % K15) EXPT	S-vL	T_{KN} (^{o}C)	T_{NI} (^{o}C)	$T_{NI}-T_{KN}$ (^{o}C)
K15	--	--	22.3	35.1	12.8
K15/S1236	62	66	5.8	21.6	15.8
K15/S1188	60	66	5.8	32.5	26.7
K15/S1115	40<x<80	63	---	41.5	>41.5

5.2.1 Effect of Temperature

The principal dielectric constants of pure K15 and three binary mixtures of K15 with a second nematic are plotted as a function of temperature in Figures 5.1-5.4. The average value of the dielectric constant, $\bar{\epsilon} = ([\epsilon_{11} + 2\epsilon_{\perp}] /3)$, is calculated from the measured values of ϵ_{11} and $\epsilon_{\perp}$ in the nematic phase and is also shown in the Figures (solid line). For direct comparison, the dielectric constant of the isotropic phase, ϵ_{is}, has been extrapolated into the nematic phase (broken line).

Our values of ϵ_{11} and $\epsilon_{\perp}$ for K15 are consistently 4% to 7% higher than those of Ratna and Shashidar[5]. This difference is believed to be due to a systematic error between the two sets of measurements. From Figures 5.1-5.4 it can be seen that the dielectric constant along the nematic director (ϵ_{11}) is about twice that in the transverse direction ($\epsilon_{\perp}$). This large dielectric anisotropy is due to the highly polar cyano end-group which lies in the director axis. The dipole moment of this moiety, as given by Minkin et al.[6], is 4.05 D. We also note that $\bar{\epsilon}$ in the nematic phase is always less than the extrapolated value of ϵ_{is} (with the single exception of the K15/S1188 mixture). Similar results have been observed by others in the case of highly polar compounds[5,7]. (This is in contrast to the behavior of non-polar molecules wherein it has been experimentally observed that $\bar{\epsilon}$ and ϵ_{is} coincide at T_{NI}[8]). Also, it is seen that $\bar{\epsilon}$ decreases as temperature decreases. These facts are in

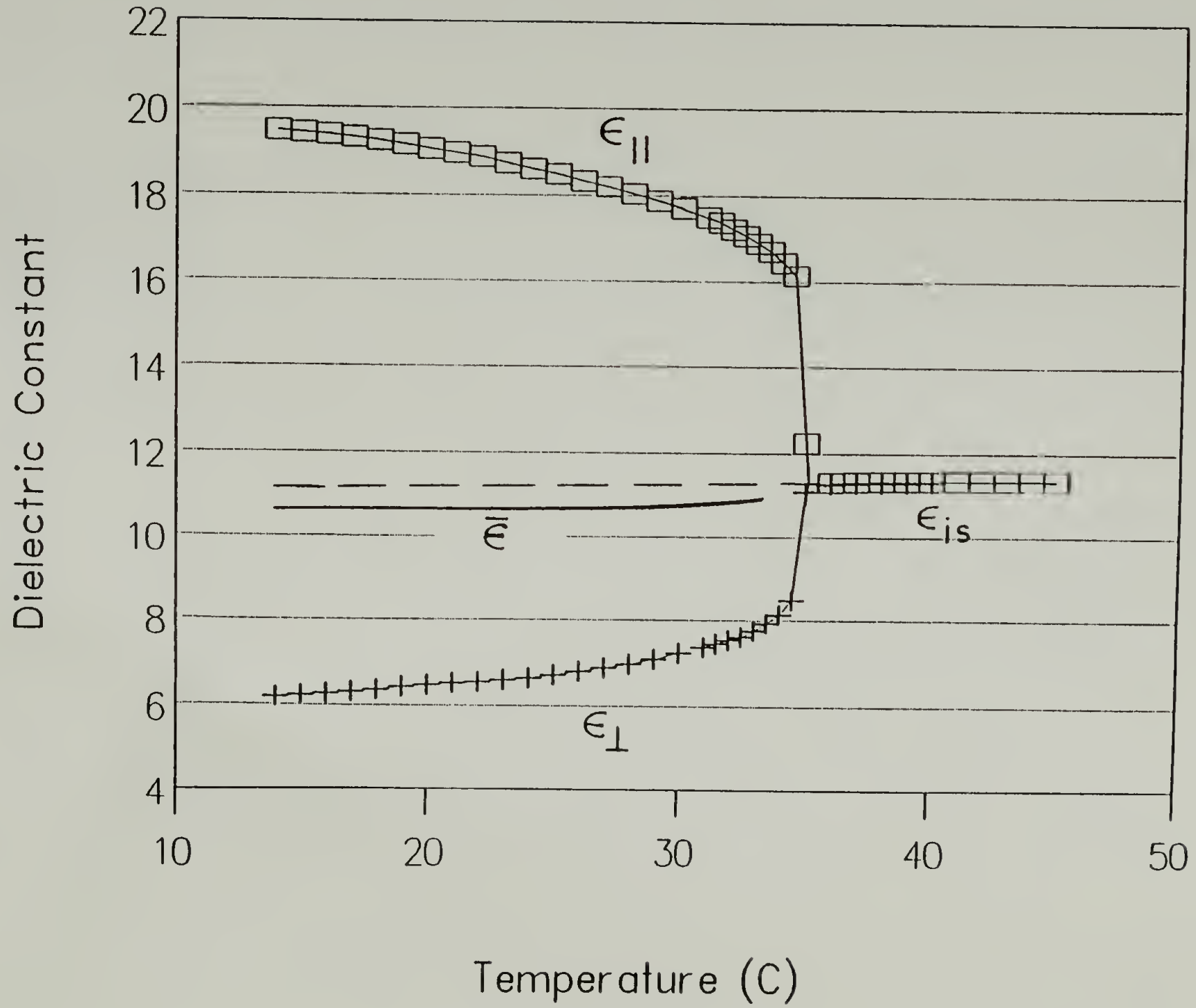

Figure 5.1. Dielectric constant of K15 as a function of temperature.

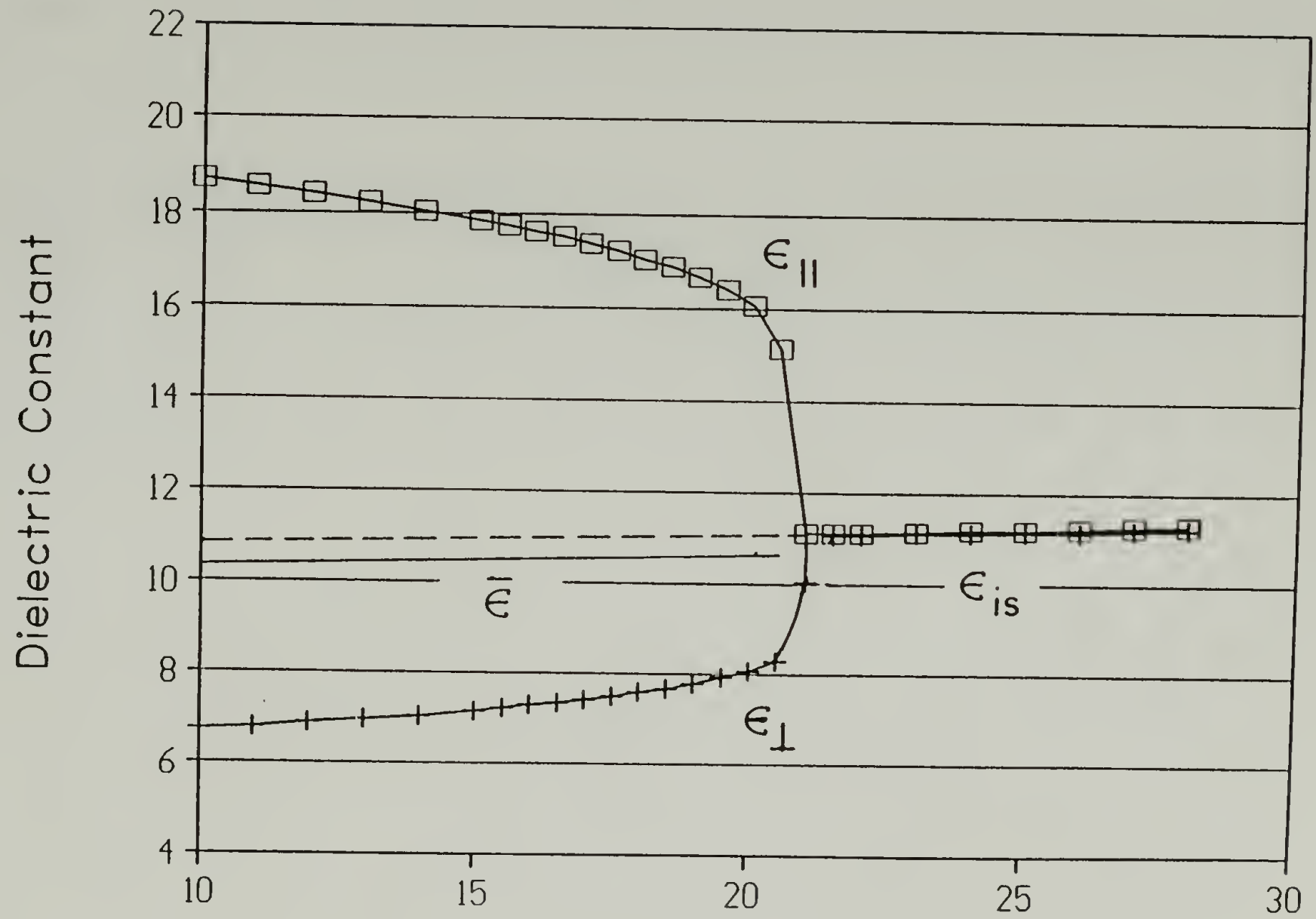

Figure 5.2. Dielectric constant of 60/40 mole percent mixture of K15/S1236 as a function of temperture.

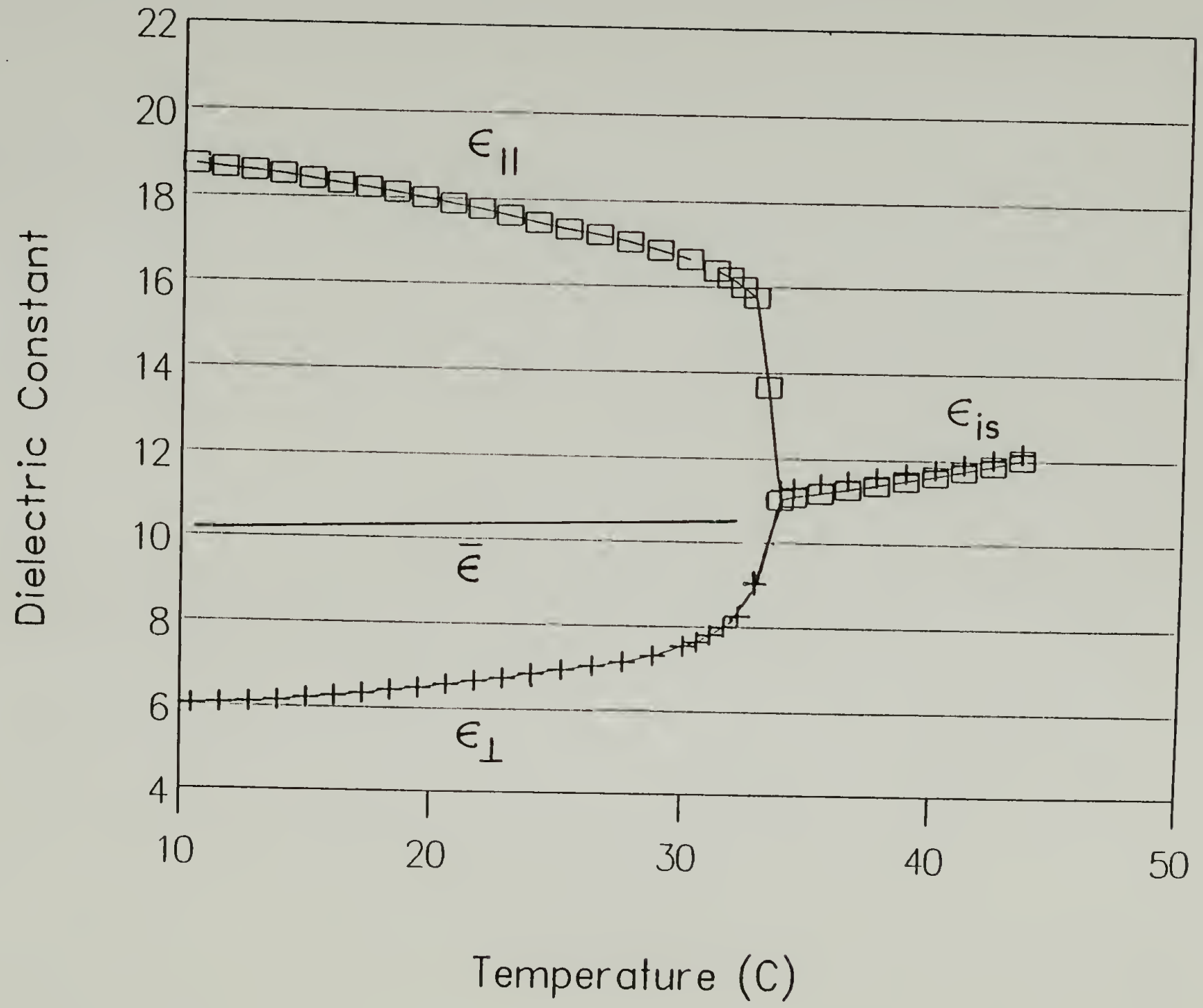

Figure 5.3. Dielectric constant of 60/40 mole percent mixture of K15/S1188 as a function of temperture.

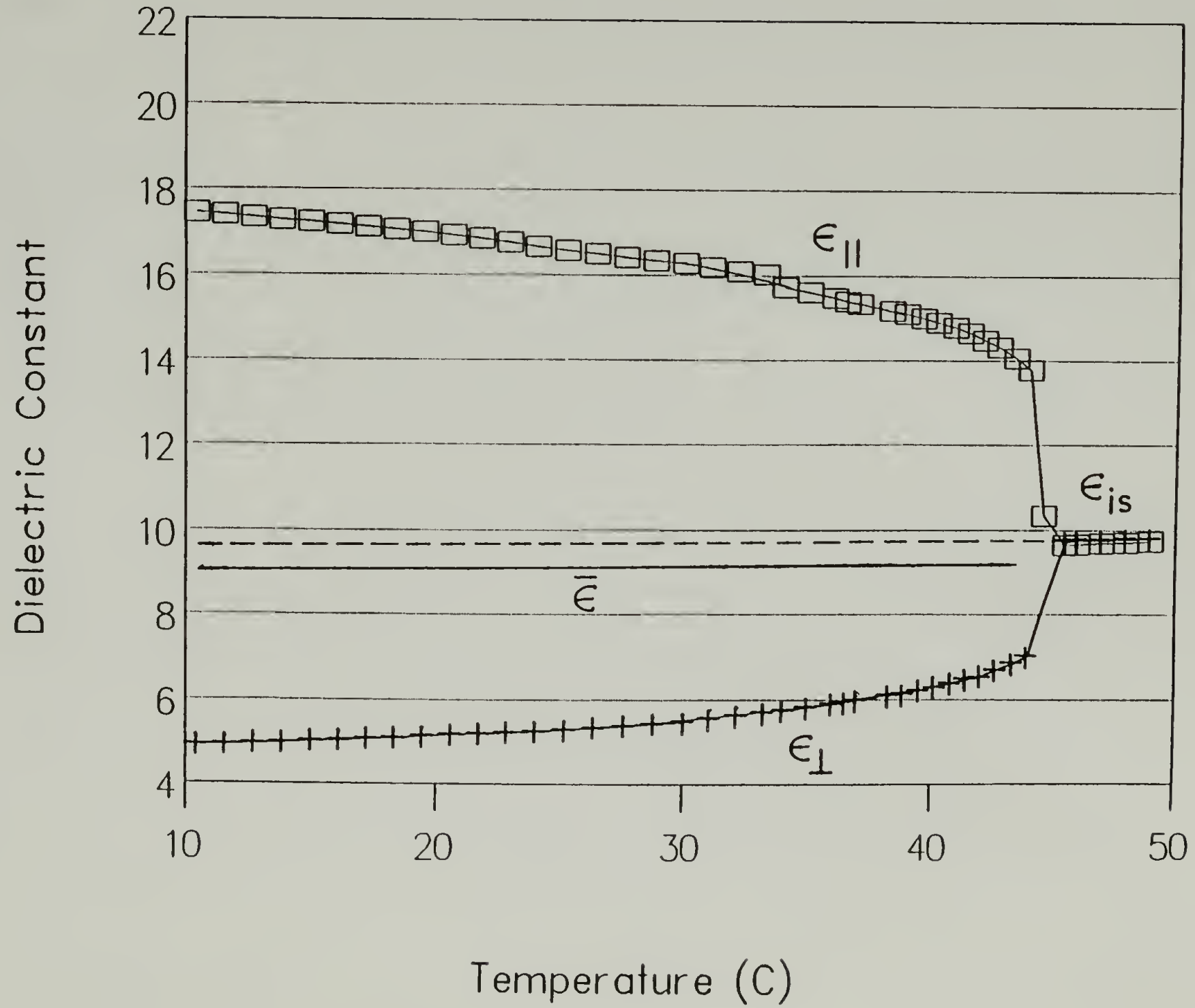

Figure 5.4. Dielectric constant of 60/40 mole percent mixture of K15/S1115 as a function of temperture.

conformity with the predictions of the statistical model of antiferroelectric short range order in nematic liquid crystals composed of polar molecules proposed by Madhusudana and Chandrasekhar[9-10]. According to this theory $\bar{\epsilon}$ should increase on going over from the nematic to the isotropic phase due to a decrease in the antiparallel correlation at the transition.

5.2.2 Effect of Composition

In Figure 5.5, the dielectric anisotropy $\Delta\epsilon$ is plotted as a function of the sub-clearing temperature, defined as $T-T_{NI}$, for the four nematic systems. One single component and three binary nematic mixtures are represented. From this Figure, the effect of adding 40 mole % of a second nematic liquid crystal on the $\Delta\epsilon$ of K15 can be seen. The trend is the same for all four fluids; $\Delta\epsilon$ decreases monotonically as $T-T_{NI}$ approaches 0.

Figure 5.5 also shows the relative ordering of $\Delta\epsilon$ for all equivalent sub-clearing temperatures to be: K15 > K15/S1236 > K15/S1188 > K15/S1115. This result was unexpected. A simple rule of mixtures states that $\Delta\epsilon$ of a binary mixture will equal the linear weighted average of the two pure components[11]. Table 5.2 shows the $\Delta\epsilon$ of S1236 to be higher than that of K15. Thus, the dielectric anisotropy of any K15/S1236 mixture is expected to be higher than that of pure K15. This anomalous result may be a consequence of the

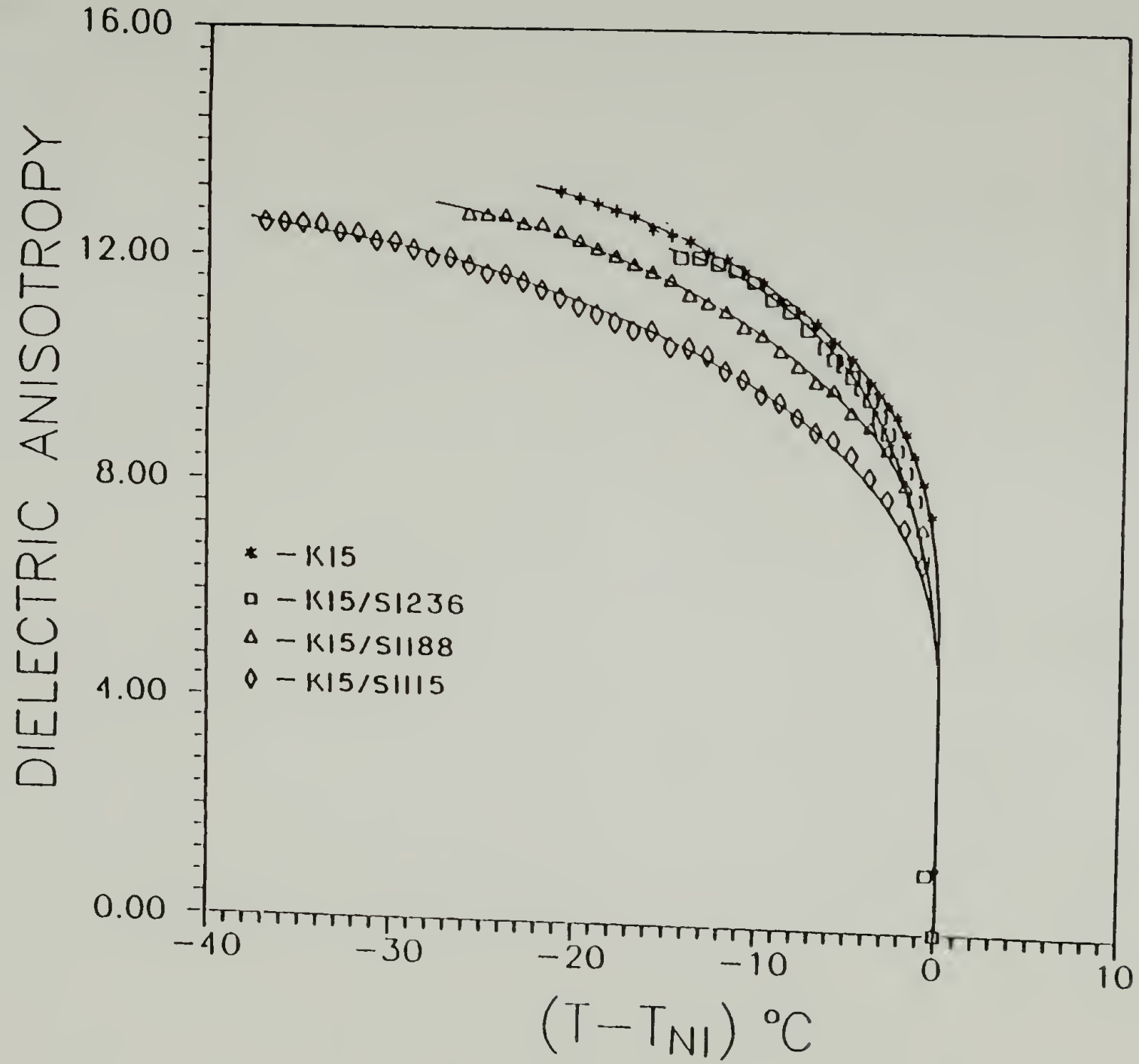

Figure 5.5. Dielectric anisotropy of four nematic fluids plotted as a function of sub-clearing temperture. * — K15, □ — K15/S1236, △ — K15/S1188, ◊ — K15/S1115.

Table 5.2 Dielectric anisotropy for four pure nematic liquid crystals; [a] our measurements at 26°C, [b] EM catalog value (temperature not specified).

Pure Nematic	Dielectric Anisotropy
K15	11.5[a]
S1236	13.7[b]
S1188	11.2[b]
S1115	8.2[b]

uncertainty in the temperature for which $\Delta\epsilon$ is reported for the pure homologs may explain . Because S1236 and S1188 are monotropic, $\Delta\epsilon$ must be determined by an extrapolation procedure rather than direct measurement. Among the binary mixtures, however, the dielectric anisotropy has the expected order, i.e. K15/S1236 > K15/S1188 > K15/S1115.

5.3 Response Time

For practical purposes, the speed of the orientation process is important. In classifying the kinetics of orientation, three values of particular interest are: 1) the delay time, t_D; 2) the rise time, t_r; and 3) the decay time, t_d. These values are defined graphically in Figure 5.6.

The time interval between the application of a voltage and the first sign of change in the measured property (e.g. capacitance) is called the delay time. The rise time is defined as that length of time required for the capacitance to rise from 10% to 90% of the total change in capacitance ($C_\infty - C_o$). And the decay time is defined as the length of time taken for the capacitance of an electrically oriented cell to decay to 10% of its initial equilibrium value.

For a Freedericksz's-type splay deformation, Robert, Labrunie and Borel[12] give the relationships:

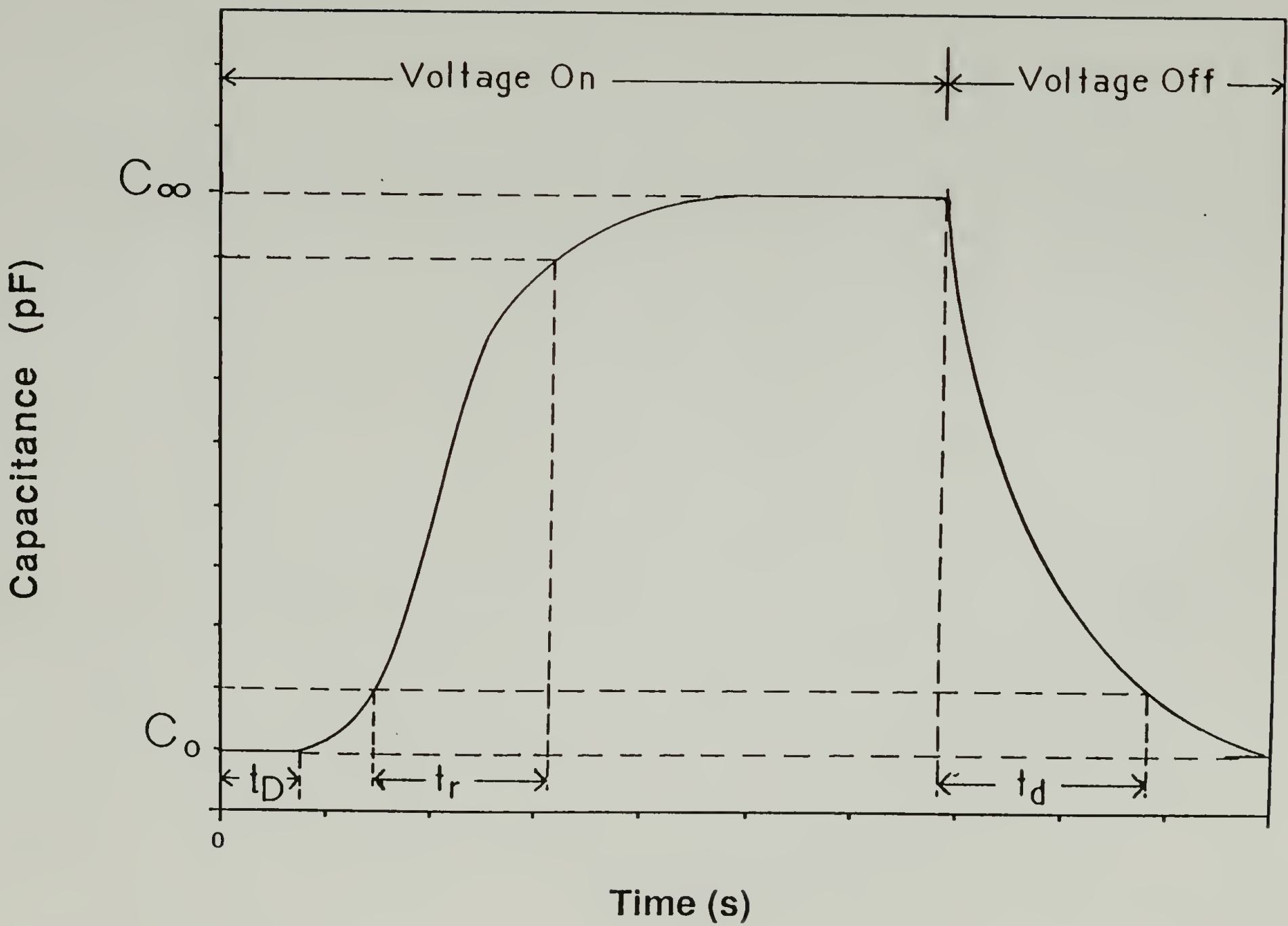

Figure 5.6. Graphical description of response times: t_D, t_r , and t_d .

$$t_d = \gamma_1 d^2/\pi^2 K_{11} \qquad (5.3)$$

$$t_r = \gamma_1 d^2/K_{11}\pi^2[(V/V_c)^2 - 1] \qquad (5.4)$$

where, γ_1 is the rotational viscosity, d is the layer thickness, V is the voltage and K_{11} is the splay elastic constant. No theoretical treatment for the delay time is known.

5.3.1 Effect of Voltage

Figure 5.7 shows the effect of voltage on the three response times defined above. From the Figure, it can be seen that the decay time is independent of voltage as expected from equation (5.3). The delay time and rise time both decrease with increasing voltage. Such a trend is expected for t_r from equation (5.4). However, this equation over estimates our experimentally measured rise time by a factor of 2 or 3.

Empirically, both the delay and rise times fit an equation of the type:

$$\text{Response Time} = A * \text{Voltage}^{X} \qquad (5.5)$$

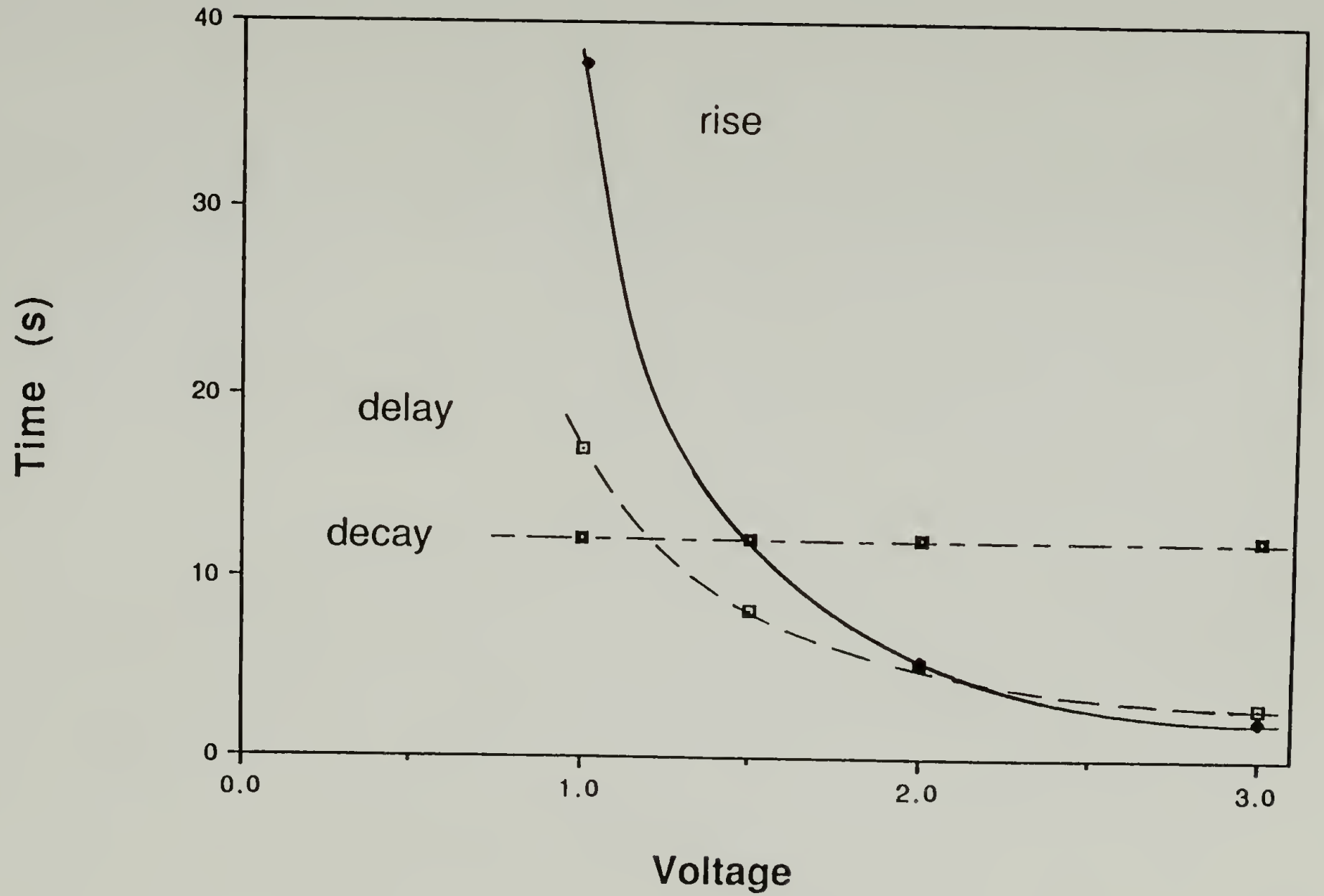

Figure 5.7. Effect of voltage on the response times of a 67 micron layer of K15 at 20°C.

where A is the front-factor and x is an exponent. The data of Table 5.3 shows the rise time is more sensitive to voltage than the dwell time due to the higher magnitude of both the front-factor and the the exponent.

5.3.2 Effect of Temperature

All three response times decrease with increasing temperature (see Figure 5.8). From equations (5.3) and (5.4), we see that the rise and decay times depend on the rotational viscosity of the nematic. The viscosity of the nematic is also temperature dependent, decreasing as temperature increases[13]. Thus, the decline in the response times are attributed principly to the decrease in the viscosity with temperature. The rise time decreases with temperature more rapidily than the decay time because the threshold voltage also decreases with temperature.

5.3.3 Effect of Layer Thickness

Figure 5.9 shows the effect of layer thickness on the response times while temperature and voltage are held constant. Using a 1 volt signal, t_D, t_r and t_d for a 12 micron layer at 14^{o}C were all found to be less than 3 seconds. Under the same conditions for a 67 micron layer, the t_D and t_d were $\approx$ 15 seconds while t_r was $\approx$ 50 seconds. Thus, thin layers orient faster than thick ones. The rise time is also found to be more sensitive to layer thickness than either the delay or decay times.

Table 5.3 A and x parameters for K15 in a 67 micron cell at 20°C.

Response Time	A	x
Delay Time	16.2	-1.6
Rise Time	36.7	-2.6

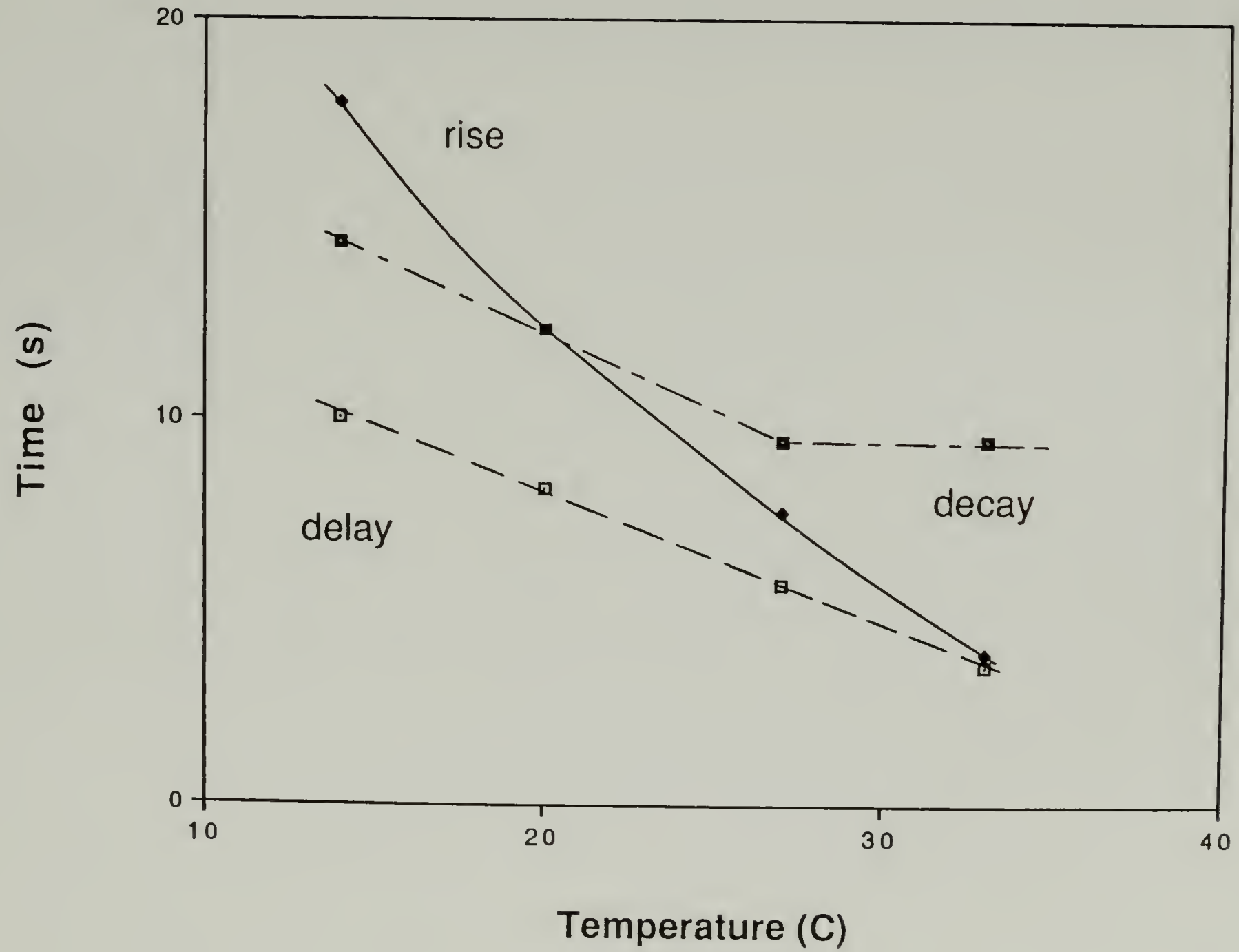

Figure 5.8. Effect of temperature on response times of K15. Layer thickness = 67 microns, V = 1.5 volts.

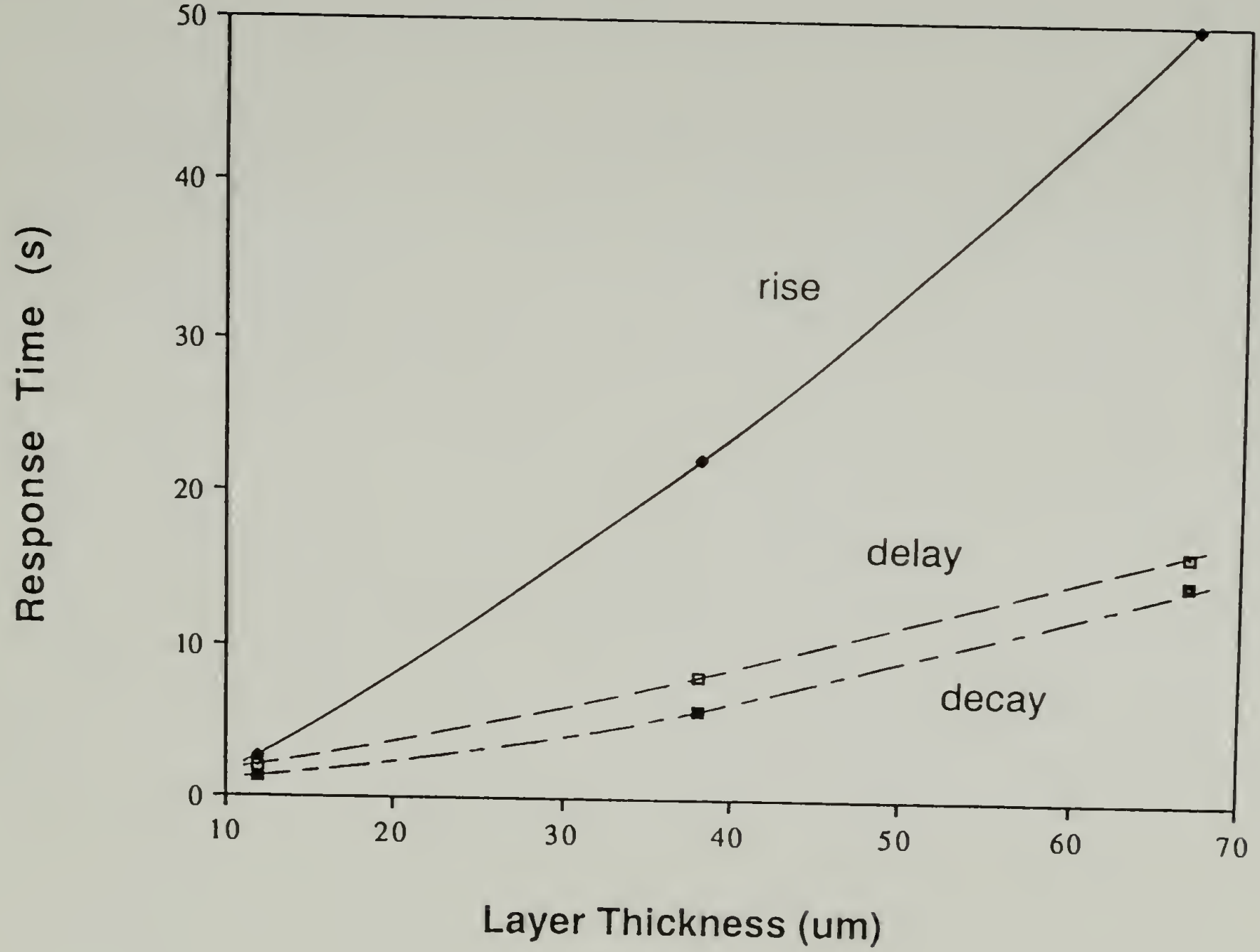

Figure 5.9. Effect of layer thickness on the response times of K15 at 14°C. V = 1.0 volts.

5.3.4 Effect of Blending

From the 60/40 blends of n-pentylcyanobiphenyl with members of a homologous series, it is possible to see the effect of the second component on the physical properties of pure n-pentylcyanobiphenyl.

Ignoring any intermolecular interactions between the mixed chemical classes, we consider the effect of the average molecular length of the nematic on the decay time. (The decay time was chosen because it is independent of the dielectric properties of the mixed nematic, whereas, t_D and t_r are not.)

10.9, 13.4, 17.2 and 15.7 A were used as the molecular lengths for S1236, S1188, S1115 and K15 respectively. The average molecular length of the 60/40 mole % mixtures were calculated as the linear weighted average. Figure 5.10 shows the decay time plotted against this average length at a constant sub-clearing of $-7^{o}C$. The Figure shows the decay time decreases significantly as the average length of the molecule increases. This is explained as an increase in the elastic constant of the mixed nematic with increasing molecular length.

Figure 5.11 shows t_D and t_r plotted as a function of the dielectric anisotropy of the mixture for a constant sub-clearing temperature of $-7^{o}C$. From the Figure, t_D and t_r appear independent of the dielectric anisotropy. This result was not anticipated. One would expect the rise time to decrease as $\Delta\epsilon$ increases due to a lowering of V_c (see

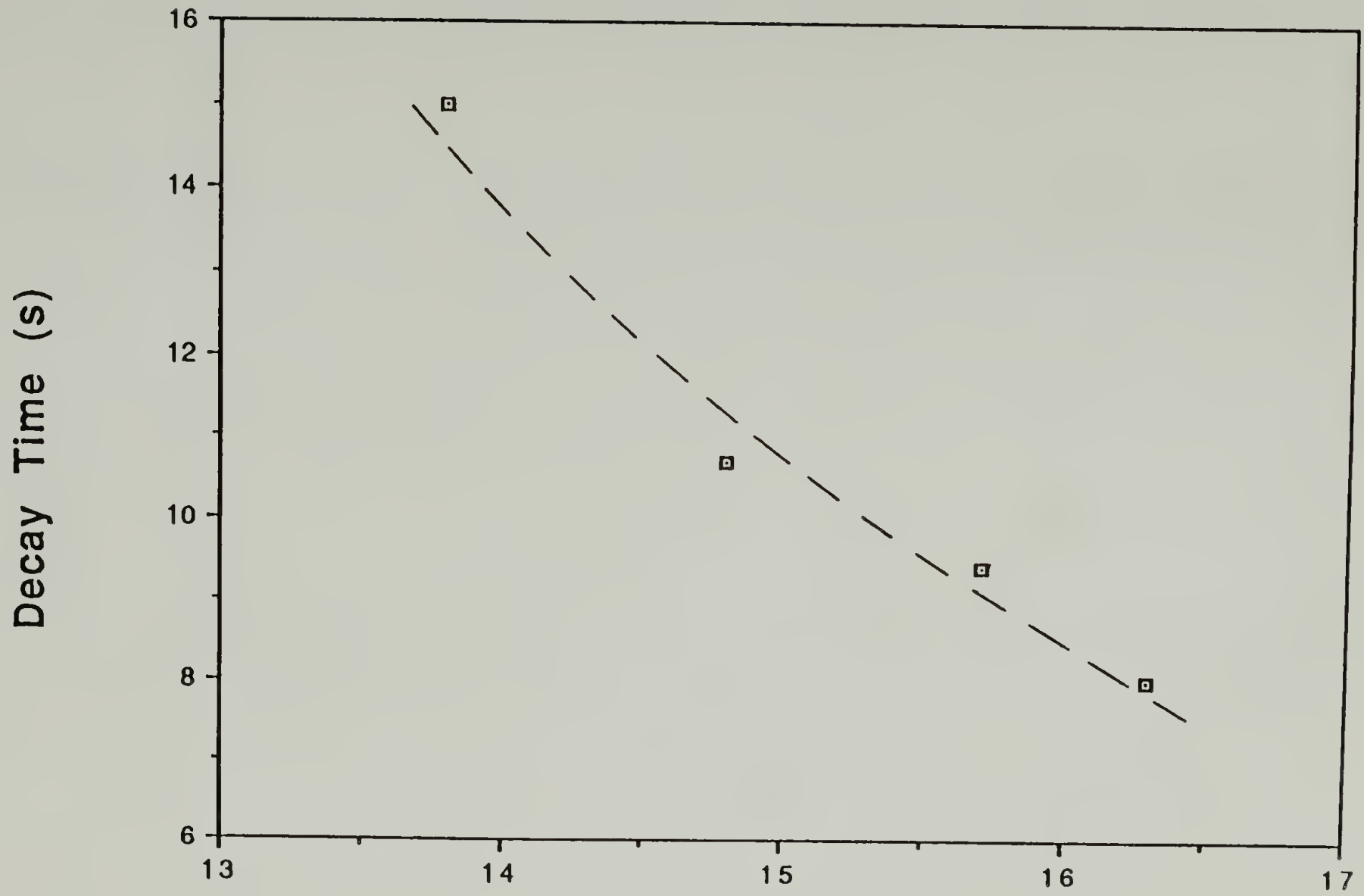

Figure 5.10. Effect of average molecular length on the decay time of four nematic fluids. Temperature = $(T_{NI}-7)^{o}C$, layer thickness = 67 microns.

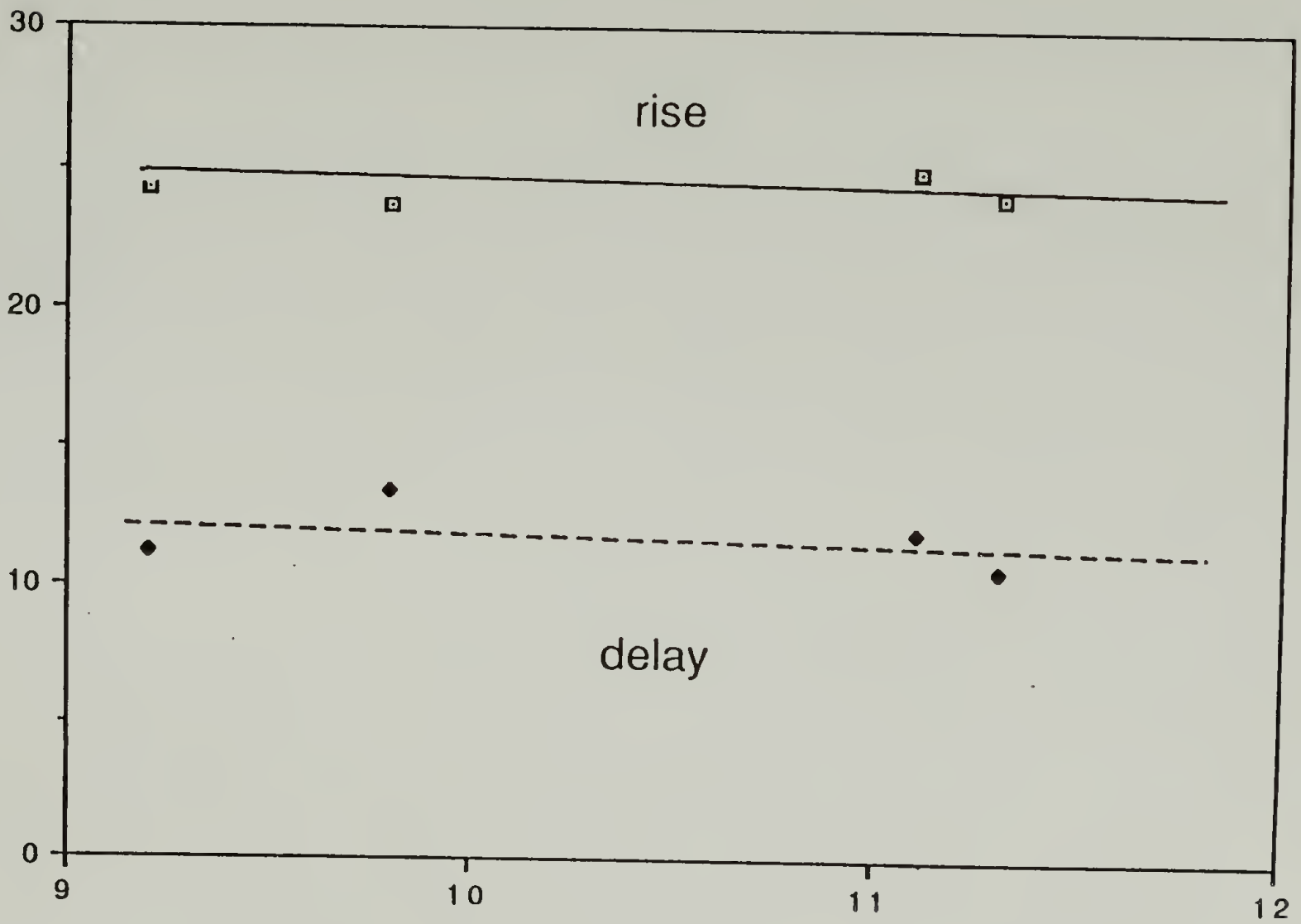

Figure 5.11. Effect of dielectric anisotropy on the rise and delay times of four nematic fluids. Temperature = $(T_{NI}- 7)^{o}C$, layer thickness = 67 microns.

equation 5.9). Apparently, the viscosities of the mixtures decrease as the dielectric anisotropy increases. The combined effect of these two influences are somewhat offsetting, thus keeping the rise time nearly constant.

5.4 Elastic Constants

The elastic constants of a nematic liquid crystal describe its propensity to return to an undeformed state when the deforming stress is removed. A uniformly oriented nematic can be deformed in one of three principle modes. These are the splay, twist and bend modes shown in Figure 5.12. The amount of energy consumed per unit volume by each deformation mode is given by one of the three terms on the left-hand side of the equation:

$$F_d = \tfrac{1}{2}K_{11}(\text{div } \mathbf{n})^2 + \tfrac{1}{2}K_{22}(\mathbf{n} \cdot \text{curl } \mathbf{n})^2 + \tfrac{1}{2}K_{33}(\mathbf{n} \times \text{curl } \mathbf{n})^2 \qquad (5.6)$$

In this equation, F_d is the total distortion-energy/unit volume of the system and K_{11}, K_{22} and K_{33} are the splay twist and bend elastic constants, respectively. Thus, for a complete energy balance of a deformed nematic, information about the elastic constants is essential.

5.4.1 Theory

The theory of electrical deformation for a nematic has been worked out. By minimizing the sum of the elastic and dielectric free energies, Deuling[14] derived expressions for

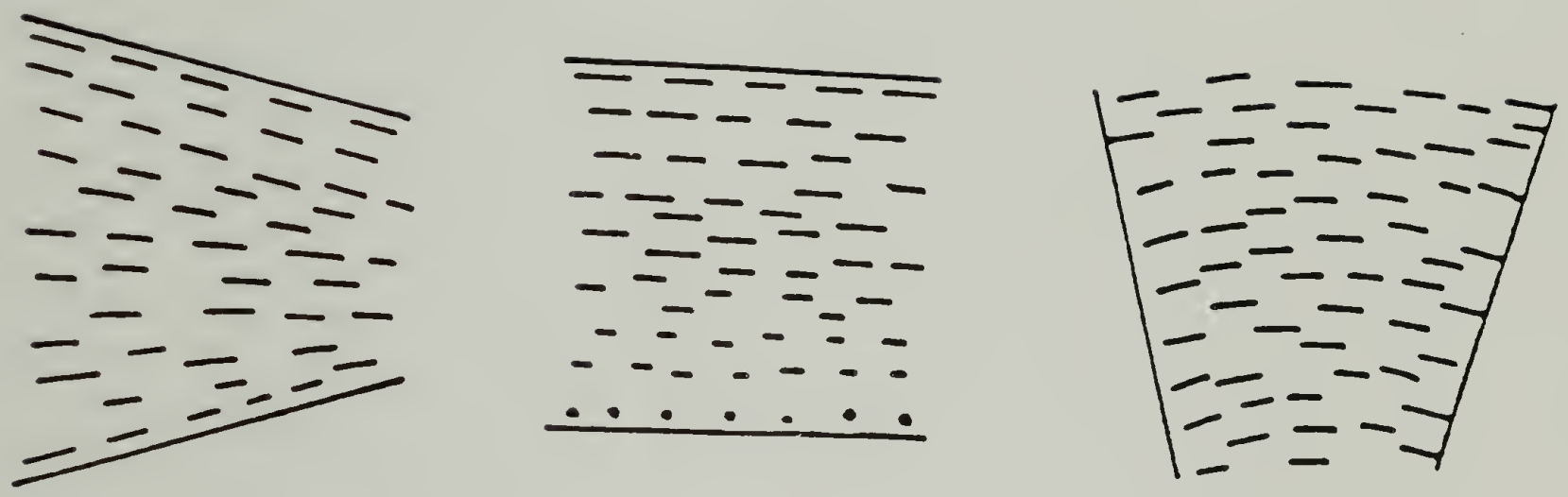

Figure 5.12. The three principle deformation modes of a nematic liquid crystal: a) splay, b) twist and c) bend.

director orientation and birefringence of a thin nematic layer. For capacitance versus voltage experiments, Maze[15] has modified Deuling's results and gives the relevant equations, in integral form, as:

$$V = \frac{2}{\sqrt{\varepsilon_o}} \int_{\theta_o}^{\theta_m} \frac{d\theta}{E(\theta)\sqrt{F(\theta)}} \qquad (5.7)$$

$$C_C = 2\,\varepsilon_o \left(\frac{A}{d}\right) \int_{\theta_o}^{\theta_m} \frac{E(\theta)\,d\theta}{\sqrt{F(\theta)}} \Bigg/ \int_{\theta_o}^{\theta_m} \frac{d\theta}{\sqrt{F(\theta)}} \qquad (5.8)$$

with the following definitions and symbols:

$F(\Theta) = \{E(\Theta)^{-1} - E(\Theta_m)^{-1}\}K(\Theta)^{-1}$

$E(\Theta) = \epsilon_{\parallel} \sin^2\Theta + \epsilon_{\perp} \cos^2\Theta$

$K(\Theta) = K_{11}\cos^2\Theta + K_{33}\sin^2\Theta$

Θ_o, Θ_m = director tilt angles at z = 0, d/2 respectively

(A/d) = cell area/thickness ratio

K_{11}, K_{33} = splay and bend elastic constants

ϵ_{11}, $\epsilon_{\perp}$ = parallel and perpendicular dielectric constants

$\epsilon_o = 8.854 \times 10^{-12}$ farads/meter

V = applied voltage

Thus, for any given voltage, equations (5.7) and (5.8) define a unique z-dependent orientation profile and a capacitance value for the nematic layer. These equations can be solved numerically. The elastic constants K_{11} and K_{33} are

found by adjusting these parameters to yield the best fit between the experimental C-V data and theory.

5.4.2 Effect of Temperature

The elastic constants of K15 versus $T-T_{NI}$ are shown in Figure 5.13. Our data compare well with that of previous workers[16-17] which are also shown. As the temperature approaches the clearing point, the elastic constants decrease, by as much as a factor of two. Note also that the bend constant is higher than that for splay.

5.4.3 Effect of Blending

Figures 5.14 and 5.15 show how the elastic properties of K15 are modified when it is blended with 40 mole % of a 4-[4-alkylcyclohexyl]cyanophenyl homolog. These Figures show that adding S1115 to K15 serves to increase the splay and bend constants of the mixture. Adding the same amount of S1188 and S1236 lowers K_{11} and K_{33} of K15. From these results, we infer the magnitude of the elastic constants, for the pure nematic substances, has the following order: S1115 > K15 > S1188 > S1236. Note that among the members of the homologous series, this ordering correlates well with the length of the alkyl tail.

5.5 Threshold Voltage

The threshold voltage, V_C, is the minimum voltage needed to overcome the elastic forces of the mesophase and,

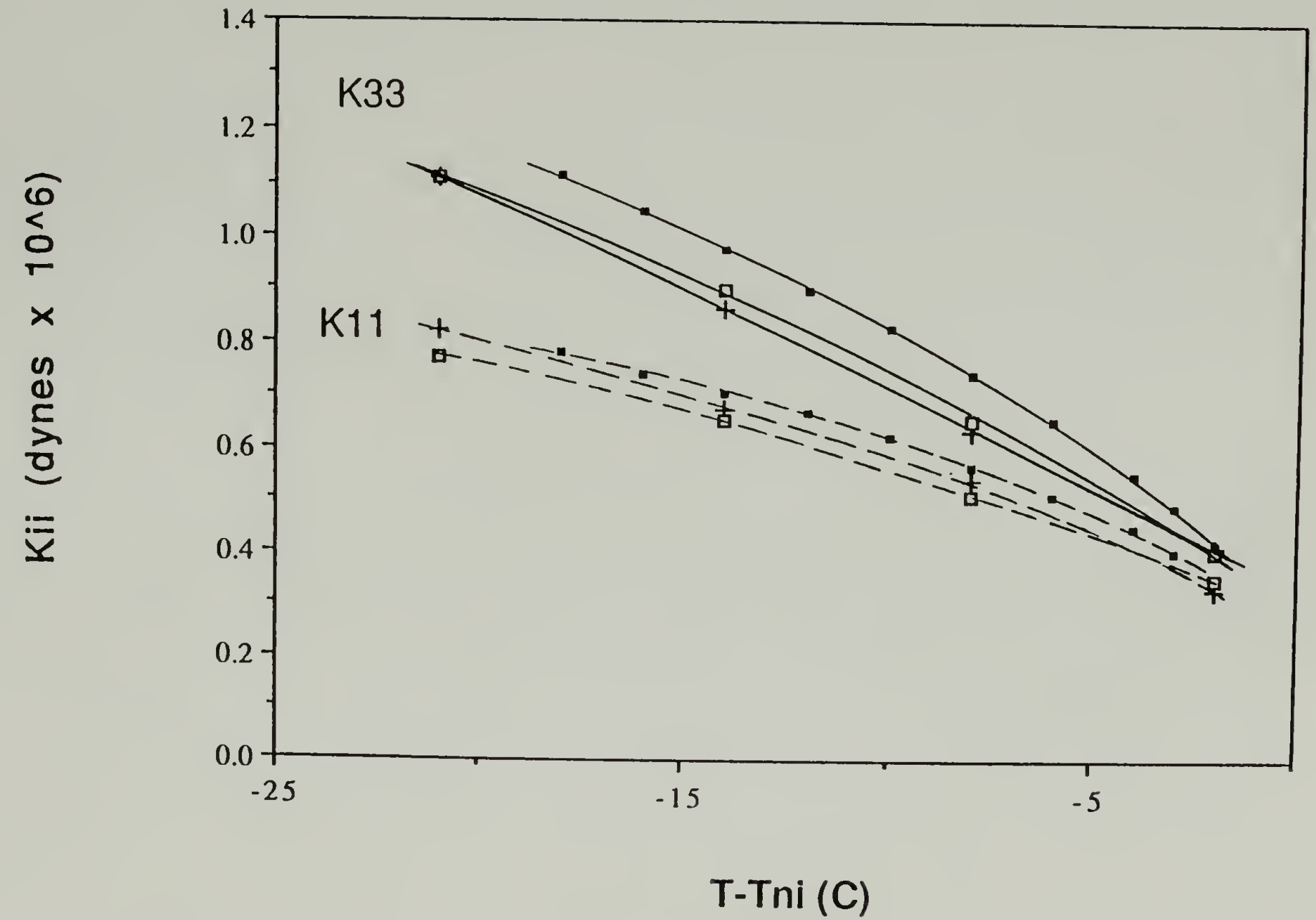

Figure 5.13. Splay, K11, and bend, K33, elastic constants of K15 as compared with the literature. + this work, ▪ - Bradshaw, ▫ - Bunning.

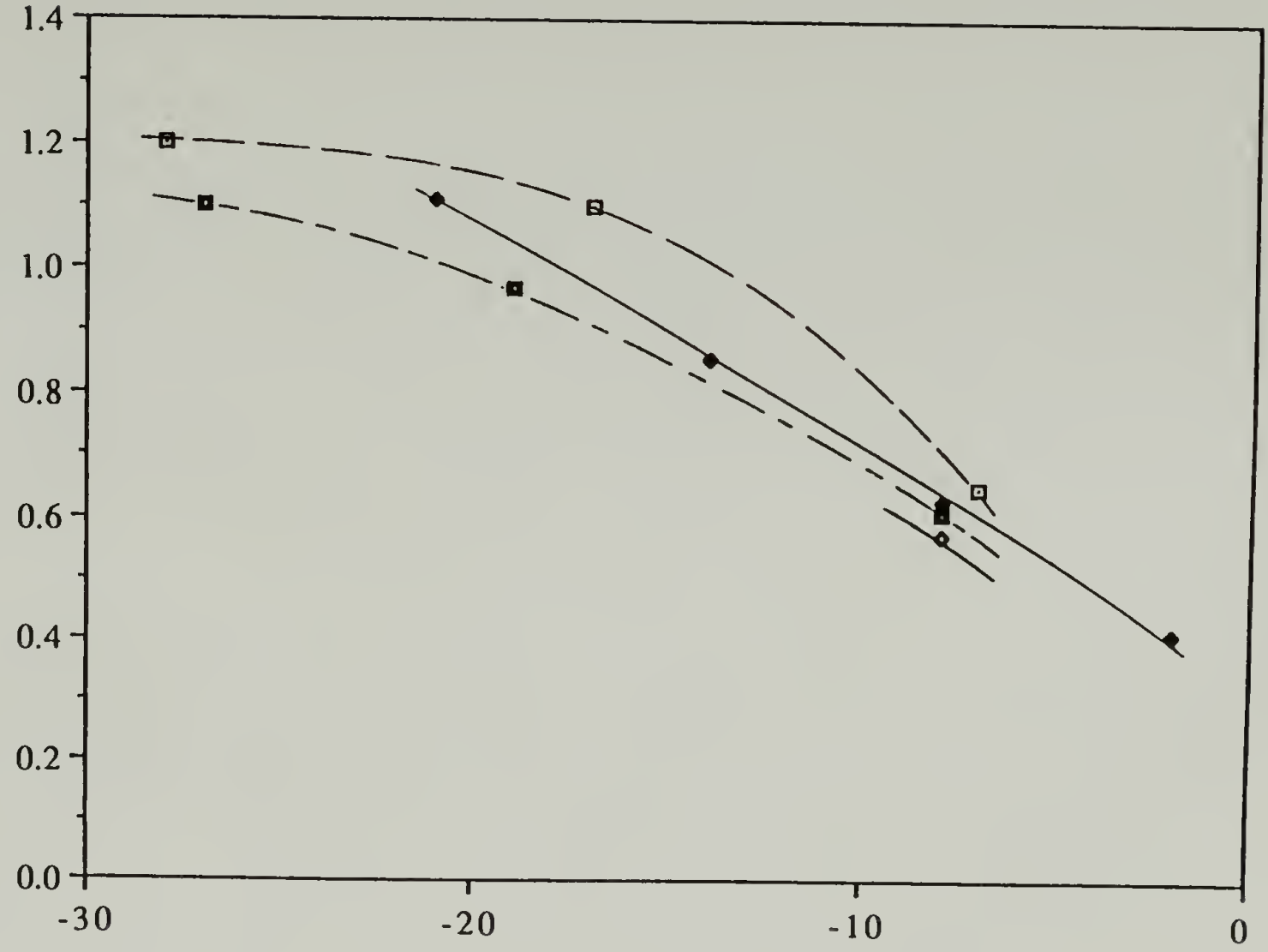

Figure 5.14. Bend elastic constant versus sub-clearing temperature for four nematic fluids. ⊡-K15/S1115, ◆-K15, ◘-K15/S1188, ◈-K15/S1236

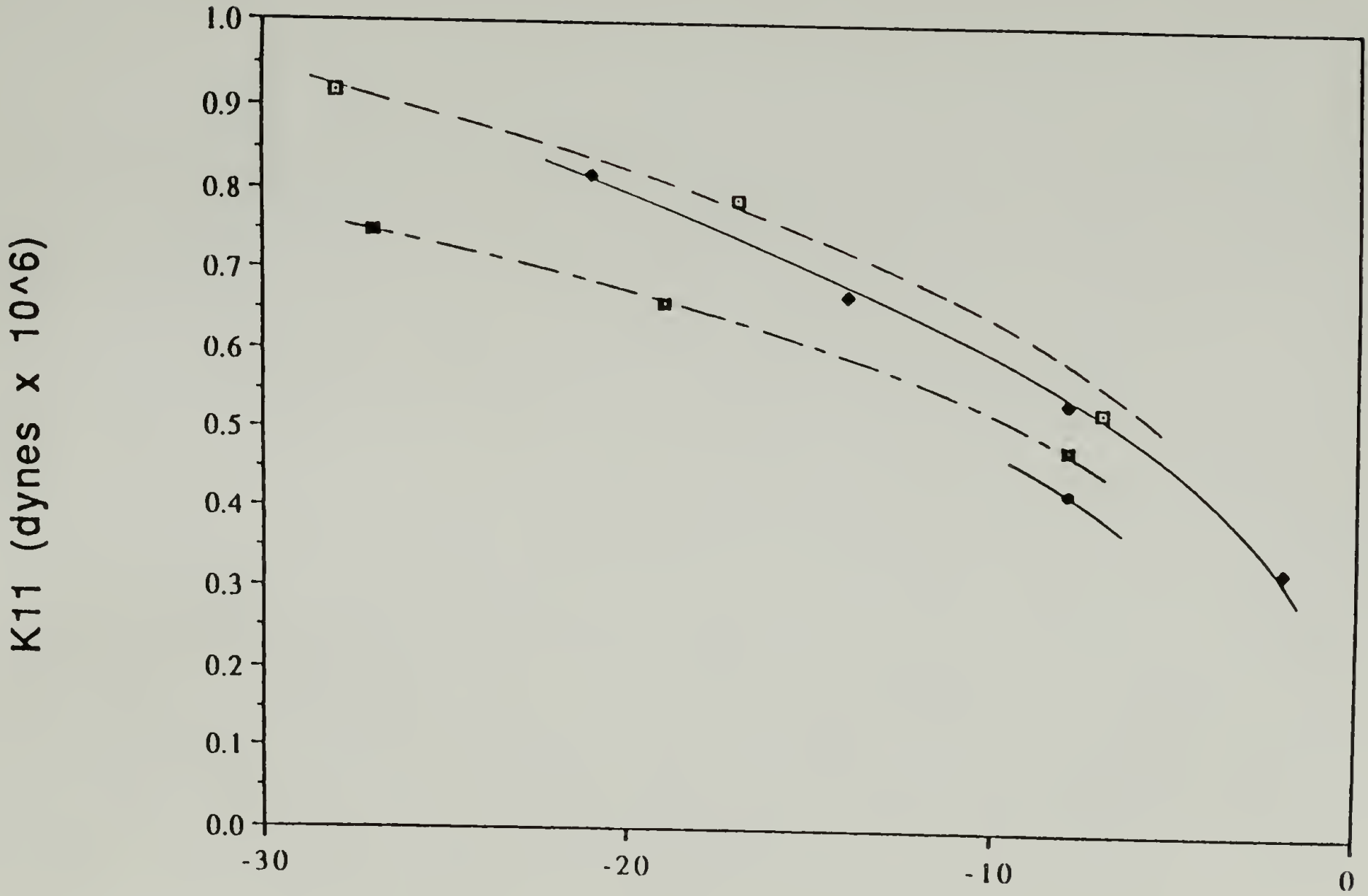

Figure 5.15. Splay elastic constant versus sub-clearing temperature for four nematic fluids. ◘ - K15/S1115, ◆ - K15, ◘ - K15/S1188, ◆ - K15/S1236

hence, produce electrical orientation of the molecules. Thus, in a capacitance versus voltage experiment, it is the voltage where the capacitance of an undeformed nematic first begins to respond to the applied field. From theoretical considerations, the threshold voltage for a splay-type deformation is given by:

$$V_c = \pi\sqrt{K_{11}/\Delta\epsilon\epsilon_o} \qquad (5.9)$$

where all the terms have been previously defined.

In Figure 5.16, V_c is plotted against $\sqrt{K_{11}/\Delta\epsilon\epsilon_o}$. From equation (5.9), a straight line plot with a slope of π is expected. The Figure shows a linear relationship having a slope of 2.61. Thus, the equation over estimates the actual threshold voltage by ≈17%. It should be noted that data for all four nematic fluids have been plotted and fall on the same line.

5.5.1 Effect of Blending

In Figure 5.17, V_c is plotted against $T-T_{NI}$ for the three nematic mixtures and K15. The Figure shows that, for all equivalent sub-clearing point temperatures, V_c for the four nematics has the following order: K15/S1115 > K15 > K15/S1188 > K15/S1236. Thus, the elastic constants play the dominant role in determining V_c for the binary blends. If the dielectric anisotropy were the dominant factor the order would be: K15/S1115 > K15/S1188 > K15/S1236 > K15 (see Figure 5.18).

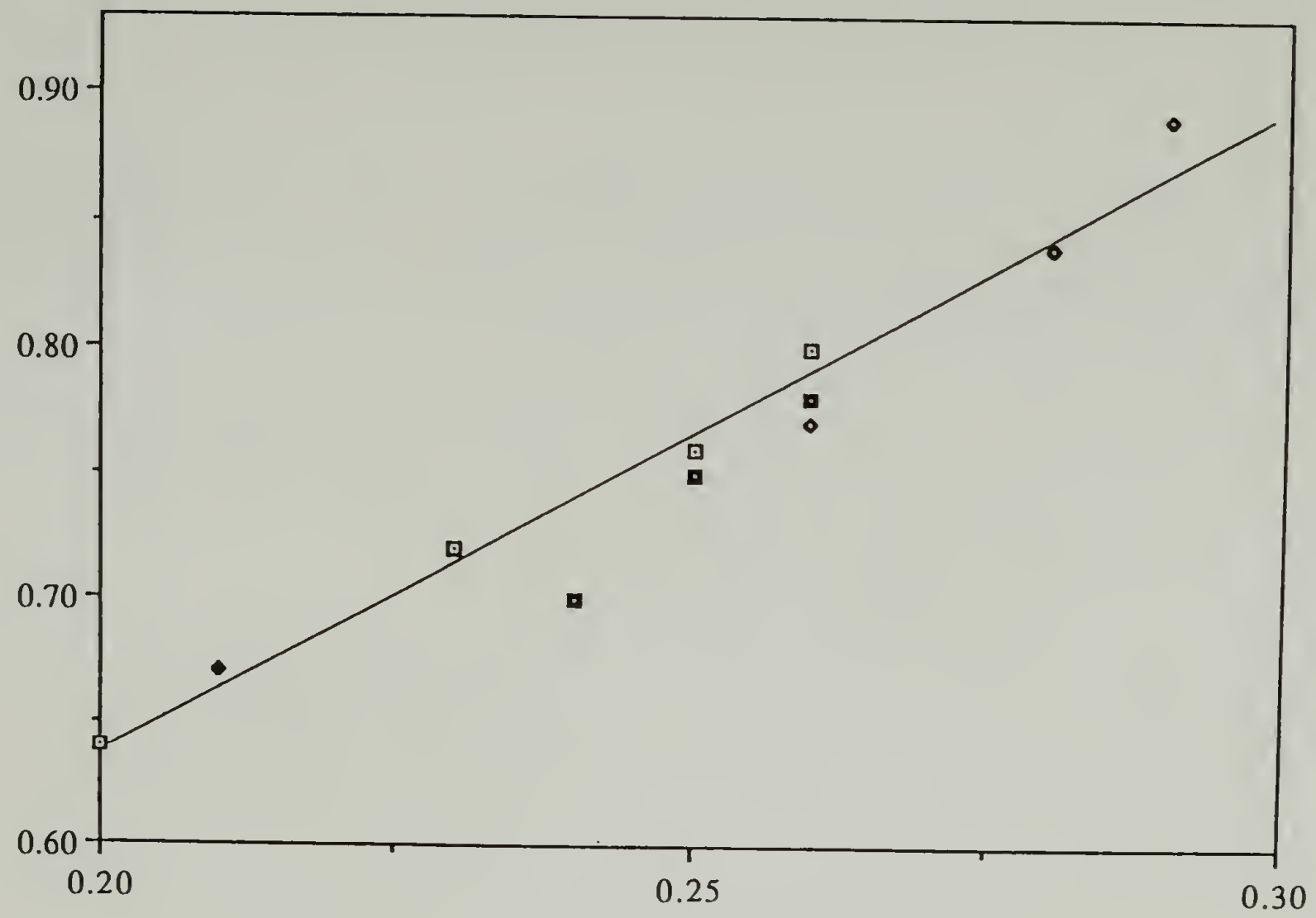

Figure 5.16. Threshold voltage plotted against $(K_{11}/\Delta\epsilon\epsilon_o)^{-\frac{1}{2}}$ for four nematic fluids. ◇-K15/S1115, ▫-K15, ▪-K15/S1188, ◆-K15/S1236.

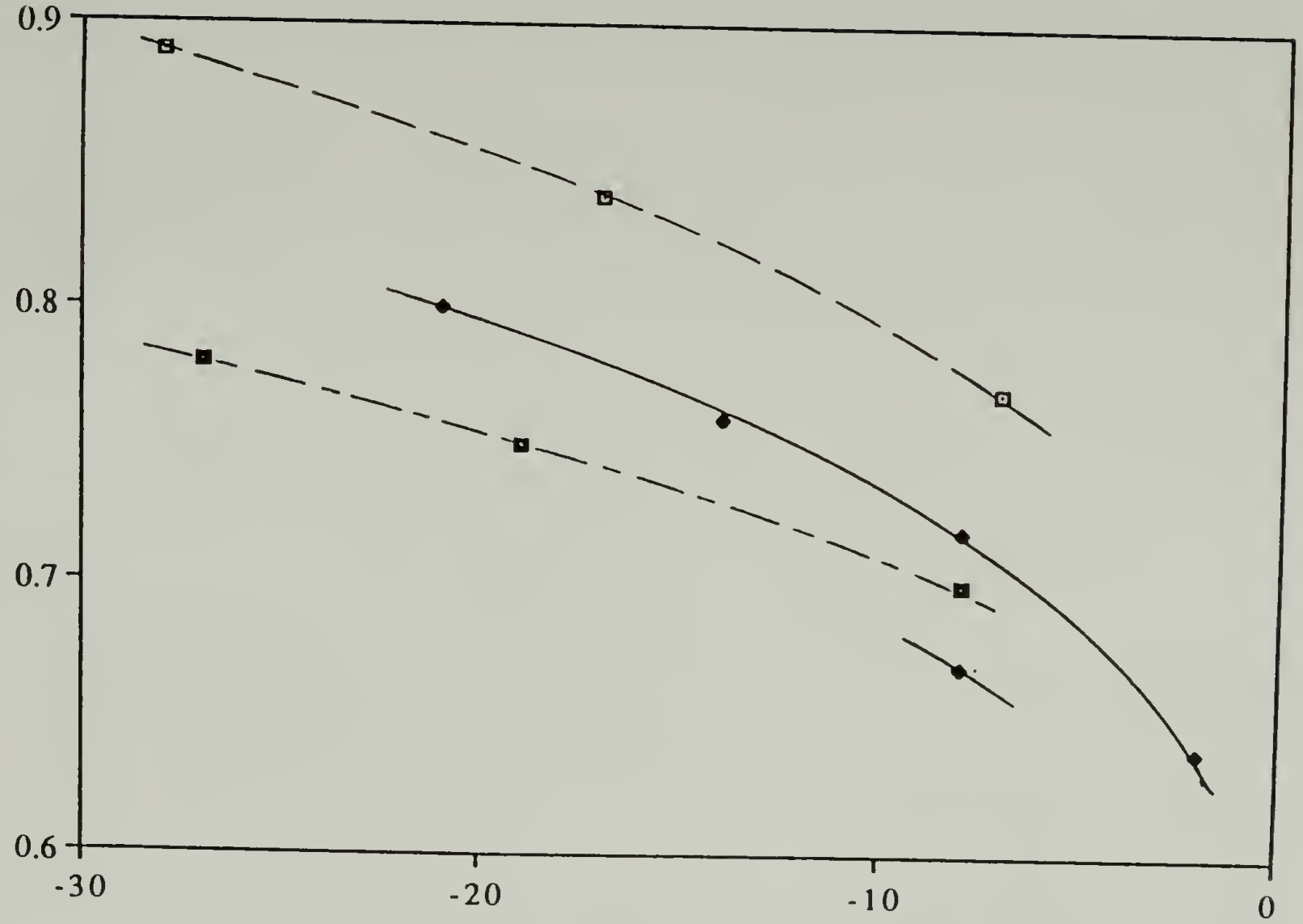

Figure 5.17. Threshold voltage versus sub-clearing temperature for four nematic fluids. ⊡ - K15/S1115, ♦ - K15, ■ - K15/S1188, ◈ - K15/S1236.

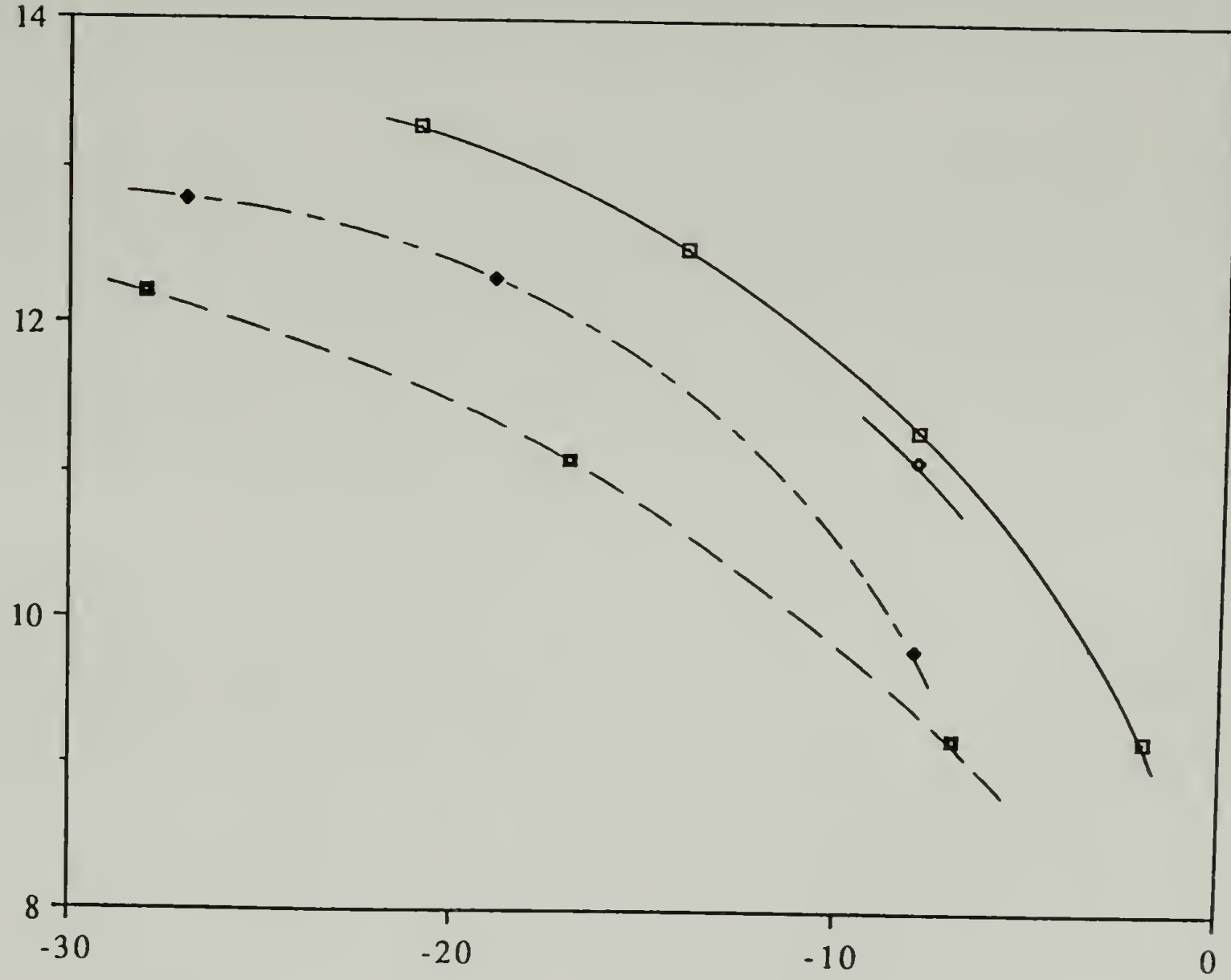

Figure 5.18. Dielectric anisotropy versus sub-clearing temperature for four nematic fluids. ⊡ K15, ◆ K15/S1236, ◆ K15/S1188, ◘ K15/S1115.

5.6 References

1. F.J. Kahn, Proc IEEE, **61**, 823 (1973).

2. R.E. Michel and G.W. Smith, J. Appl. Phys., **45**, 3234 (1974).

3. M. Schadt and F. Müller, J. Phys., **14**, 265 (1978).

4. M. Schadt and P.R. Gerber, Z. Naturforsch., **37a**, 165 (1982).

5. B.R. Ratna and R. Shashidar, Mol. Cryst. Liq. Cryst., **42**, 113 (1977).

6. V.I. Minkin, O.A. Osipov, and Y.A. Zhdanov, Dipole Moments in Organic Chemistry, Plenum (1970), p91.

7. M. Schadt, J. Chem Phys., **56**, 1494 (1972).

8. W.H. de Jeu and T.W. Lathouwers, Z. Naturforsch., **29a**, 905 (1974).

9. N.V. Madhusudana and S. Chandrasekhar, Proc. Int. Liq. Cryst. Conf., Bangalore, 1973 --Pramana Suppl., **1**, p57.

10. N.V. Madhusudana, K.L. Savithramma, and S. Chandrasekhar, Pramana, **8**, 22 (1977).

11. M. Schadt and P. Gerber, Z. Naturforsch., **37a**, 165 (1982).

12. J. Robert, G. Labrunie and J. Borel, Mol. Cryst. Liq. Cryst., **23**, 197 (1973).

13. P.R. Gerber and M. Schadt, Z. Naturforsch., **37a**, 179 (1982).

14. H. Deuling, Mol. Cryst. Liq. Cryst., **19**, 123 (1972).

15. C. Maze, Mol. Cryst. Liq. Cryst., **48**, 273 (1978).

16. M.J. Bradshaw, E.P. Raynes, J.D. Bunning and T.E. Faber, J. Physique, **46**, 1513 (1985).

17. J.D. Bunning, T.E. Faber and P.E. Sherrell, J. Physique, **42**, 1175 (1981).

CHAPTER 6

ELECTRO-OPTICAL STUDIES OF BINARY NEMATIC MIXTURES

In chapter 2, an interesting electrical deformation for the room-temperature nematic liquid crystal n-pentylcyanobiphenyl was discussed. One of the goals towards understanding this phenomenon is to correlate the behavior of the deformation with the physical properties of the mesophase. One approach towards this goal is to modify the properties of the mesophase through blending. This rationale led to the phase study of three binary systems of n-pentylcyanobiphenyl with homologs of 4-[4-alkylcyclohexyl]cyanophenyl. Three binary mixtures, one from each phase diagram, were chosen for further characterization. In this final experimental chapter, an attempt is made to correlate the physical properties of the binary mixtures characterized in chapters 4 and 5 with their deformation behavior.

6.1 Experimental

Four nematic fluids were electrically deformed in a transverse-electrode cell such as the one shown in Figure 2.1. The electrode spacing, L, was ~1.1 mm and the plate separation, d, was ~17 microns. Thermocouples were mounted in each sample for accurate temperature readings to within $\pm 1^{o}C$. The deformation experiment of chapter 2 was repeated for all four fluids. The nematic fluids used were pure n-

pentylcyanobiphenyl (K15) and the 60/40 mole % mixtures of K15 with three 4-[4-alkylcyclohexyl]cyanophenyl homologs. The phase behavior and physical properties of these fluids are discussed in the previous chapters. Deformation of the nematic fluids were carried out at two temperature: 14°C and $(T_{NI}-7)$°C. Values of the wave-onset field, wavelength and interface position were recorded for these four nematics.

6.2 Transverse Electric-Field Deformation

6.2.1 At Constant Temperature (14°C)

Figure 6.1 shows the interface position plotted as a function of the electric-field squared at 14°C. The Figure shows a linear relationship for all four fluids. The slope of such a plot has the units of m^3/V^2, and thus, is inversely related to the energy density of the mesophase. In other words, the greater the slope the less efficient the nematic is in storing energy in a given volume. The Figure shows the efficiency of energy storage in the four nematic fluids has the following order: K15/S1236 < K15/S1188 < K15/S1115 < K15.

Two factors are important in considering the ability of a nematic to store electrical energy: the elastic and dielectric properties. From the data listed in Table 6.1, we can quantitatively explain the ordering seen above. The nematic fluids of Table 6.1 are listed in increasing order of their elastic constants. Thus, more energy is required to

produce the same distortion as we proceed down the Table. This is the same order as the magnitude of the slopes shown in Figure 6.1 with the exception that K15/S1115 and K15 are transposed. To explain this reversal of order, note the dielectric anisotropy of these two systems also given in Table 6.1. The dielectric anisotropy of K15 is greater than that of the K15/S1115 mixture. Thus, the couple between the electrical field and the dipole moment of the cyano group is greater in the case of K15. This implies that at any given cell position, x/L, K15 has undergone more rotation than the K15/S1115 mixture, thus storing more energy in the z-direction. A comparison of the orientation profile between these two systems, in the same vein as the work of chapter 4, should bear out this conclusion.

In Table 6.2, the wave-onset field and the wavelength of the undulations at constant temperature and energy are shown. No general correlations between E_W or wavelength with the physical properties of Table 6.1 were found.

6.2.2 At Constant Sub-Clearing

Figure 6.2 shows the interface position plotted as a function of the electric field squared for a constant sub-clearing temperature of $-7^{o}C$. The slopes of the four nematics have the same order and are higher than those given in Table 6.2. Thus, more mechanical work is done on the system as the clearing point is approached.

The physical properties of the four nematic systems are given in Table 6.3 for easy reference. In Table 6.4, the wave onset field andwavelength of the undulations at -7°C sub-clearing are given. Again, clear correlations between the deformation behavior and the material properties of Table 6.3 were not found, with the following exception.

In Figure 6.3, the slope of the deformation is plotted as a function of the dielectric anisotropy of the nematic. The Figure shows that, in general, as $\Delta\epsilon$, increases the slope of the interface position versus electric-field squared curve decreases. This is attributed to the effectiveness of the nematic to shield interior molecules from the applied field as $\Delta\epsilon$ increases.

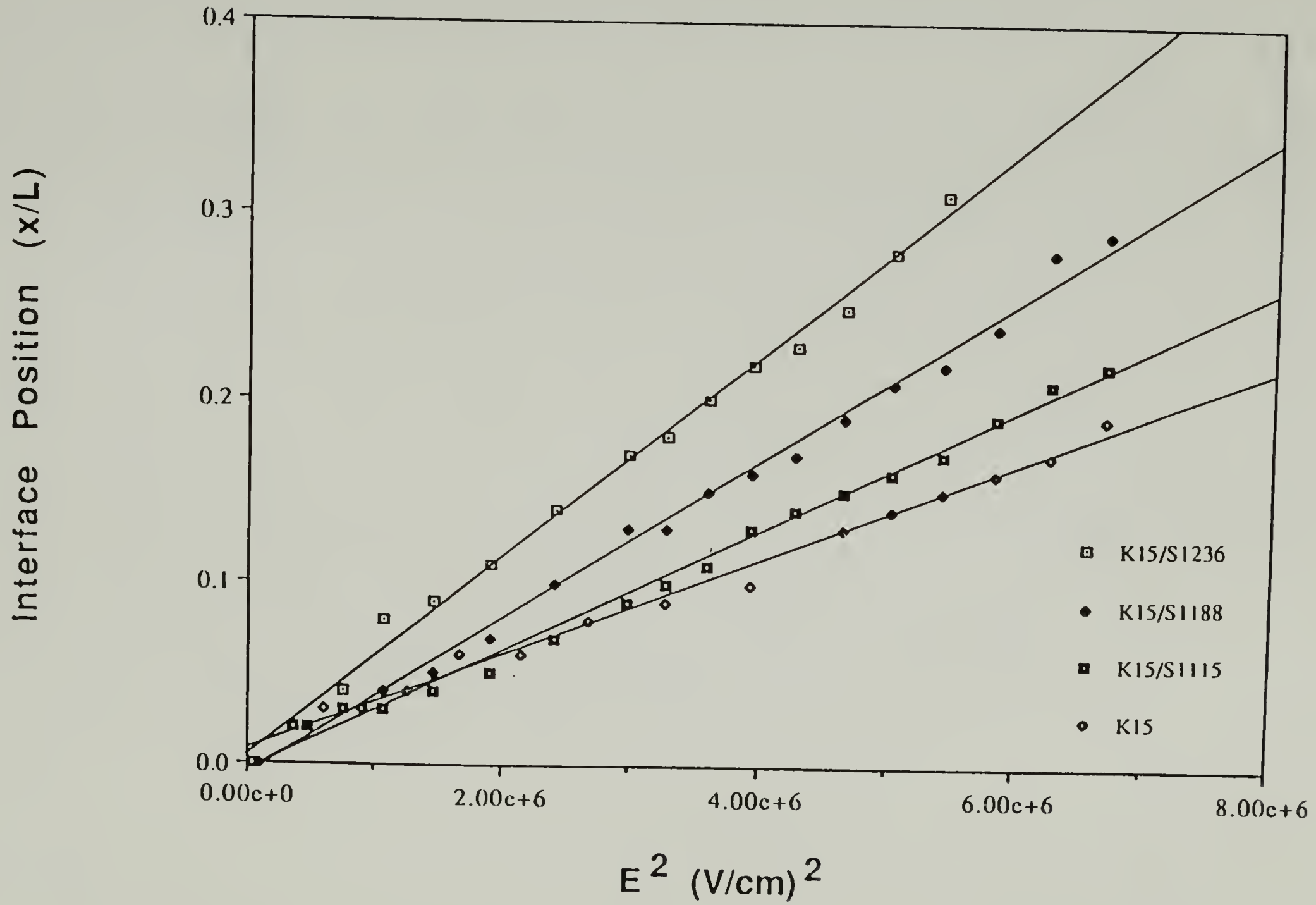

Figure 6.1. Interface position vs electric field squared at 14°C.

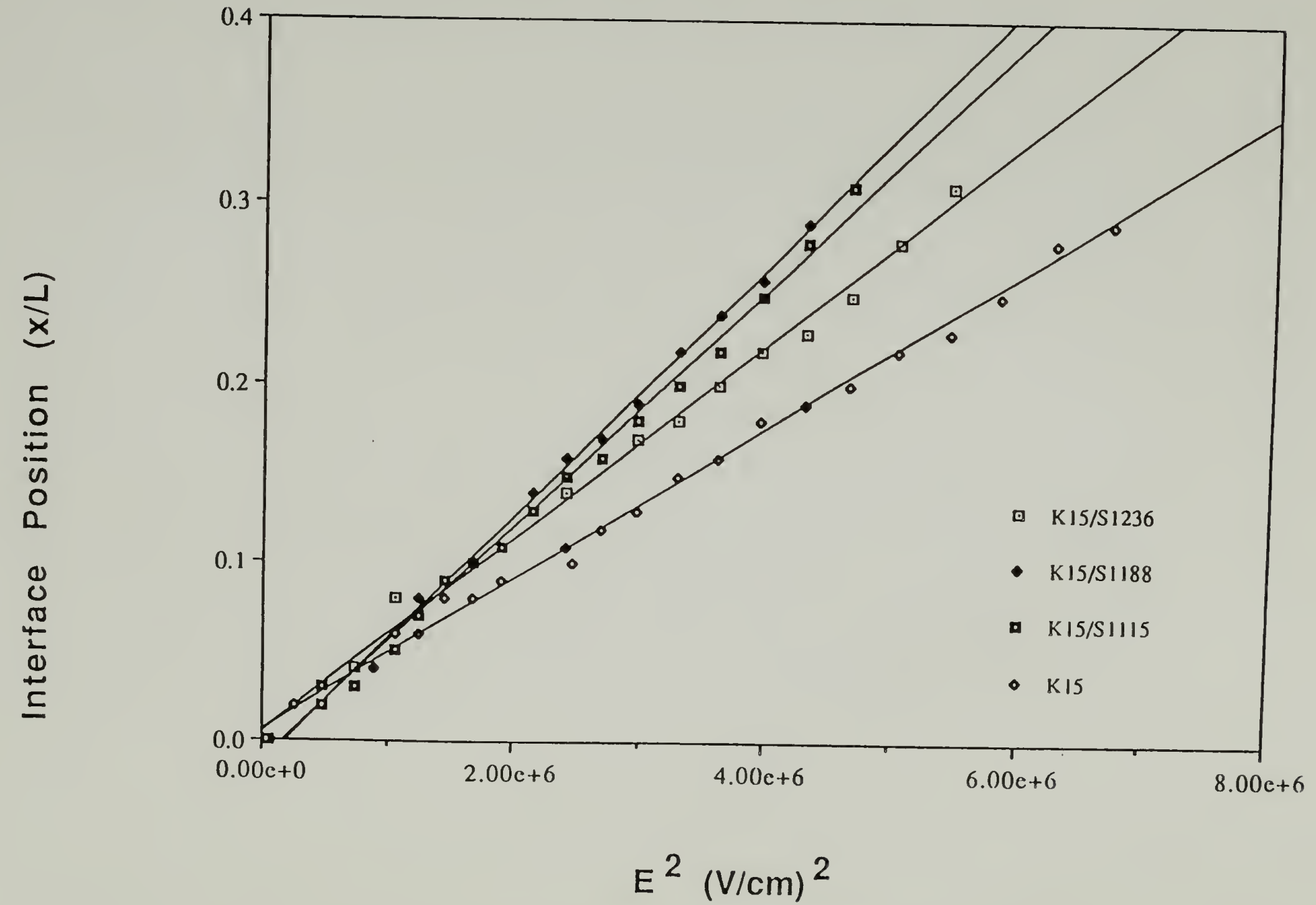

Figure 6.2 Interface position vs electric field squared at (Tni-7)°C.

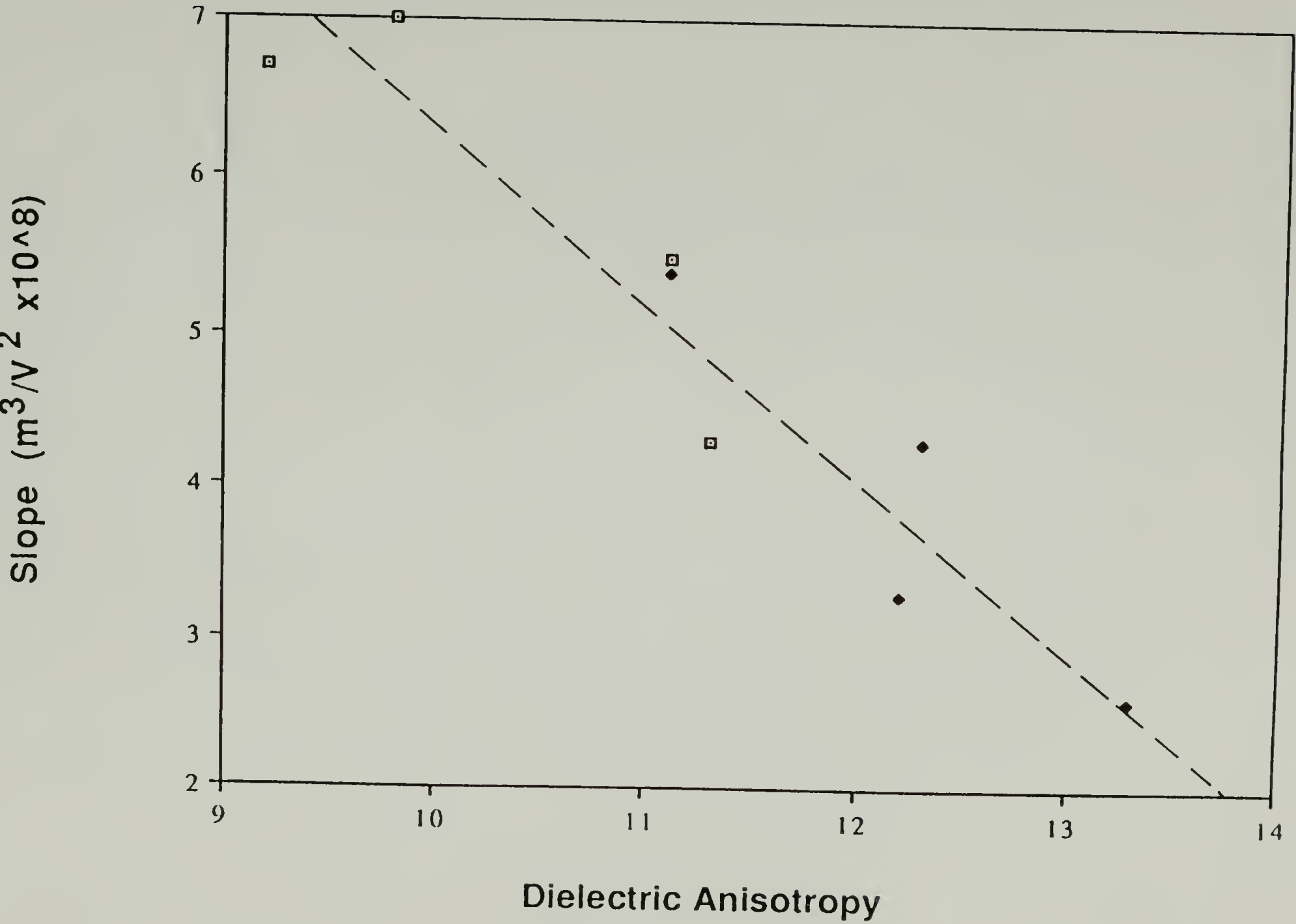

Figure 6.3. Slope of interface position vs. electric field squared curve plotted as a function of dielectric anisotropy.

Table 6.1 Physical properties of four nematic systems at 14°C. Binary systems are 60/40 mole % mixtures.

System	V_c	$\Delta\epsilon$	K_{11} dynes x 10^6	K_{33}
K15/S1236	.67	11.1	.44	.57
K15/S1188	.75	12.3	.66	.97
K15	.80	13.3	.82	1.11
K15/S1115	.89	12.2	.92	1.20

Table 6.2 Electrical deformation data for four nematic fluids at 14°C.

System	E_w (V/cm)	λ (μm)	$T_{NI}-T$ (°C)	slope (m^3/V^2) x 10^8
K15/S1236	2327	100	7	5.4
K15/S1188	2192	60	19	4.3
K15	1769	80	21	2.6
K15/S1115	2019	60	28	3.3

Table 6.3 Physical properties of four nematic systems at (TNI-7)°C. Binary systems are 60/40 mole % mixtures.

System	V_c	$\Delta\epsilon$	K_{11} dynes x 10^6	K_{33}
K15/S1236	.67	11.1	.44	.57
K15/S1188	.70	12.3	.66	.97
K15	.72	11.3	.54	.63
K15/S1115	.77	9.2	.53	.65

Table 6.4 Electrical deformation data for four nematic fluids at (TNI-7)°C.

System	E_w (V/cm)	λ (μm)	$T_{NI}-T$ (°C)	slope (m^3/V^2) x 10^8
K15/S1236	2327	100	7	5.4
K15/S1188	2280	120	7	7.0
K15	2301	90	7	4.3
K15/S1115	2019	90	7	6.7

CHAPTER 7

FUTURE WORK

It is common, in the course of a doctoral program, to uncover questions relating to the subject of interest which cannot be answered during the matriculation of the graduate student. This is understandable and needs to be accepted by the student as well as the thesis committee. However, it is the responsibility of the maturing scientist to suggest those areas he sees as the most interesting or fruitful for further work. It is the goal of this chapter to highlight some of those areas.

A novel deformation pattern was discussed in chapter 2. The most interesting feature of this deformation is the wave-like undulation structure. The birefringent bands in the immediate vicinity of these undulations are not parallel to the electrodes as are the bands closer to the electrode (see Figure 1.2c). However, both sets of bands become extinct under the same conditions, i.e. when the electric-field direction and the analyzer or polarizer directions are coincident. This indicates all deformed molecules have rotated only in planes normal to the electrodes. From this fact, it is simple to show that twist deformation occurs in the vicinity of the undulations while splay occurs in regions farther away.

Given the different energy storage capacities of these distortions, by controlling the ratio K_{11}/K_{22} while holding

the other material parameters constant it should be possible to significantly vary the wavelength of the undulations. This would be of practical interest in the design of a diffraction grating as well as fundamental, academic interest.

One means of controlling K_{11}/K_{22} is to synthesize a series of compounds from the same chemical class having longer and longer molecular lengths. As the length increases, splay becomes much more difficult while twist increases moderately.

The work of chapter 3 set out to quantify the deformation structures observed. Using theoretical approaches, two orientation profiles for the x-direction were given. One allows for a z-dependent orientation angle and the other holds this value constant. It would be a great experimental challenge to design a cell which could directly view the molecular orientation in the x-z plane to assess which of these descriptions is more accurate.

In chapter 6, the energy storage capacity of four nematic fluids was discussed qualitatively. A method of quantitative analysis for comparison would be desirable. Perhaps an analysis of the deforamtion for the four systems following the same algorithm as demonstrated in chapter 2 might provide such a method.

Finally, we also noted in chapter 6 that there were no general correlations found between the wave-onset field E_W or the wavelength of the undulations with any of the

physical properties measured in chapter 5. This result is unsatisfying. It would be desirable to study a larger number of nematic fluids and seek other possible physical parameters that yield a correlation between the mesophase structure and the deformation properties. This would give a greater understanding of the phenomenon and could possibly lead to a new technique for measuring all three elastic constant of the mesophase in a single deformation experiment.

APPENDIX

MEASURING FILM THICKNESS INTERFEROMETRICALLY

The thickness of very thin films can be measured interferometrically from optical fringe patterns. These fringe patterns are often seen in the mid-IR region of polystyrene spectra. Two conditions must be met for such a fringe pattern to exist: a) the index of refraction, n, for the layer of unknown thickness must be sufficiently different from the index of refraction for the adjacent layers and b) the surfaces of the film must be nearly parallel. When these conditions are met and a spectral band of appropriate wavelengths, λ ,is used, interference fringes such as those shown in Figure A.1 can be recorded. Such fringe patterns are simply plots of intensity vs wavelength for the sample.

The thickness of the film, d, can be found using

$$d = n/2(\nu_1 - \nu_2) \qquad (A.1)$$

where ν_1 and ν_2 are the wavenumbers of two spectral frequencies and n is the number of fringes between them.

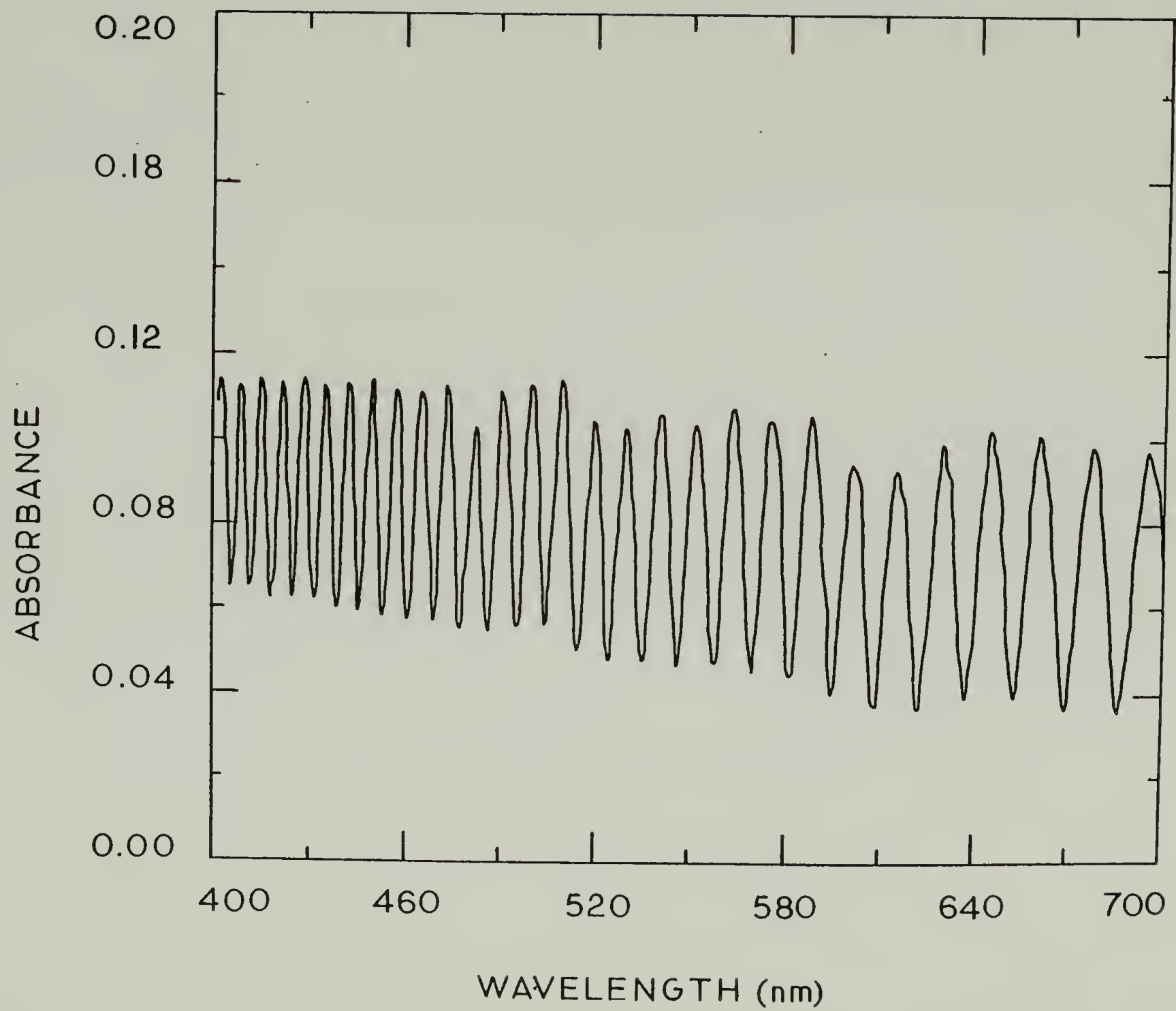

Figure A.1 Interference pattern for a 12 micron LC cell.

BIBLIOGRAPHY

Berezin, P.D., I.N. Kompanets, V.V. Nikitin, and S.A. Pikin, Zh. Esp. Teor. Fiz. **64**, 599 (1972) [Sov. Phys. JETP **37**, 305 (1973)].

Berreman, D.W., in Nonemissive Electro-optic Displays, edited by A.R. Kmetz and F.K. Willisen (Plenum Press, New York and London, 1975), p9.

Bihrandar, B., Mol. Cryst. Liq. Cryst. **99**, 345 (1983).

Bogojawlensky, A, and N. Winogradow, Z. Physik. Chem. (Leipzig), **60**, 433 (1907).

Bradshaw, M.J., E.P. Raynes, J.D. Bunning and T.E. Faber, J. Physique, **46**, 1513 (1985).

Bunning, J.D., T.E. Faber and P.E. Sherrell, J. Physique, **42**, 1175 (1981).

Chistyakov, I.G. and L.K. Vistin, Kristallografiya, **19**, 195 (1974).

Creagh, L.T. and A.R. Kmetz, Mol. Cryst. Liq. Cryst., **24**, 59 (1974).

Dave, J.S. and K.L. Vasanth, Ind. J. Chem., **7**, 498 (1968).

DeGennes, P.G., The Physics of Liquid Crystals, Oxford Press University, Oxford, 1974.

DeJeu, W.H., and T.W. Lathouwers, Z. Naturforsch., **29a**, 905 (1974).

Demus, D., C. Fietkau, R. Schubert and H. Kehlen, Mol. Cryst. Liq. Cryst., **25**, 215 (1972).

Deuling, H., Mol. Cryst. Liq. Cryst., **19**, 123 (1972).

Dubois, J.C., M. Gazard and A. Zann, J. Appl. Phys. **47**, 1270 (1976).

Dubois-Violette, E., P.G. deGennes and O. Parodi, J. Physique, **32**, 305 (1971).

Engelen, B. and F. Schneider, Z. Naturforsch., **33A**, 1077 (1978).

Frank, F.C., Disc. Faraday Soc. **25**, 19 (1958).

Freederickz, V. and I.V. Tsvetkov, Dokl. Akad. Nauk. SSSR **4**, 123 (1935).

Gerber, P.R., and M. Schadt, Z. Naturforsch., **37a**, 179 (1982).

Gruler, H., T.J. Scheffer and G. Meier, Z. Naturforsch. **27A**, 966 (1972).

Haas, W., J. Adams and J.B. Flannery, *Phys. Rev. Lett.*, **25**, 1326 (1970).

Haller, I., Appl. Phys. Lett. **24**, 349 (1974).

Heilmeier, G.H., and L.A. Zanoni, Appl. Phys. Lett. **13**, 91 (1968).

Heilmeier, G.H., L.A. Zanoni and L.A. Barton, *Proc. IEEE*, **56**, 1162 (1968).

Helfrich, W., J. Chem Phys., **51**, 4092 (1969).

Hollaway, W.W., Jr. and M.J. Rafuse, *J. Appl. Phys.*, **42**, 5395 (1971).

Horn, R.G., J. Physique, **39**, 105 (1978).

Hsu, E.C.H., and J.F. Johnson, Mol. Cryst. Liq. Cryst., 27, 95-104 (1973).

Ivashcenko, A.V., V.V. Titov and E.I. Kovshev, Mol. Cryst. Liq. Cryst., **33**, 195 (1976).

Jakeman, E., and E.P. Raynes, Phys. Lett. **A39**, 69 (1972). Orsay Liquid Crystal Group, J. Chem. Phys. **54**, 816 (1969).

Kahn, F.J., *Appl. Phys. Lett.*, **20**, 199 (1972).

Kahn, F., G.N. Taylor and H. Schonhorn, Proc. IEEE **61**, 823 (1973).

Kapustin, A.P., and L.S. Larinova, Kristallogr. **9**, 297 (1963).

Karat, P.P., and N.V. Madhusudana, Mol. Cryst. Liq. Cryst., **40**, 239 (1977).

Madhusudana, N.V., and S. Chandrasekhar, Proc. Int. Liq. Cryst. Conf., Bangalore, 1973 --Pramana Suppl., **1**, p57.

Madhusudana, N.V., K.L. Savithramma, and S. Chandrasekhar, Pramana, **8**, 22 (1977).

Maze, C., and D. Johnson, Mol. Cryst. Liq. Cryst. **33**, 213 (1976).

Michel, R.E., and G.W. Smith, J. Appl. Phys., **45**, 3234 (1974).

Minkin, V.I., O.A. Osipov, and Y.A. Zhdanov, *Dipole Moments in Organic Chemistry,* Plenum (1970), p91.

Ong, H.L., A.J. Hurd and R.B. Meyer, J Appl. Phys., **57**, 186 (1984).

Oseen, C.W., Arkiv Matematik Astron. Fysik **A19**, 1 (1925), Fortschr. Chem. Physik u. Physik Chem. **20**, 1 (1929), Trans. Faraday Soc. **29**, 883 (1933).

Osman, M.A., Z. Naturforsch., 38A, 779-787 (1983).

Penz, P.A., Proc. S.I.D., **19**, 43 (1978).

Ramo, S., J.R. Whinnery, T.V. Duzer, Fields and Waves in Communication Electronics, John Wiley & Sons, Inc., New York, 1965, p186.

Ratna, B.R., and R. Shashidar, Mol. Cryst. Liq. Cryst., **42**, 113 (1977).

Raynes, E.P., IEEE Trans. Electr. Dev., **26**, 1116 (1979).

Robert, J., G. Labrunie and J. Borel, Mol. Cryst. Liq. Cryst., **23**, 197 (1973).

Saupe, A., Z. Naturforsch. **15a**, 815 (1960); P. Pincus, J. Appl. Phys. **41**, 974 (1970).

Schadt, M., J. Chem Phys., **56**, 1494 (1972).

Schadt, M., and P.R. Gerber, Z. Naturforsch. **37a**, 165 (1982).

Schadt, M., and W. Helfrich, Appl. Phys Lett., **18**, 127 (1971).

Schadt, M., and F. Müller, J. Phys., **14**, 265 (1978).

Schell, K.T., and R.S. Porter, Mol. Cryst. Liq. Cryst., **174**, 141 (1989).

Schiekel, M.F., and K. Fahrenschon, Appl. Phys. Lett. **19**, 391 (1971).

Soref, R.A., Appl. Phys. Lett. **22**, 165 (1972).

Soref, R.A., S.I.D. Symposium, New York, 1973.

Soref, R.A., S.I.D. Symposium, New York, 1973.

Soref, R.A., J. Appl. Phys. **45**, 5466 (1974).

Soref, R.A., Proc. IEEE **62**, 1710 (1974).

Soref, R.A., Sperry Rand Research Report SRRC-RR-73-1, (1973).

Soref, R.A., and M.J. Rafuse, J. Appl. Phys., **43**, 2029 (1971).

Soref, R.A., Appl. Phys. Lett., **22**, 165 (1973).

Soref, R.A., in S.I.D. Symposium Digest of Technical Papers (Lewis Winner, New York, 1972), p34.

Uchida, T., M. Ohgawara and Y. Shibata, Mol. Cryst. Liq. Cryst. **98**, 149 (1983).

Urbach, W., M. Boix and E. Guyon, Appl. Phys. Lett., **25**, 479 (1974).

Vistin, L.K., and V.M. Ivanov, 1st Scientific Conference on Liquid Crystals, Ivanovo Pedagogical Institute, Ivanovo (1970).

Walter, R., Ber. Deut. Chem. Ges., 58, 2303 (1925).

Williams, R., J.Chem. Phys. **56**, 147 (1971).

Zocher, H., Z. Phisik **28**, 790 (1927).